

Electronic Supplementary Materials for

X-ray Characterization of core-modified N-confused fused porphyrinogen and genesis of $\pi(\sigma)$ (anti)Aromatic N-confused fused porphyrinoids

Manik Jana,^a Gunasekaran Velmurugan,^b Peter Comba,^{*b} and Harapriya Rath^{*a}

^a School of Chemical Sciences, Indian Association for The Cultivation of Science, 2A/2B Raja S. C. Mullick Road, Jadavpur, Kolkata 700 032, India, E-mail: ichr@iacs.res.in

^b1Heidelberg University, Institute of Inorganic Chemistry and Interdisciplinary Center for Scientific Computing, Im Neuenheimer Feld 270, 69120 Heidelberg, GERMANY. E-mail: peter.comba@aci.uni-heidelberg.de

Table of Contents

Materials and Methods	S2-S4
General Synthetic Procedure	S4-S6
Spectroscopic Data	S7-S21
Electrochemistry	S21-S22
X-ray crystal Data	S23-S24
Theoretical Calculations	S25-S48
X,Y,Z Coordinates	S49-S59

Materials and Methods:

1.1 Electronic absorption spectra were measured with a Perkin Elmer Lambda 950 UV-visible-NIR spectrophotometer. ^1H NMR spectra were recorded on a Bruker AVIII 500 MHz spectrometer, Bruker AVIII 400 MHz, Bruker DPX-300 MHz spectrometer and chemical shifts were reported as the delta scale in ppm relative to CHCl_3 ($\delta = 7.26$ ppm) and CH_2Cl_2 ($\delta = 5.32$ ppm) as internal reference for ^1H and ^{13}C NMR CHCl_3 ($\delta = 77.00$ ppm) and CH_2Cl_2 ($\delta = 55.00$ ppm). MALDI-TOF MS data were recorded using Bruker Daltonics flex Analyser and ESI HR-MS data were recorded using Waters QTOF Micro YA263 spectrometer. Cyclic voltammograms were recorded using a platinum working electrode, a platinum wire counter electrode and a Ag/AgCl reference electrode in Bioanalytical Systems EC epsilon. The measurements were carried out in CH_2Cl_2 solution using 0.1 M Bu_4NPF_6 as the supporting electrolyte at a scan rate of 0.1 V/s. Peak potentials were determined from differential pulse voltammetry experiments. The Fc/Fc^+ redox couple was used as an internal standard. All solvents and chemicals were of reagent grade quality, obtained commercially and used without further purification except as noted. For spectral measurements, anhydrous dichloromethane was obtained by refluxing and distillation over CaH_2 . Dry THF was obtained by refluxing and distillation over pressed Sodium metal. Thin layer chromatography (TLC) was carried out on alumina sheets coated with silica gel 60 F₂₅₄ (Merck 5554) and gravity column chromatography were performed using Merck Silica Gel 230-400 mesh. Aluminum Oxide (Basic) grade II was purchased from Sigma Aldrich.

1.2 X-Ray structure determination.

A specimen of $\text{C}_{50}\text{H}_{39}\text{Cl}_2\text{F}_4\text{N}_3\text{S}_2$, approximate dimensions 0.200 mm x 0.200 mm x 0.500 mm, was used for the X-ray crystallographic analysis. The X-ray intensity data were measured ($\lambda = 0.71073$ Å). The total exposure time was 1.09 hours. The frames were integrated with the Bruker SAINT Software package using a narrow-frame algorithm. The integration of the data using an monoclinic unit cell yielded a total of 70188 reflections to a maximum θ angle of 27.55° (0.77 Å resolution), of which 10045 were independent (average redundancy 6.987, completeness = 98.7%, $R_{\text{int}} = 5.57\%$, $R_{\text{sig}} = 6.12\%$) and 6830 (67.99%) were greater than 2σ (F^2). The final cell constants of $a = 24.971(3)$ Å, $b = 14.4865(19)$ Å, $c = 12.3630(15)$ Å, volume = $4399.9(9)$ Å³, are based upon the refinement of the XYZ-centroids of 9939 reflections above 20σ (I) with $4.884^\circ < 2\theta < 54.83^\circ$. Data were corrected for absorption effects using the Multi-Scan method (TWINABS). The ratio of minimum to maximum apparent transmission was 0.757. The calculated minimum and maximum transmission coefficients (based on crystal size) are 0.8650 and 0.9430. The structure was solved and refined using the Bruker SHELXTL Software Package, using the space group P 1 21/c1 with $Z = 4$ for the formula unit, $\text{C}_{50}\text{H}_{39}\text{Cl}_2\text{F}_4\text{N}_3\text{S}_2$. The final anisotropic full-matrix least-squares refinement on F^2 with 556 variables converged at $R1 = 7.23\%$, for the observed data and $wR2 = 18.95\%$ for all data. The goodness-of-fit was 1.040. The largest peak in the final difference electron density synthesis was 0.393 e/Å³ and the largest hole was -0.660 e/Å³ with an RMS deviation of 0.072 e/Å³. On the basis of the final model, the calculated density was 1.348 g/cm³ and $F(000)$, 1848 e⁻.

1.3 Theoretical Calculation

All the calculations have been computed using the Gaussian16 program¹ at B3LYP/6-31G(d,p) level of theory.² The electronic absorption spectra, singlet vertical excitation energies and oscillator strengths on the ground state optimized geometries have been computed using time dependent density functional theory (TD-DFT).³ We have used dichloromethane as solvent using the polarized continuum model (PCM).⁴ The contribution of various fragments of the macrocycle have been analyzed using the QMForge program.⁵ The nucleus independent chemical shift (NICS) values were calculated at the non-weighted mass of conjugation π -pathway of the macrocycles (1-8 Å above and below the molecular plane).⁶ The NICS values are scanned along the trajectory orthogonal to the plane of the macrocycle based on the Stranger method.⁷ The NMR shielding tensors were computed using the Gauge-Independent Atomic Orbital (GIAO) at the non-weighted mass of conjugation π -pathway of the macrocycle.⁸ On the other hand, the harmonic oscillator model of aromaticity (HOMA) index, electron localization function (ELF), multi center index (MCI), AV1245, AVmin and localized orbital locator (LOL) topology analysis, the NBO analysis based decomposition of the Wiberg bond index has been calculated using Multiwfn.⁹ The anisotropy of the current (induced) density (ACID) has been done using ACID plot.¹⁰

References:

1. M. Frisch, G. Trucks, H. Schlegel, G. Scuseria, M. Robb, J. Cheeseman, G. Scalmani, V. Barone, B. Mennucci, G. Petersson, H. Nakatsuji, M. Caricato, X. Li, H. Hratchian, A. Izmaylov, J. Bloino, G. Zheng, J. Sonnenberg, M. Hada, M. Ehara, K. Toyota, R. Fukuda, J. Hasegawa, M. Ishida, T. Nakajima, Y. Honda, O. Kitao, H. Nakai, T. Vreven, J. Montgomery, Jr, J. E. Peralta, F. Ogliaro, M. Bearpark, J. J. Heyd, E. Brothers, K. N. Kudin, V. Staroverov, R. Kobayashi, J. Normand, K. Raghavachari, A. Rendell, J. Burant, S. Iyengar, J. Tomasi, M. Cossi, N. Rega, N. Millam, M. Klene, J. E. Knox, J. B. Cross, V. Bakken, C. Adamo, J. Jaramillo, R. Gomperts, R. Stratmann, O. Yazyev, A. Austin, R. Cammi, C. Pomelli, J. Ochterski, R. L. Martin, K. Morokuma, V. Zakrzewski, G. Voth, P. Salvador, J. Dannenberg, S. Dapprich, A. Daniels, Ö. Farkas, J. Foresman, J. Ortiz, J. Cioslowski and D. Fox, Gaussian 16, revision C. 01, Gaussian, Inc., Wallingford, CT 2010.
2. (a) A. D. Becke, Density-functional thermochemistry. III. The role of exact exchange, *J. Chem. Phys.*, 1993, **98**, 5648-5652; (b) J. P. Perdew, Density-functional approximation for the correlation energy of the inhomogeneous electron gas, *Phys. Rev. B*, 1986, **33**, 8822-8824; (c) A. D. Becke, Density-functional exchange-energy approximation with correct asymptotic behaviour, *Phys. Rev. A*, 1988, **38**, 3098-3100; (d) C. Lee, W. Yang and R. G. Parr, Development of the Colle-Salvetti correlation-energy formula into a functional of the electron density, *Phys. Rev. B*, 1988, **37**, 785-789.
3. (a) E. Runge and E. K. U. Gross, Density-Functional Theory for Time-Dependent Systems, *Phys. Rev. Lett.*, 1984, **52**, 997-1000; (b) R. E. Stratmann, G. E. Scuseria and M. J. Frisch, An efficient implementation of time-dependent density-functional theory for the calculation of excitation energies of large molecules, *J. Chem. Phys.*, 1998, **109**, 8218-8224; (c) R. Bauernschmitt and R. Ahlrichs, Treatment of electronic excitations within the adiabatic approximation of time dependent density functional theory, *Chem. Phys. Lett.*, 1996, **256**, 454-464.
4. (a) M. Cossi, G. Scalmani, N. Rega and V. Barone, New developments in the polarizable continuum model for quantum mechanical and classical calculations on molecules in solution, *J. Chem. Phys.*, 2002, **117**, 43-54; (b) E. Cancès, B. Mennucci and J. Tomasi, A new integral equation formalism for the polarizable continuum model: Theoretical background and applications to isotropic and anisotropic dielectrics, *J. Chem. Phys.*, 1997, **107**, 3032-3041; (c) B. Mennucci and J. Tomasi, Continuum solvation models: A new approach to the problem of solute's charge distribution and cavity boundaries, *J. Chem. Phys.*, 1997, **106**, 5151-5158.
5. (a) A. Tenderholt, "QMForge: A Program to Analyze Quantum Chemistry Calculations", Version 2.3.2, <http://qmforge.sourceforge.net>; (b) G. Velmurugan and P. Venuvanalingam, Luminescent Re(I) terpyridine complexes for OLEDs: what does the DFT/TD-DFT probe reveal?, *Dalton Trans.*, 2015, **44**, 8529-8542; (c) G.

- Velmurugan, B. K. Ramamoorthi and P. Venuvanalingam, Are Re(I) phenanthroline complexes suitable candidates for OLEDs? Answers from DFT and TD-DFT investigations, *Phys. Chem. Chem. Phys.*, 2014, **16**, 21157-21171; (d) G. Velmurugan, S. A. Vedha and P. Venuvanalingam, Computational evaluation of optoelectronic and photophysical properties of unsymmetrical distyrylbiphenyls, *RSC Adv.*, 2014, **4**, 53060-53071.
- (a) P. v. R. Schleyer, C. Maerker, A. Dransfeld, H. Jiao and N. J. R. V. E. Hommea, Nucleus-Independent Chemical Shifts: A Simple and Efficient Aromaticity Probe, *J. Am. Chem. Soc.*, 1996, **118**, 6317-6318. (b) K. K. Zborowski, I. Alkorta, J. Elguero and L. M. Proniewicz, Calculation of the HOMA model parameters for the carbon–boron bond, *Struct. Chem.*, 2012, **23**, 595-600.
 - A. Stanger, Nucleus-Independent Chemical Shifts (NICS): Distance Dependence and Revised Criteria for Aromaticity and Antiaromaticity, *J. Org. Chem.*, 2006, **71**, 883-893.
 - K. Wolinski, J. F. Hinton and P. Pulay, Efficient Implementation of the Gauge-Independent Atomic Orbital Method for NMR Chemical Shift Calculations, *J. Am. Chem. Soc.*, 1990, **112**, 8251-8260.
 - (a) S. Ostrowski and J. C. Dobrowolski, What does the HOMA index really measure?, *RSC Adv.*, 2014, **4**, 44158-44161; (b) T. Lu and F. Chen, Multiwfn: A multifunctional wavefunction analyzer, *J. Comput. Chem.*, 2012, **33**, 580-592.
 - (a) D. Geuenich, K. Hess, F. Köhler and R. Herges, Anisotropy of the Induced Current Density (ACID), a General Method To Quantify and Visualize Electronic Delocalization, *Chem. Rev.*, 2005, **105**, 3758-3772; (b) R. Herges and D. Geuenich, Delocalization of Electrons in Molecules, *J. Phys. Chem. A*, 2001, **105**, 3214-3220.

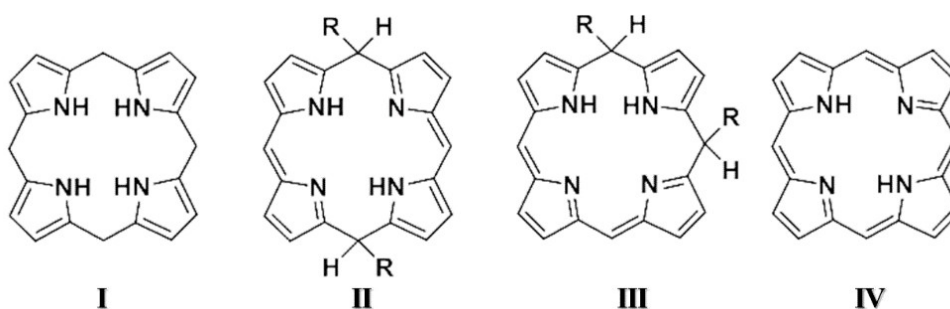
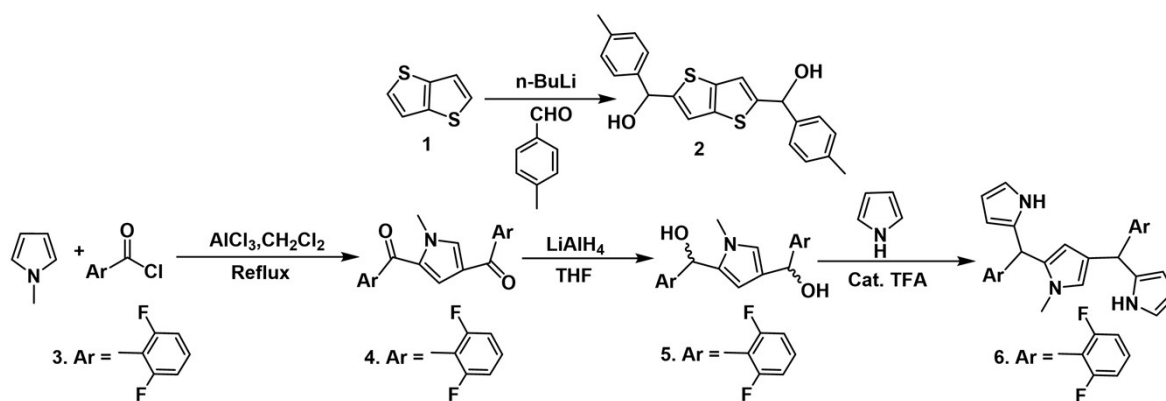
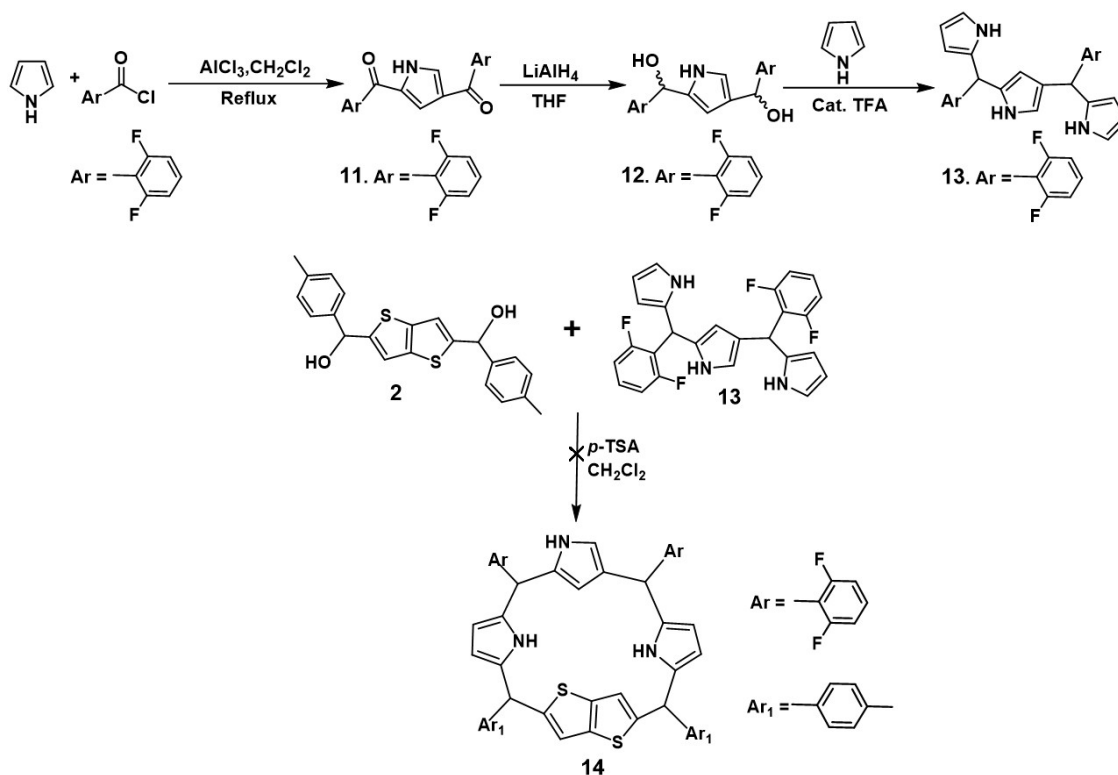


Chart S1 Structural relationship between porphyrinogen (I)-calixphyrin (II, III)-porphyrin(IV)

1.4 Synthesis:



Scheme S1. Synthesis of all precursors used for the macrocycles reported in the manuscript



Scheme S2. Attempted Synthesis of macrocycle **14**

General Synthesis of **7**:

Tripyrrane **6** (0.463 g, 1 mmol) and diol **2** (0.380 g, 1 mmol) were taken in a round bottom flask, to it 100 mL of dry DCM was added and stirred for 15 minutes under nitrogen atmosphere to get a clear solution. After that p -Toluenesulfonic acid (0.035 g, 0.185 mmol) was added to the reaction mixture and stirred for 120 minutes under dark condition. After complete removal of solvent from crude mixture by rotary evaporator, the compound was purified using basic alumina followed by repeated silica gel (200–400 mesh) chromatographic separation and preparative thin layer chromatography (PTLC) yielded 60% of extra pure macrocycle **7** as an orange solid.

Compound **7**: Yield. ~420 mg (60%). $R_f = 0.4$ ($\text{CH}_2\text{Cl}_2/\text{Hexane} = (1:4)$). $\text{Mp} > 350^\circ\text{C}$

HR-ESI-TOF MS (m/z): calc. for $[\text{M} + \text{H}]^+$ $[\text{C}_{49}\text{H}_{38}\text{F}_4\text{N}_3\text{S}_2]^+$ 808.2443, found 808.2444.

Elemental analysis Calc. for $\text{C}_{49}\text{H}_{37}\text{F}_4\text{N}_3\text{S}_2$: C, 72.84; H, 4.62; N, 5.20. Found: C, 72.91; H, 4.67; N, 5.18.

UV-vis-NIR (CH_2Cl_2 , λ [nm], (ϵ [$\text{M}^{-1}\text{cm}^{-1} \times 10^4$]), 298K): 461 (1.26).

[**7**] ^1H NMR (400 MHz, CDCl_3 , 298K) δ : 7.99 (s, 1H), 7.75 (s, 1H), 7.60 (d, $J = 8.0$ Hz, 2H), 7.29 (d, $J = 8.0$ Hz, 2H), 7.23 – 7.18 (m, 2H), 7.15 (d, $J = 8.0$ Hz, 2H), 7.07 (d, $J = 8.0$ Hz, 2H), 7.00 (s, 1H), 6.94 – 6.78 (m, 4H), 6.68 (s, 1H), 6.12 (s, 1H), 6.06 (d, $J = 4.0$ Hz, 1H), 6.04 (d, $J = 4.0$ Hz, 1H), 5.85 (s, 1H), 5.78 (d, $J = 4.0$ Hz, 1H), 5.74 (d, $J = 4.0$ Hz, 1H), 5.70 (s, 1H), 5.65 (s, 1H), 5.59 (s, 1H), 5.50 (s, 1H), 3.05 (s, 3H), 2.40 (s, 3H), 2.30 (s, 3H).

^{13}C NMR (101 MHz, CDCl_3 , 298K) δ : 151.02, 141.83, 139.33, 136.98, 136.44, 135.94, 135.81, 134.56, 132.54, 131.50, 129.83, 129.55, 129.44, 129.24, 128.90, 128.79, 128.52, 128.26, 127.69, 126.51, 126.40, 126.25, 125.83, 120.93, 119.79, 118.54, 117.52, 115.75, 112.81, 112.38, 112.35, 112.13, 112.11, 111.63, 111.60, 111.49, 111.37, 109.65, 109.31, 107.19, 46.85, 37.27, 34.42, 33.00, 29.86, 21.38, 21.10.

General Synthesis of **9**:

Porphyrinogen **7** (20 mg, 0.0248 mmol) was taken in a round bottom flask; to it 20 mL of dry DCM was added and stirred for 15 minutes to get a clear solution. Chloranil (15.2 mg, 0.062 mmol) was added to the reaction mixture and stirred for 60 minutes. After complete removal of solvent from crude mixture by rotary evaporator, the compound was purified using basic alumina followed by preparative thin layer chromatography (PTLC) leading to extra pure macrocycle **9** as an air-stable green solid in 80% yields.

Compound **9**: Yield. ~16.5 mg (80%). $R_f = 0.3$ ($\text{CH}_2\text{Cl}_2/\text{Hexane} = (3:2)$). $\text{Mp} > 350^\circ\text{C}$

HR-ESI-TOF MS (m/z): calc. for $[\text{M}]^+$ $[\text{C}_{49}\text{H}_{29}\text{F}_4\text{N}_3\text{OS}_2]^+$ 815.1688, found 815.1689. Elemental analysis
Calc. for $\text{C}_{49}\text{H}_{29}\text{F}_4\text{N}_3\text{OS}_2$: C, 72.13; H, 3.58; N, 5.15. Found: C, 72.16; H, 3.59; N, 5.12.

UV-vis-NIR (CH_2Cl_2 , λ [nm], (ϵ [$\text{M}^{-1}\text{cm}^{-1} \times 10^4$]), 298K): 329 (3.66), 455 (5.44), 678 (1.36).

[**9**]: ^1H NMR (400 MHz, CD_2Cl_2 , 298K) δ : 7.57 (d, $J = 8.0$ Hz, 2H), 7.52 (d, $J = 8.0$ Hz, 2H), 7.35 (d, $J = 8.0$ Hz, 2H), 7.28 (d, $J = 8.0$ Hz, 2H), 7.25 (s, 1H), 7.01 (d, $J = 4.0$ Hz, 1H), 6.94 (d, $J = 8.0$ Hz, 1H), 6.89 - 6.92 (m, 6H), 6.88 (d, $J = 4.0$ Hz, 1H), 6.67 (d, $J = 4.0$ Hz, 1H), 6.19 (d, $J = 8.0$ Hz, 1H), 3.53 (s, 3H), 2.47 (s, 3H), 2.39 (s, 3H). ^{13}C NMR (101 MHz, CD_2Cl_2 , 298K) δ : 145.53, 145.35, 140.23, 137.99, 137.25, 136.80, 133.81, 132.89, 132.32, 131.08, 130.97, 130.74, 130.07, 129.67, 129.55, 129.30, 128.66, 127.58, 126.45, 124.42, 120.63, 112.91, 112.04, 111.84, 111.53, 77.23, 37.73, 30.06, 23.06, 21.50, 21.31.

General Synthesis of **10**:

Porphyrinogen **7** (20 mg, 0.0248 mmol) was taken in a round bottom flask; to it 20 mL of dry DCM was added and stirred for 15 minutes to get a clear solution. DDQ (14 mg, 0.062 mmol) was added to the reaction mixture and stirred for 15 minutes. After complete removal of solvent from crude mixture by rotary evaporator, the compound was purified using basic alumina followed by preparative thin layer chromatography (PTLC) leading to extra pure macrocycle **10** as dark brown solid in 75% yields.

Compound **10**: Yield. ~15.3 mg (75%). $R_f = 0.2$ ($\text{CH}_2\text{Cl}_2/\text{Hexane} = (4:1)$). $\text{Mp} > 350^\circ\text{C}$

HR-ESI-TOF MS (m/z): calc. for $[\text{M}]^+$ $[\text{C}_{49}\text{H}_{29}\text{F}_4\text{N}_3\text{O}_2\text{S}_2]^+$ 831.1637, found. 831.1639. Elemental analysis
Calc. for $\text{C}_{49}\text{H}_{29}\text{F}_4\text{N}_3\text{O}_2\text{S}_2$: C, 70.75; H, 3.51; N, 5.05. Found: C, 70.78; H, 3.59; N, 5.01.

UV-vis-NIR (CH_2Cl_2 , λ [nm], (ϵ [$\text{M}^{-1}\text{cm}^{-1} \times 10^4$]), 298K): 329 (1.96), 426 (3.13), 647(0.09).

[**10**]: ^1H NMR (400 MHz, CD_2Cl_2 , 298K) δ : 7.55 (d, $J = 8.0$ Hz, 2H), 7.39 – 7.34 (m, 2H), 7.28 (d, $J = 8.0$ Hz, 2H), 7.23 – 7.17 (m, 4H), 7.00 (s, 1H), 6.98 – 6.89 (m, 4H), 6.75 (t, $J = 8.0$ Hz, 2H), 6.60 (s, 1H), 6.12 (d, $J = 4.0$ Hz, 1H), 6.10 (d, $J = 4.0$ Hz, 1H), 3.85 (s, 3H), 2.44 (s, 3H), 2.43 (s, 3H). ^{13}C NMR (101 MHz, CD_2Cl_2 , 298K) δ : 177.05, 171.75, 161.87, 160.22, 160.10, 160.05, 158.44, 158.39, 144.35, 142.22, 138.80, 138.03, 137.94, 136.72, 135.06, 134.99, 134.40, 131.55, 131.35, 131.04, 130.90, 130.48,

129.81, 129.09, 128.96, 128.66, 128.37, 126.73, 126.05, 123.29, 123.02, 122.59, 121.91, 121.27, 117.48, 116.87, 113.94, 111.76, 111.43, 111.29, 106.37, 37.54, 30.62, 21.01, 20.96.

2. Supplementary Data:

2.1 Mass Spectra

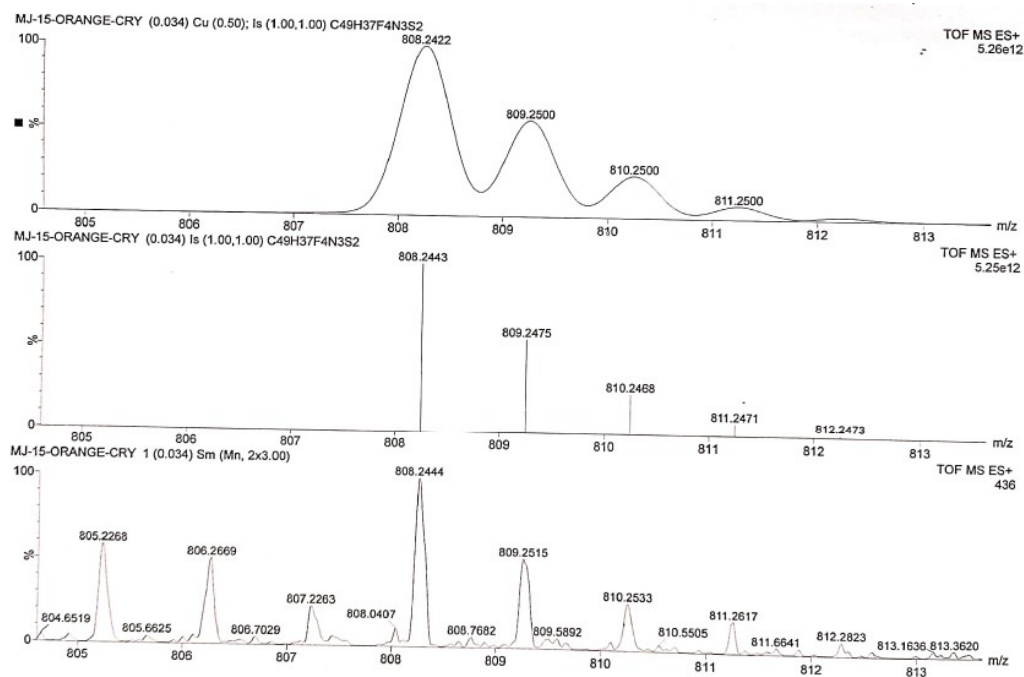


Fig. S1 HRMS Spectra of 7

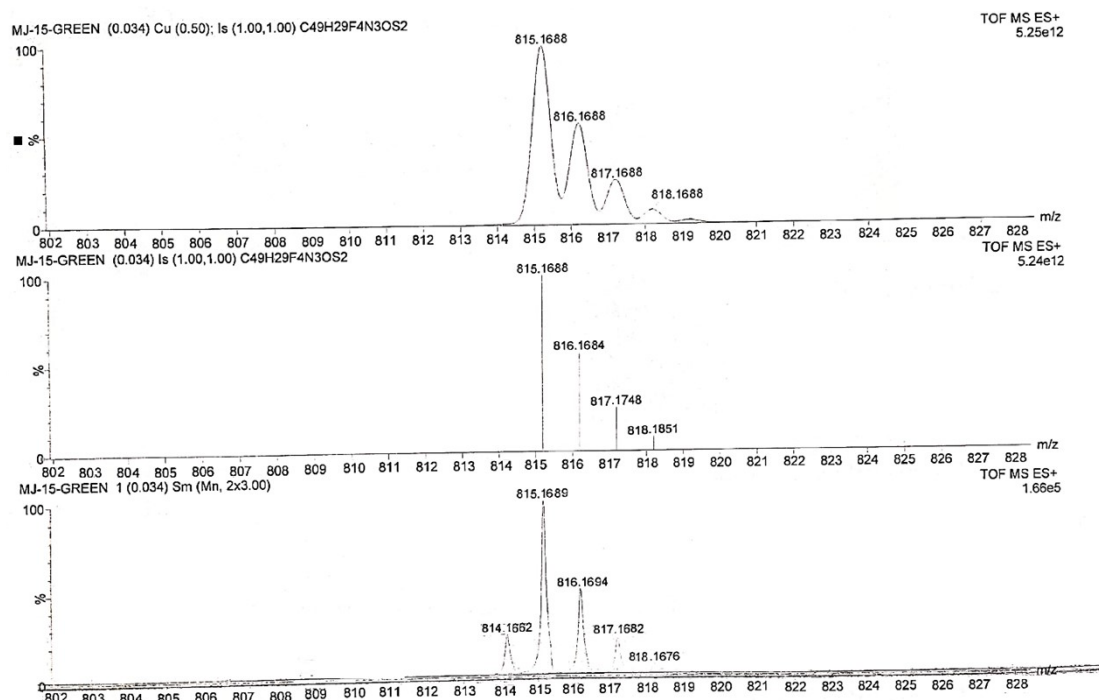


Fig. S2 HRMS Spectra of 9

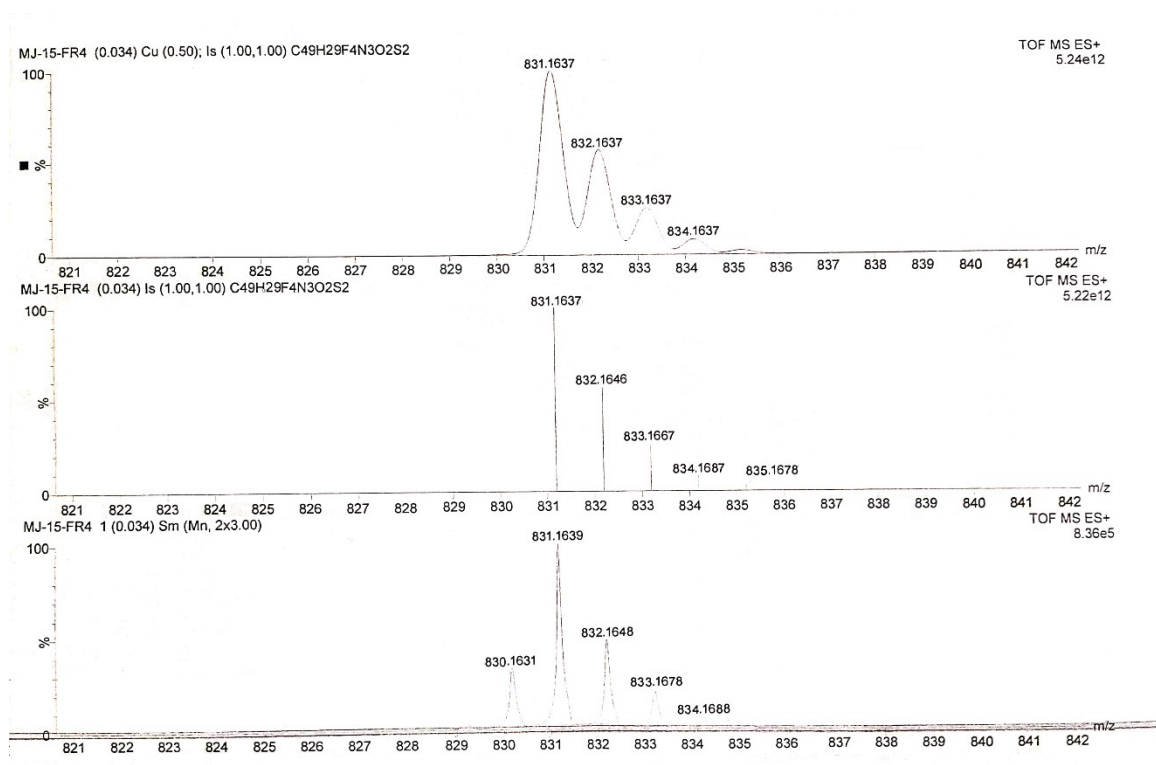


Fig.S3 HRMS Spectra of 10

2.2 IR spectra:

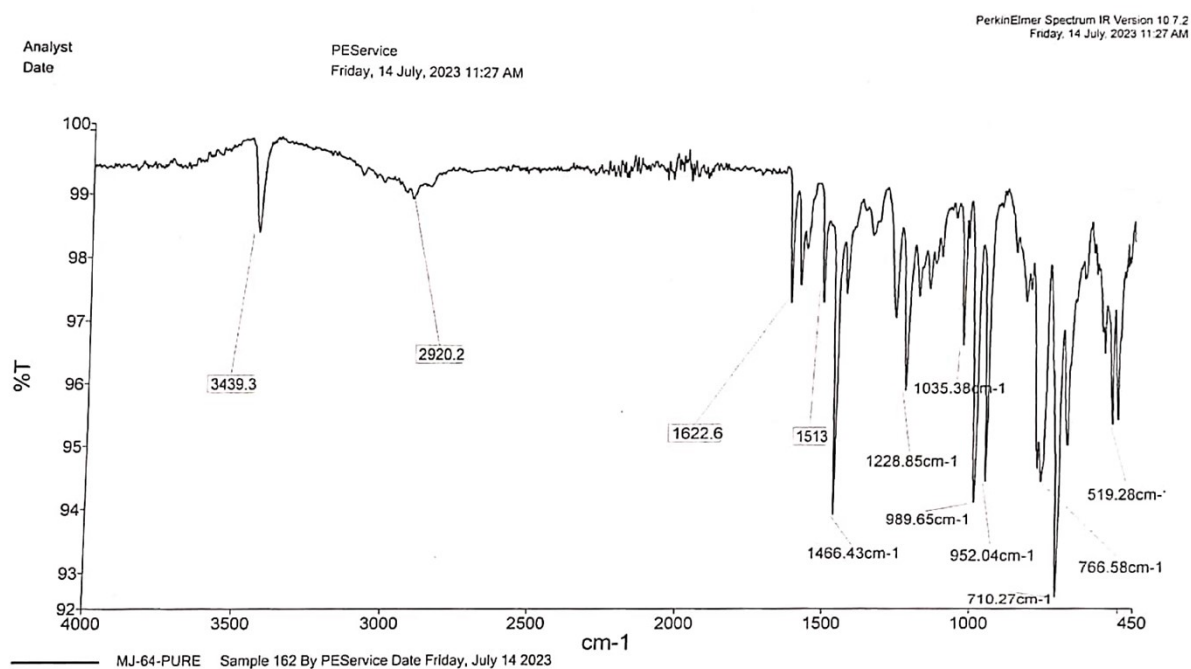


Fig. S4 IR Spectrum of 7

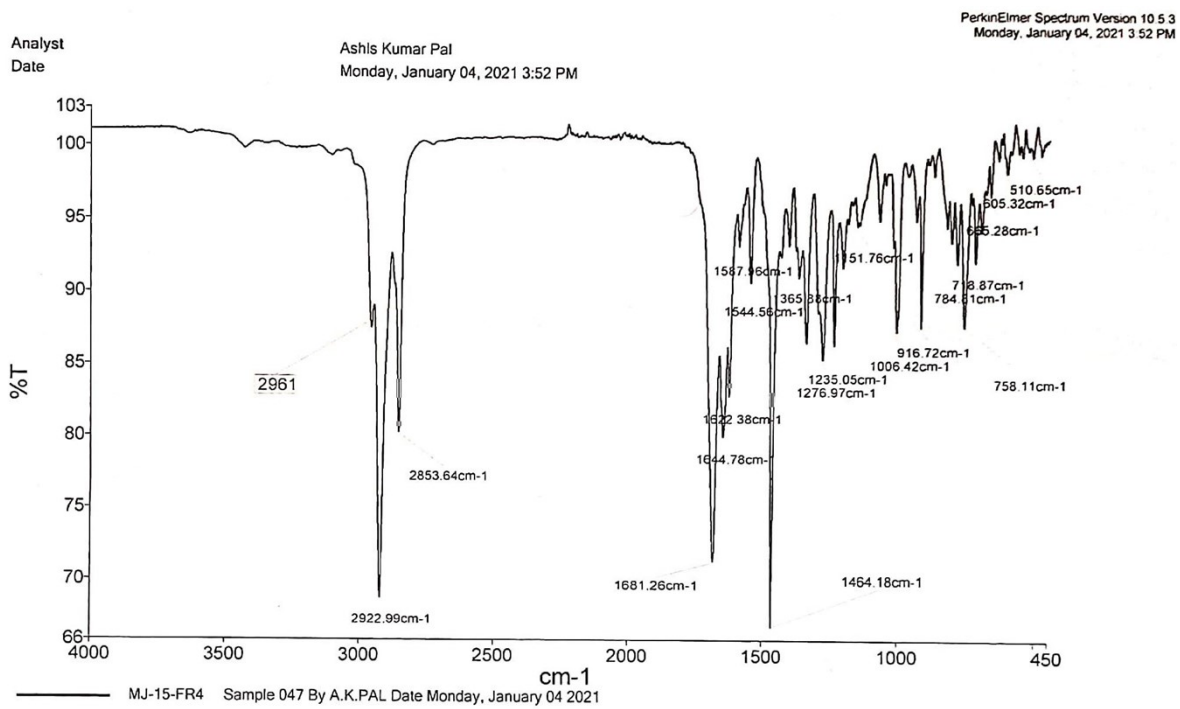


Fig. S5 IR Spectrum of 9

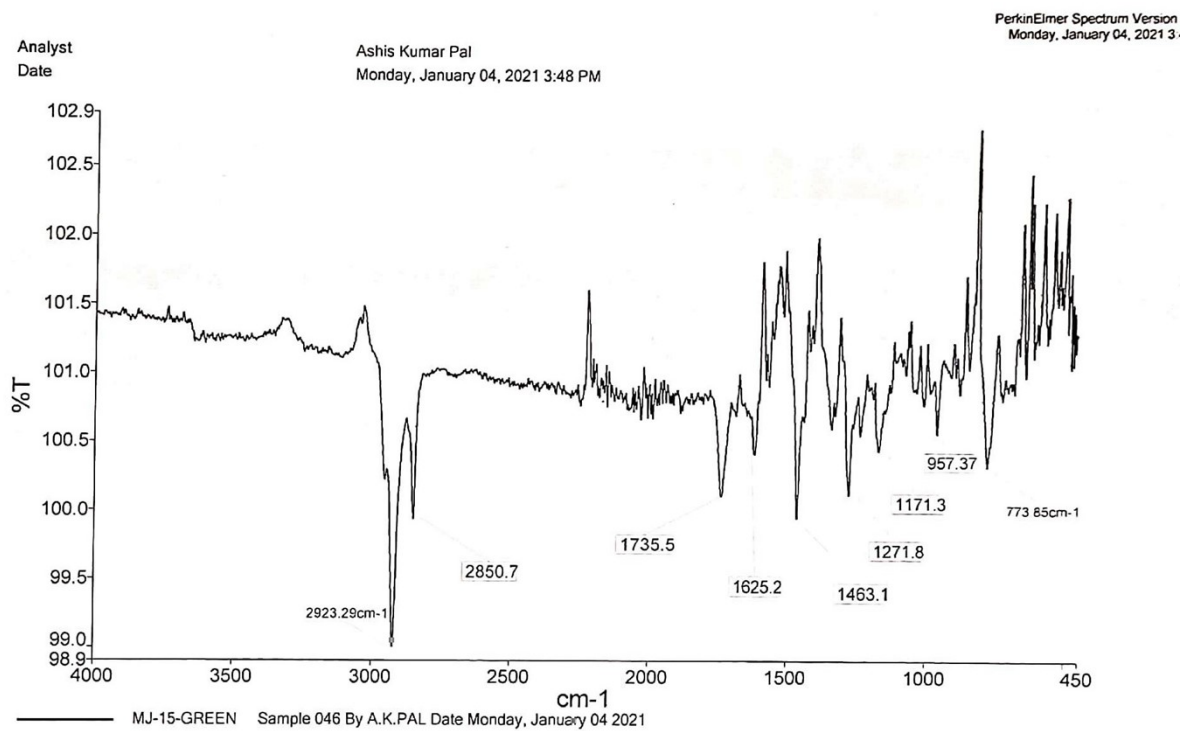


Fig. S6 IR Spectrum of 10

2.3 UV-vis spectra:

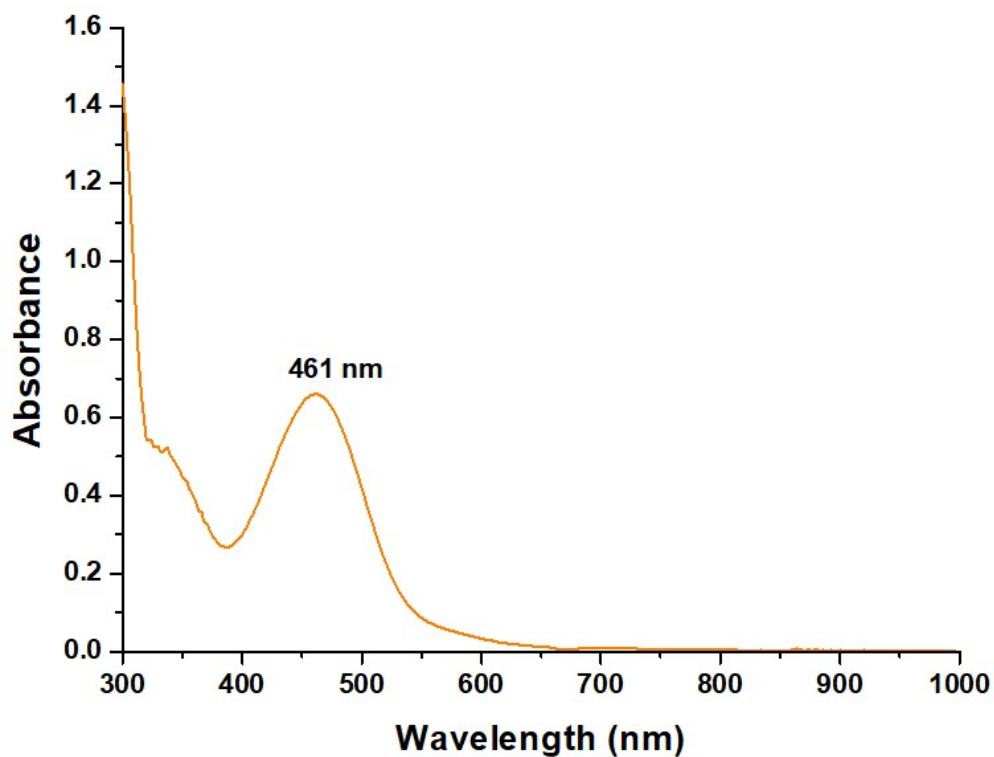


Fig. S7 UV-vis Spectrum of **7** in CH_2Cl_2 at 298 K

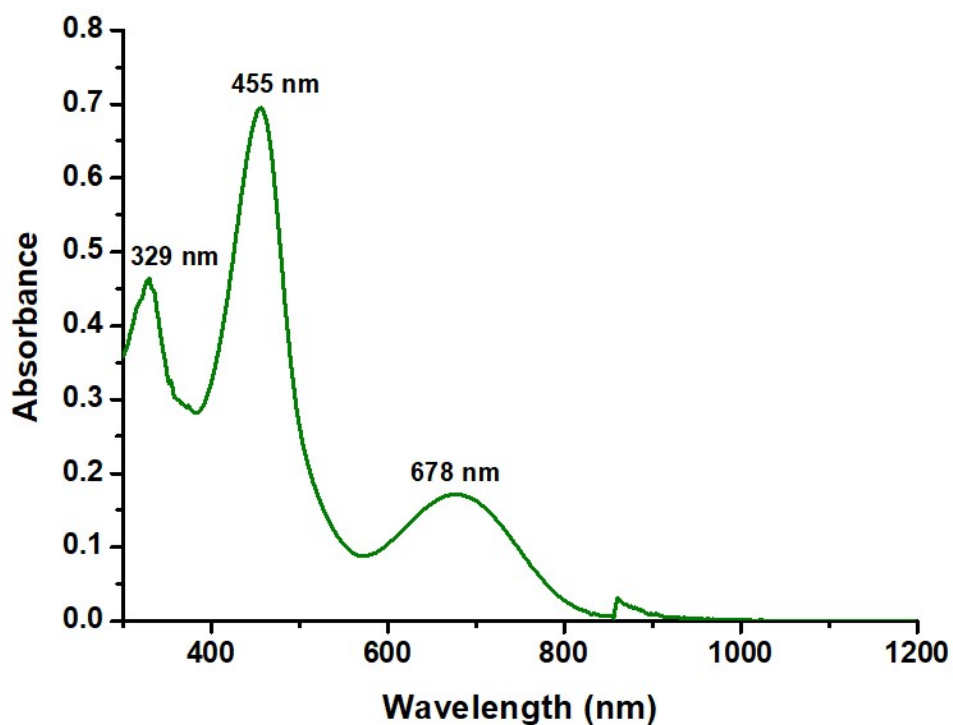


Fig. S8 UV-vis Spectra of **9** in CH_2Cl_2 at 298 K

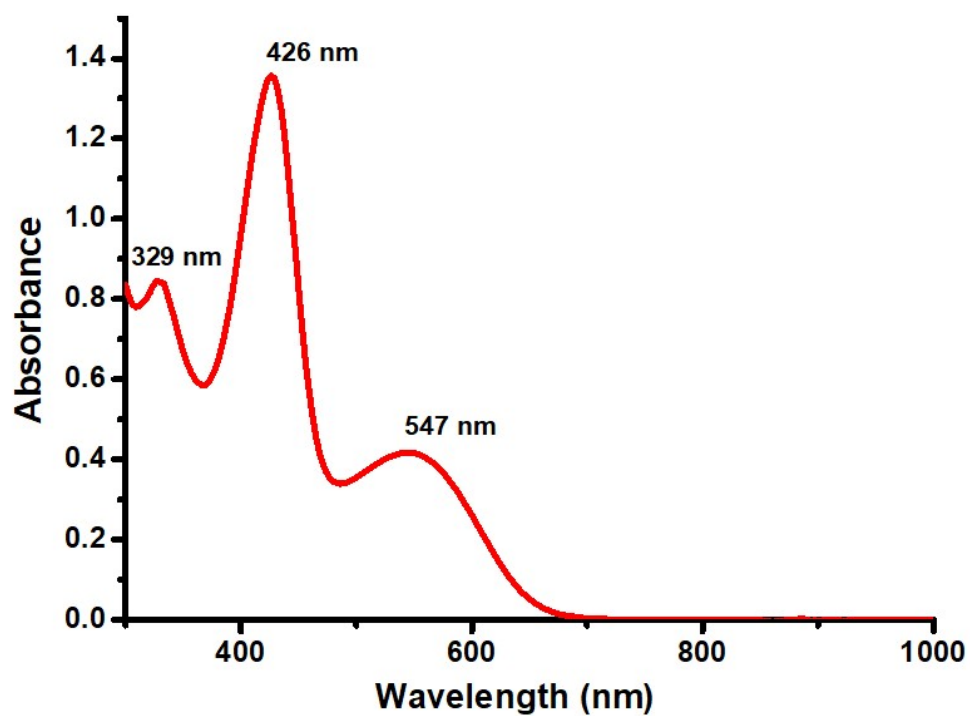


Fig. S9 UV-vis Spectra of **10** in CH₂Cl₂ at 298 K

2.4 NMR spectra:

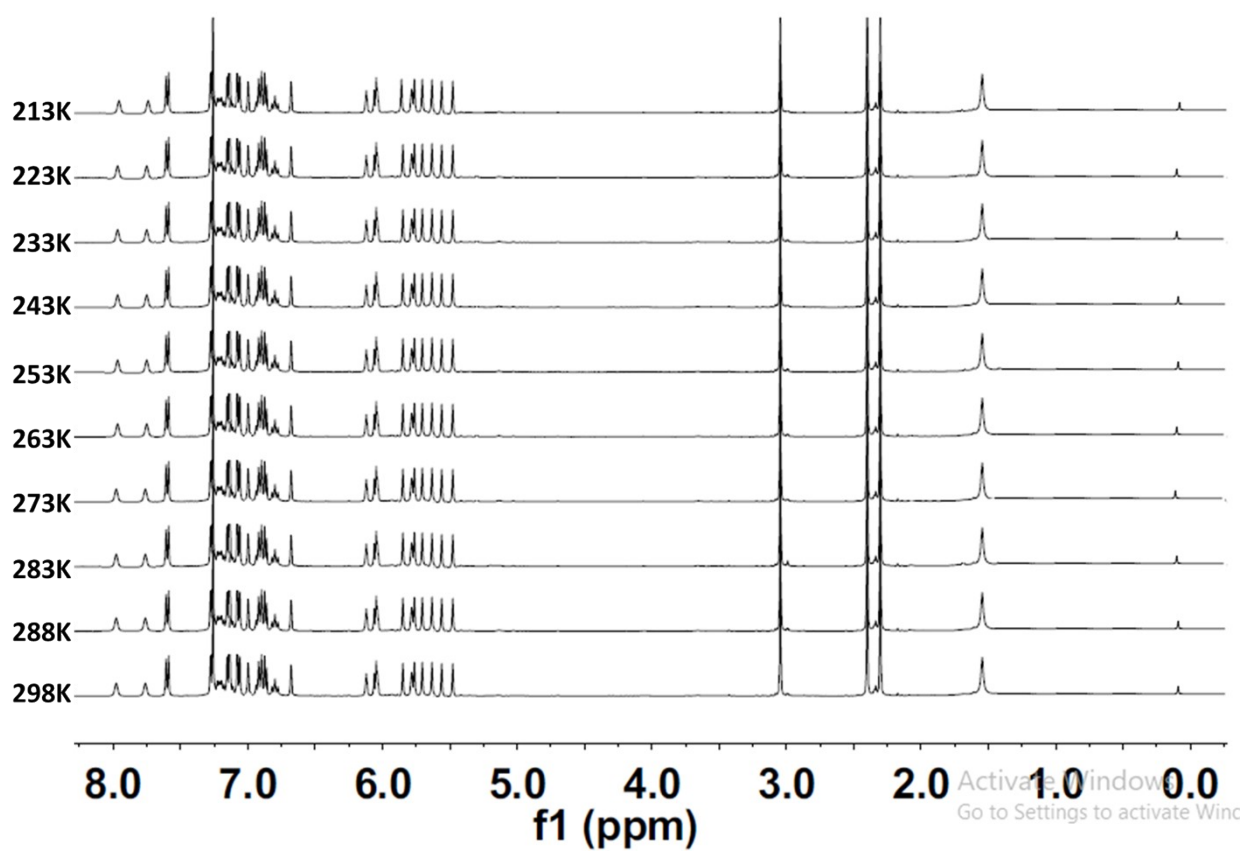


Fig. S10 Low VT ¹H NMR spectra of **7** in CDCl₃

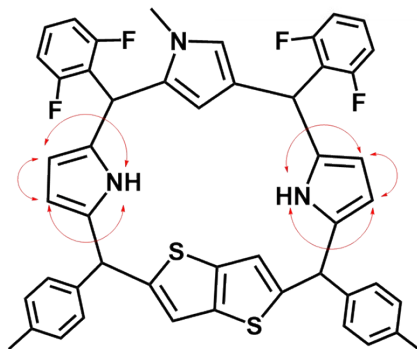
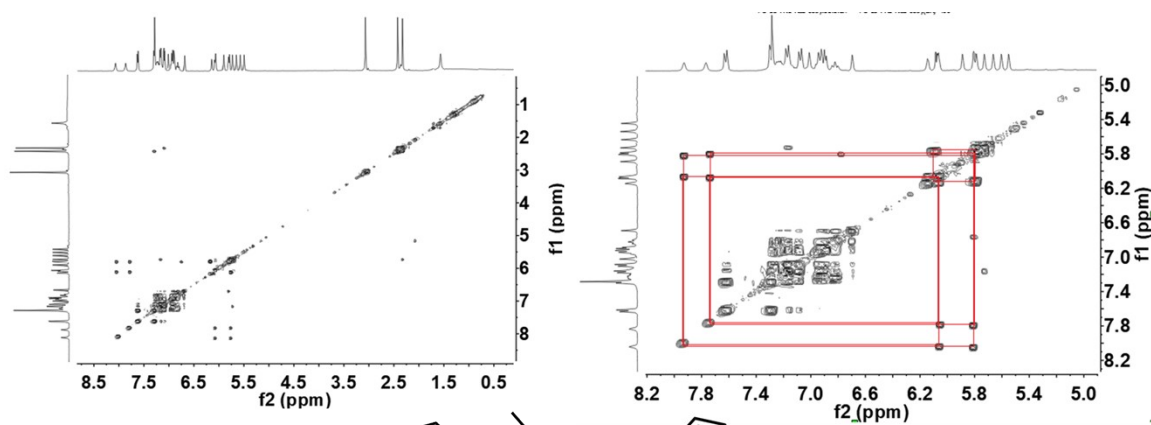


Fig. S11 ^1H - ^1H 2D COSY NMR spectra of **7** in CDCl_3 at 298 K

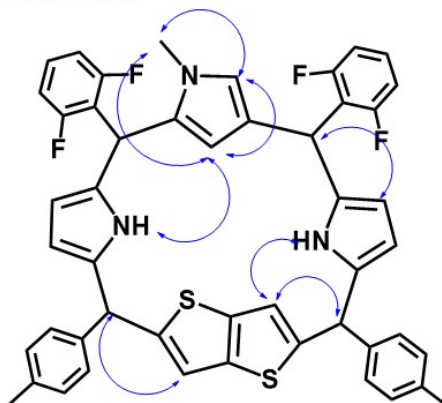
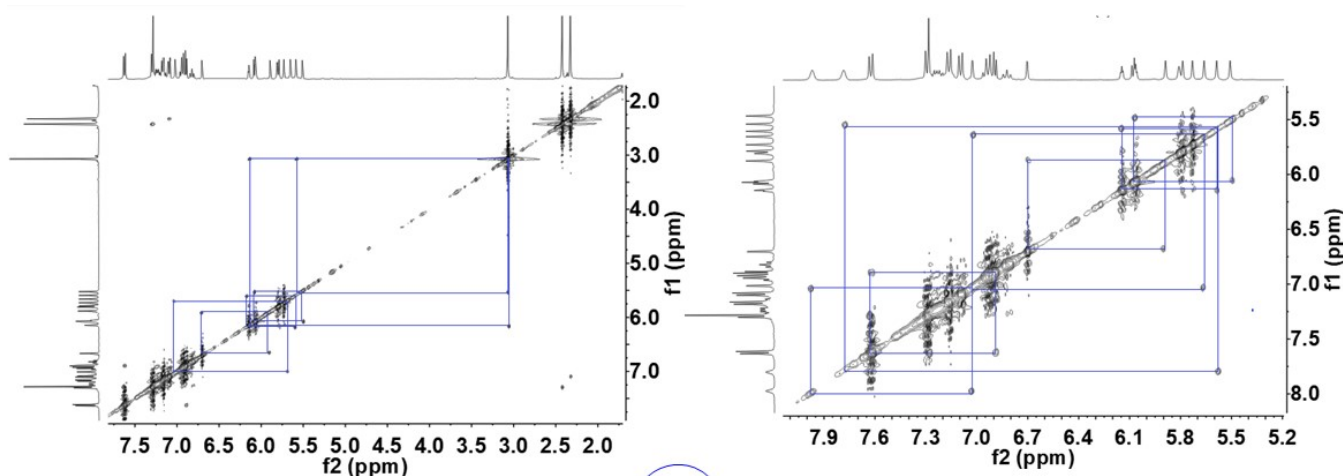


Fig. S12 ^1H - ^1H 2D ROESY NMR spectra of **7** in CDCl_3 at 298 K

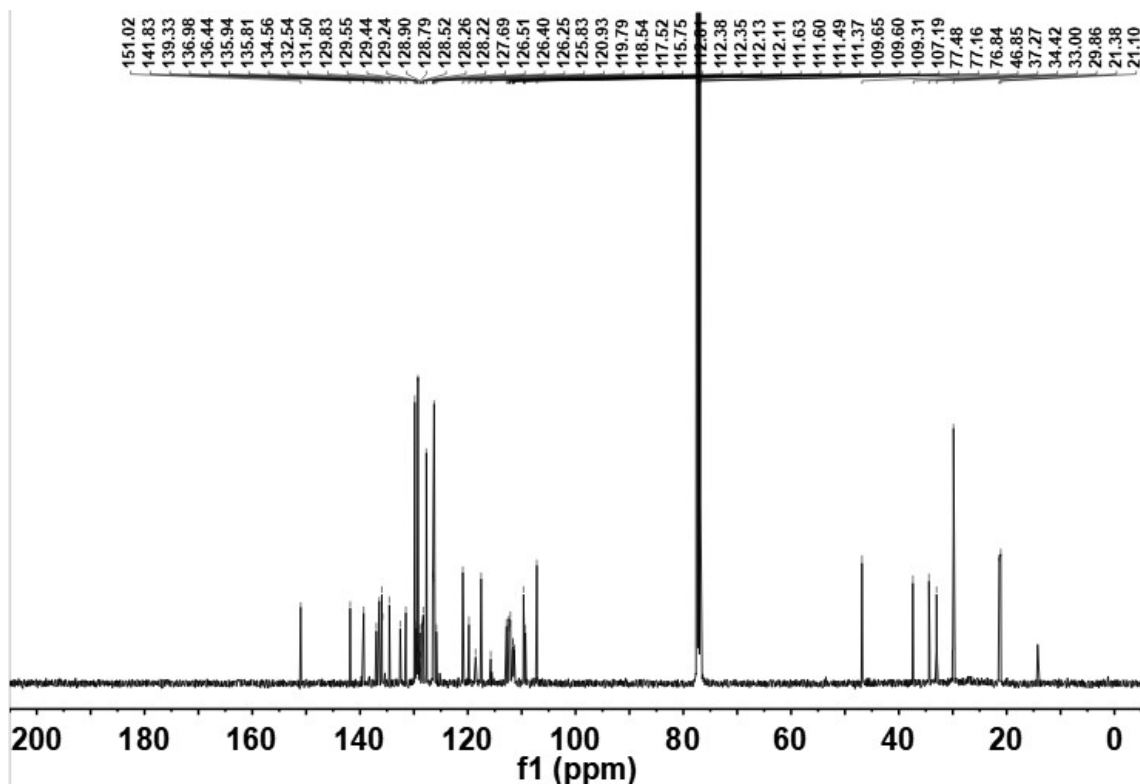
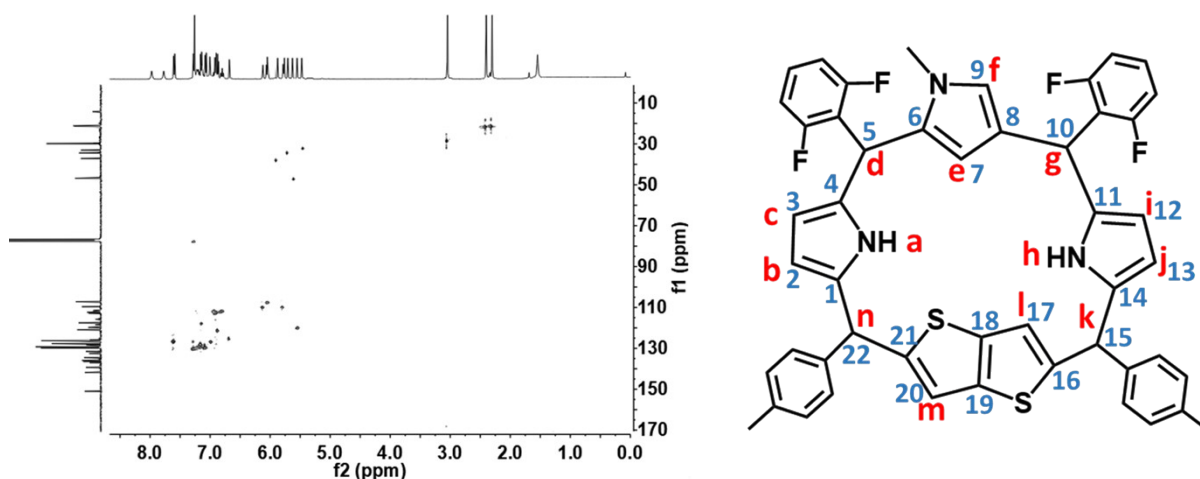


Fig. S13 ^{13}C NMR spectra of **7** in CDCl_3 at 298 K



^1H (ppm)	^{13}C (ppm)	^1H (ppm)	^{13}C (ppm)
7.99 (h)	-	5.78, 5.74 (j, b)	109.65
7.75 (a)	-	5.70 (d)	33.00
7.00 (l)	128.20	5.65 (k)	46.85
6.68 (m)	126.51	5.59 (e)	120.93
6.12 (f)	109.31	5.50 (g)	34.42
6.06, 6.04 (i, c)	107.19	3.05 (N-Me)	29.86
5.85 (n)	37.27	2.40, 2.30 (Tol-Me)	21.38, 21.10

Fig. S14 ^1H - ^{13}C 2D HSQC NMR spectra of **7** in CDCl_3 at 298 K

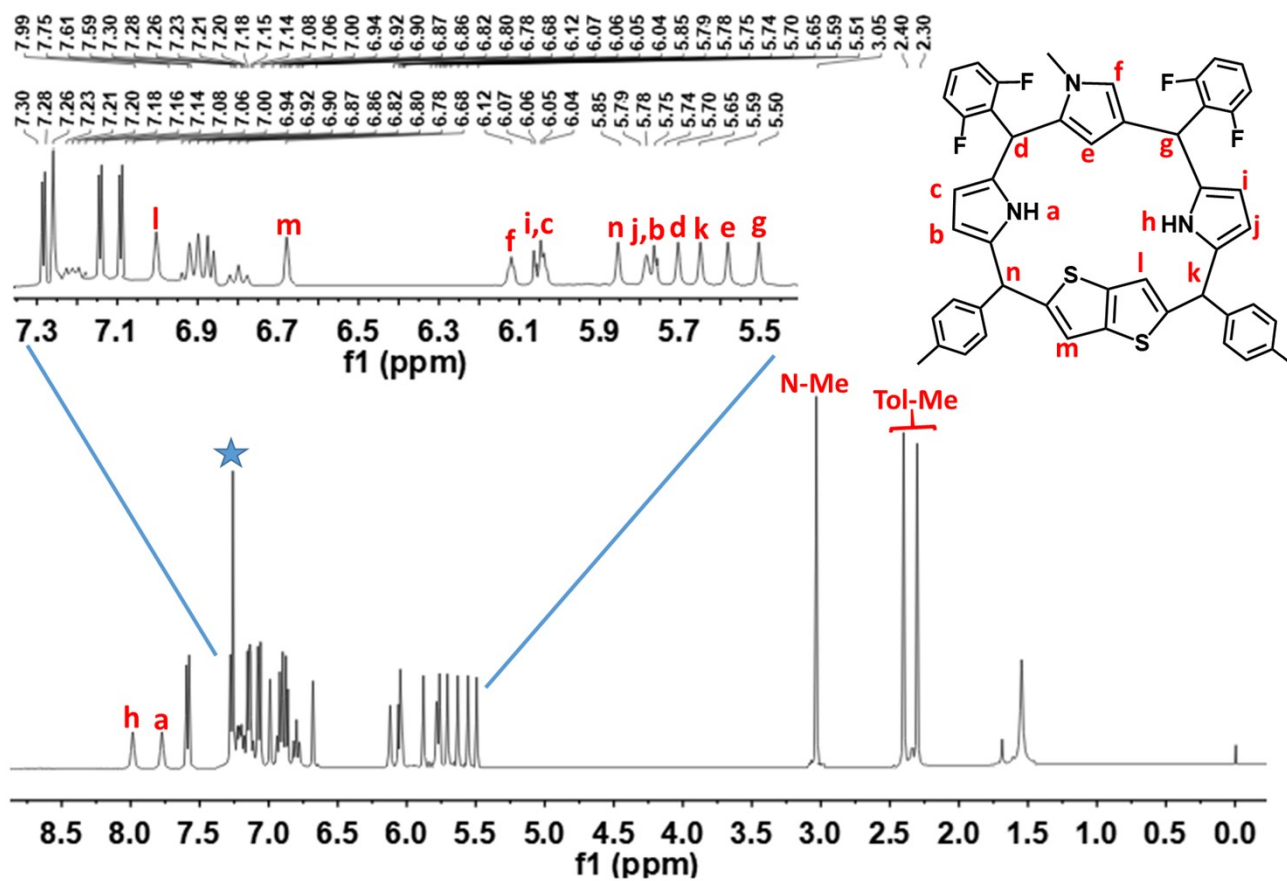


Fig.S15 Complete ^1H NMR spectral assignment of **7** in CDCl_3 at 298 K

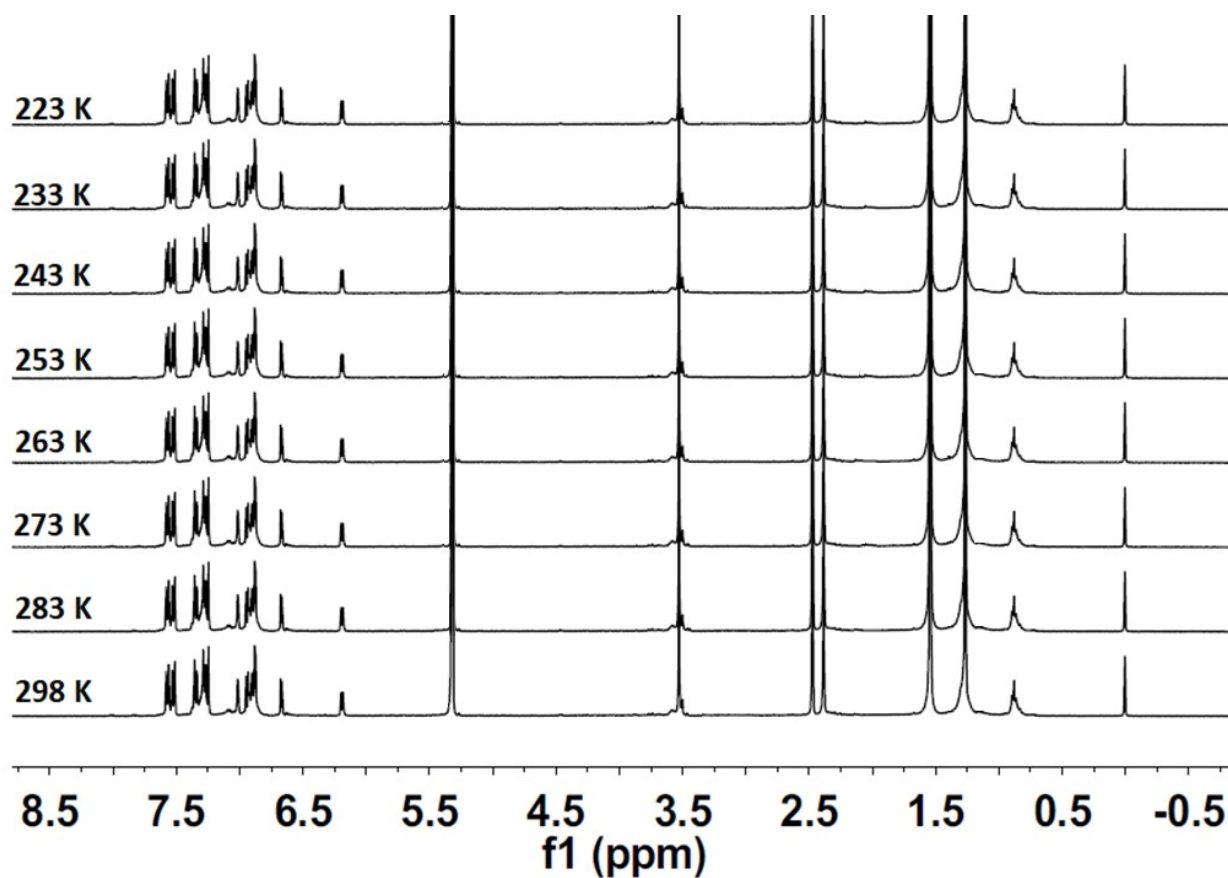


Fig. S16 Low VT ^1H NMR spectra of **9** in CD_2Cl_2

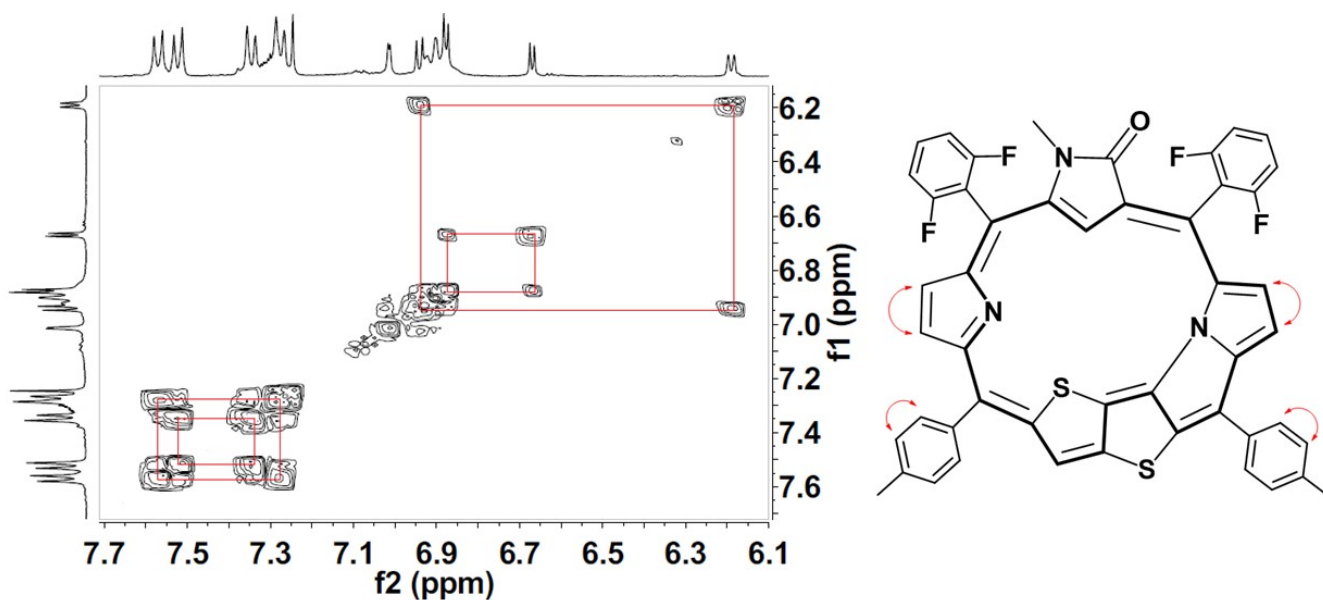


Fig. S17 ^1H - ^1H 2D COSY NMR spectra of **9** in CD_2Cl_2 at 298 K

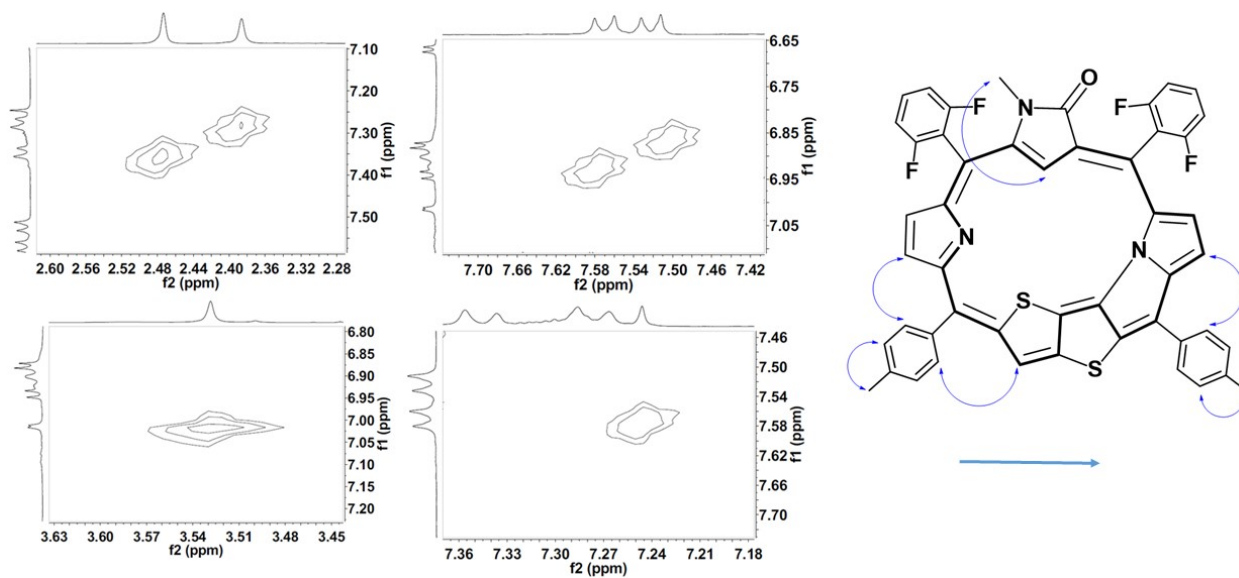


Fig. S18 ^1H - ^1H 2D ROESY NMR spectra of **9** in CD_2Cl_2 at 298 K

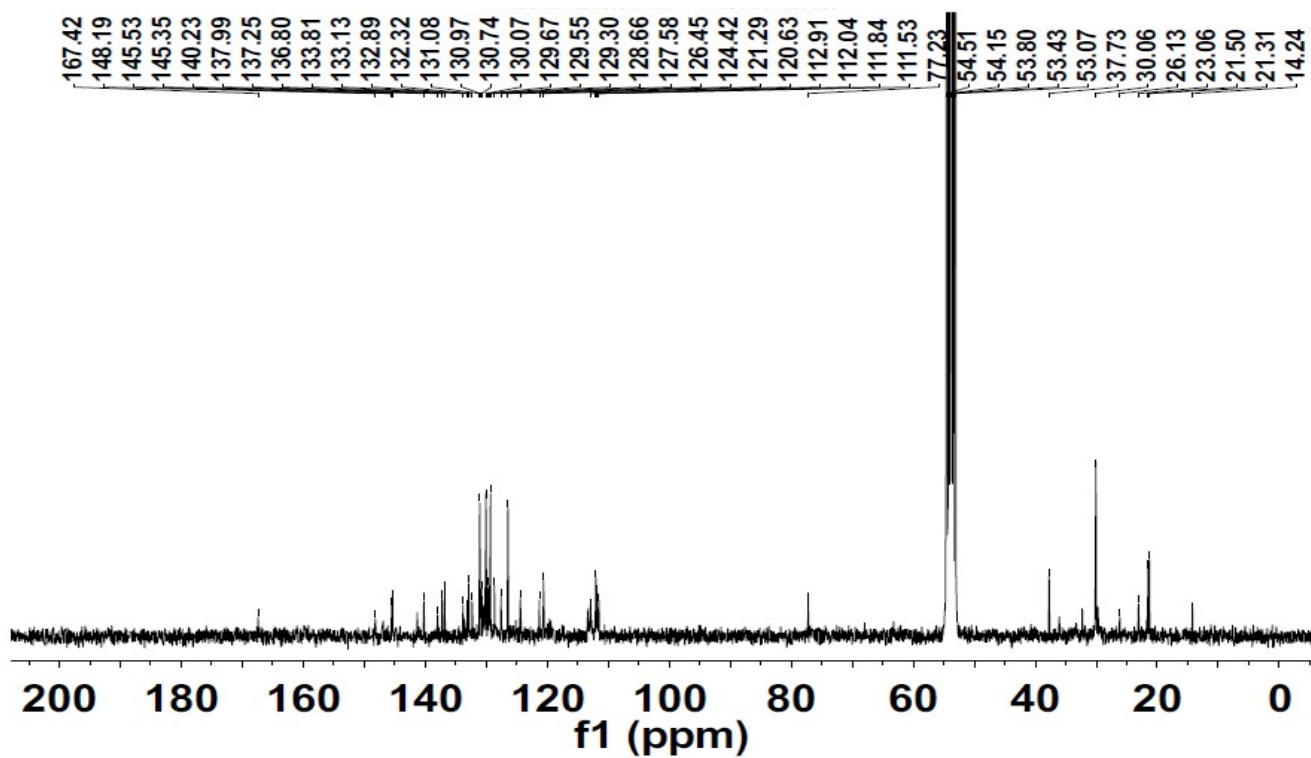


Fig. S19 ^{13}C NMR spectra of **9** in CD_2Cl_2 at 298 K

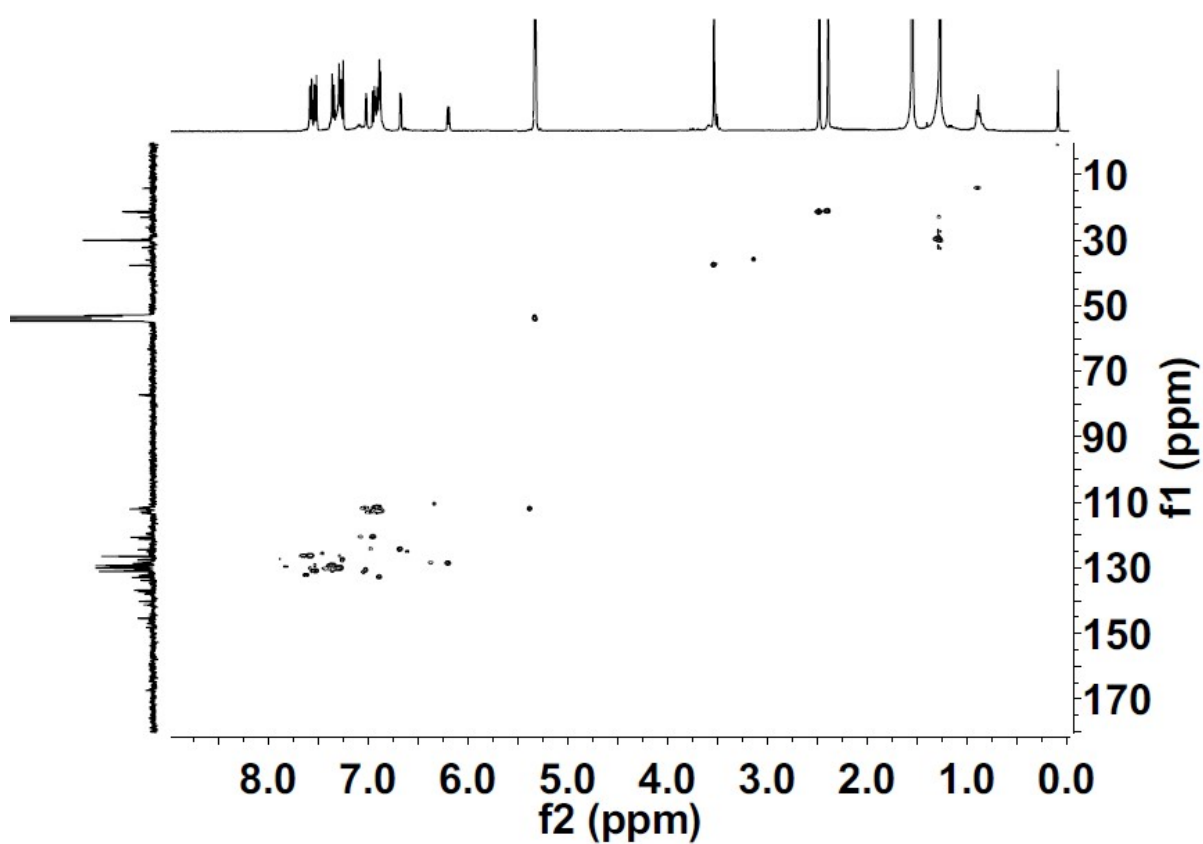


Fig. S20 HSQC NMR spectra of **9** in CD_2Cl_2 at 298 K

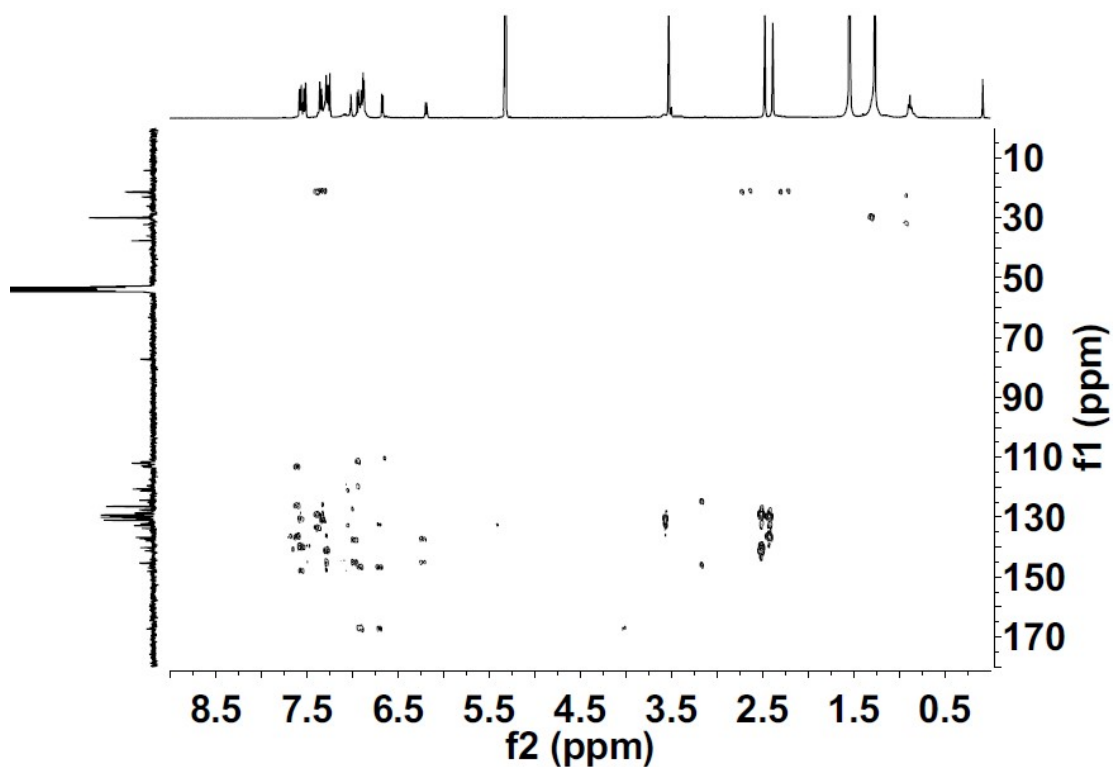


Fig. S21 HMBC NMR spectra of **9** in CD₂Cl₂ at 298 K

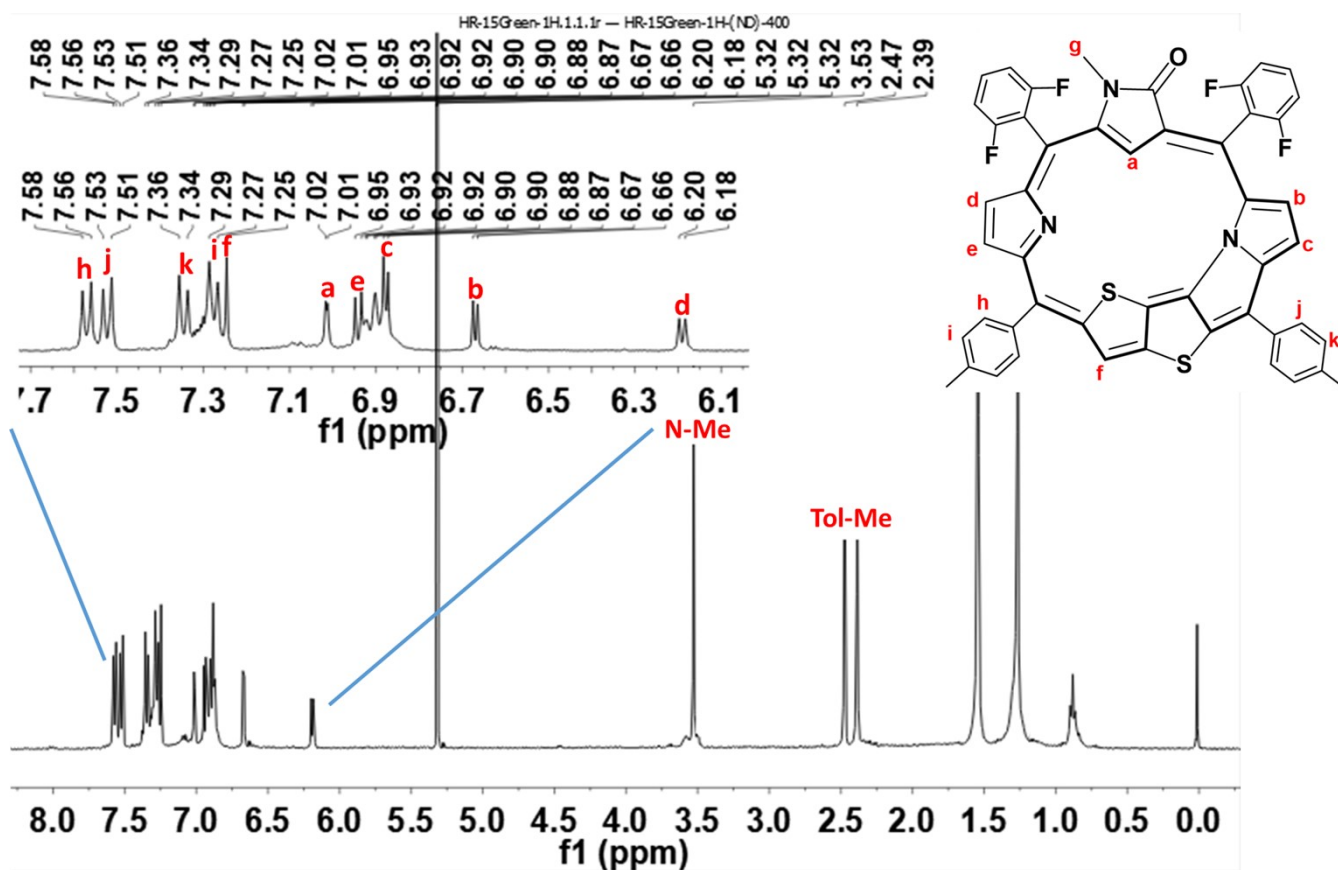


Fig. S22 Complete ¹H NMR spectral assignment of **9** in CD₂Cl₂ at 298 K

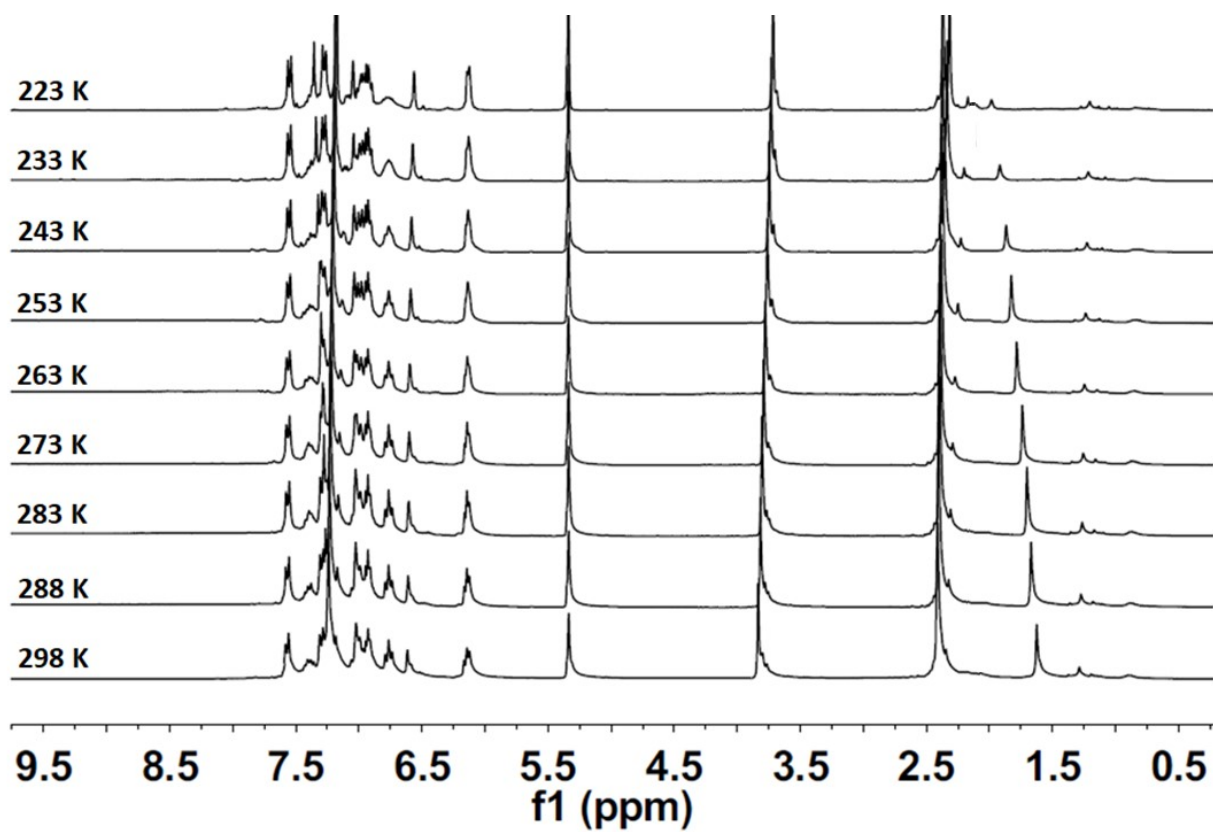


Fig. S23 Low VT ^1H NMR spectra of **10** in CD_2Cl_2

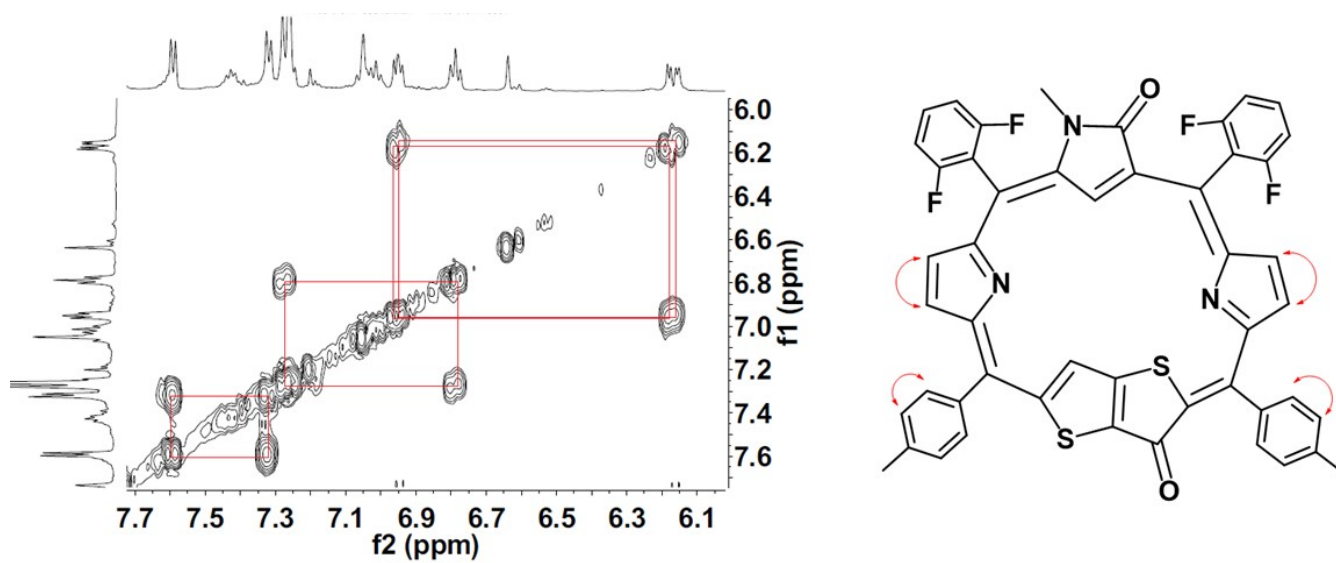


Fig. S24 ^1H - ^1H 2D COSY NMR spectra of **10** in CD_2Cl_2 at 298 K

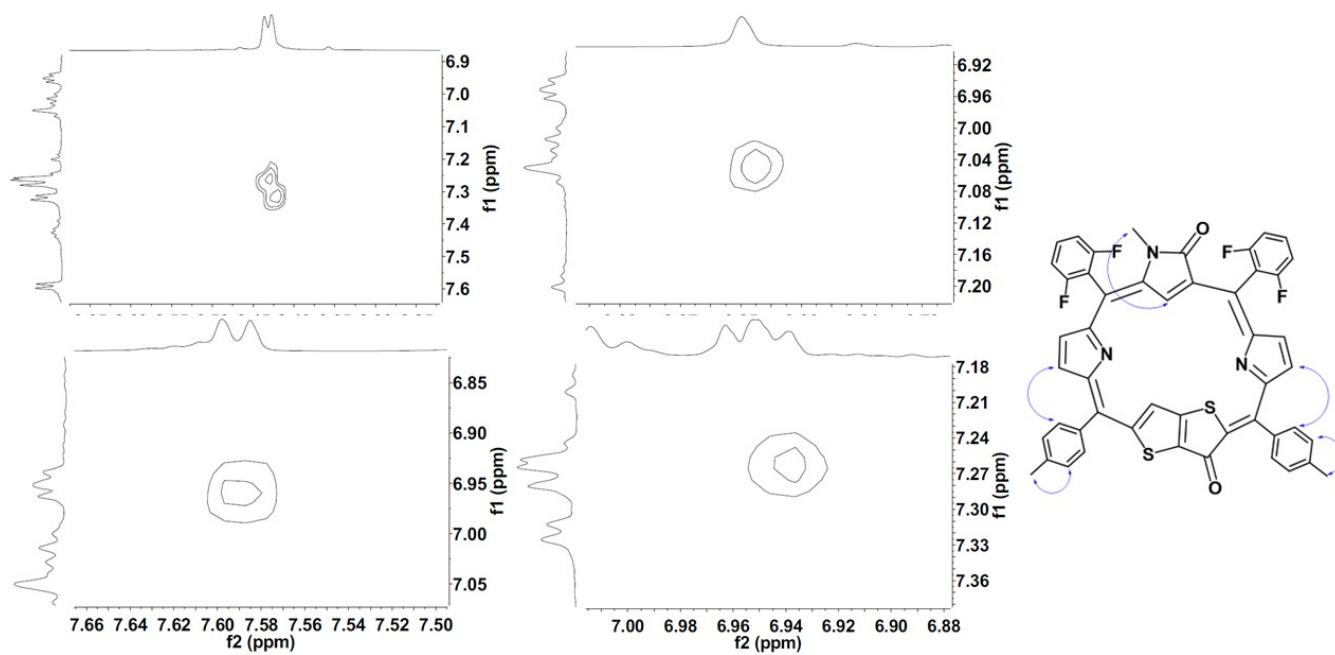


Fig. S25 ^1H - ^1H 2D ROESY NMR spectra of **10** in CD_2Cl_2 at 298 K

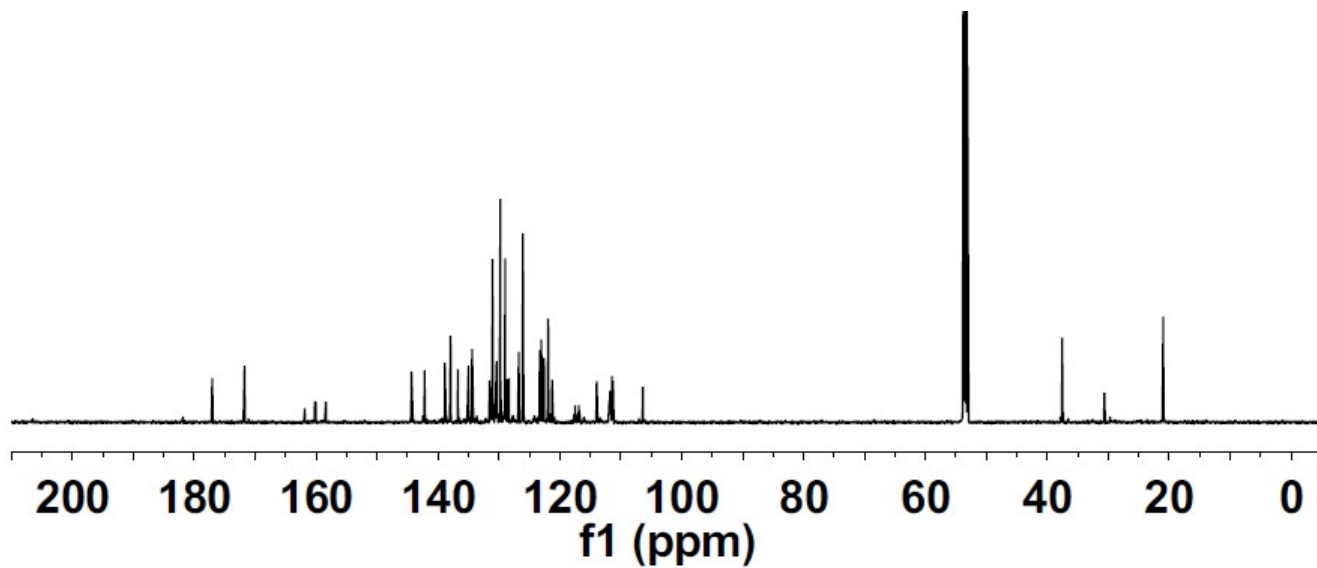


Fig. S26 ^{13}C NMR spectra of **10** in CD_2Cl_2 at 298 K

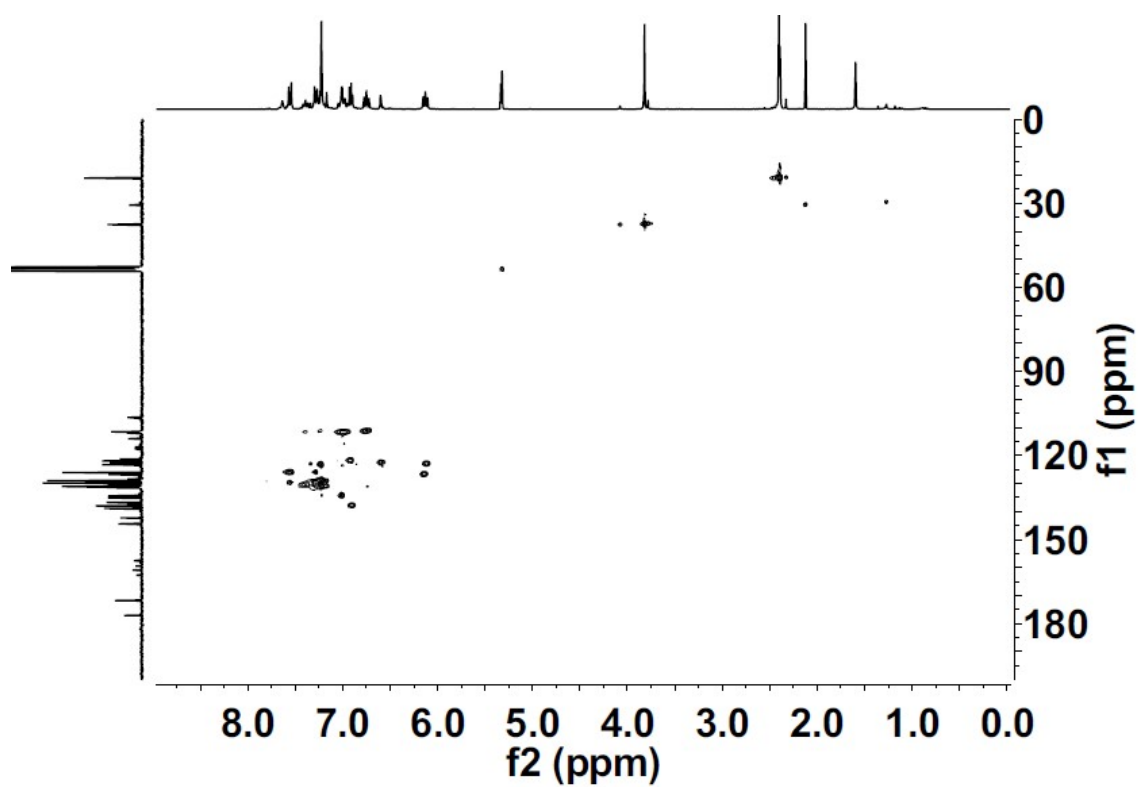


Fig. S27 HSQC NMR spectra of **10** in CD_2Cl_2 at 298 K

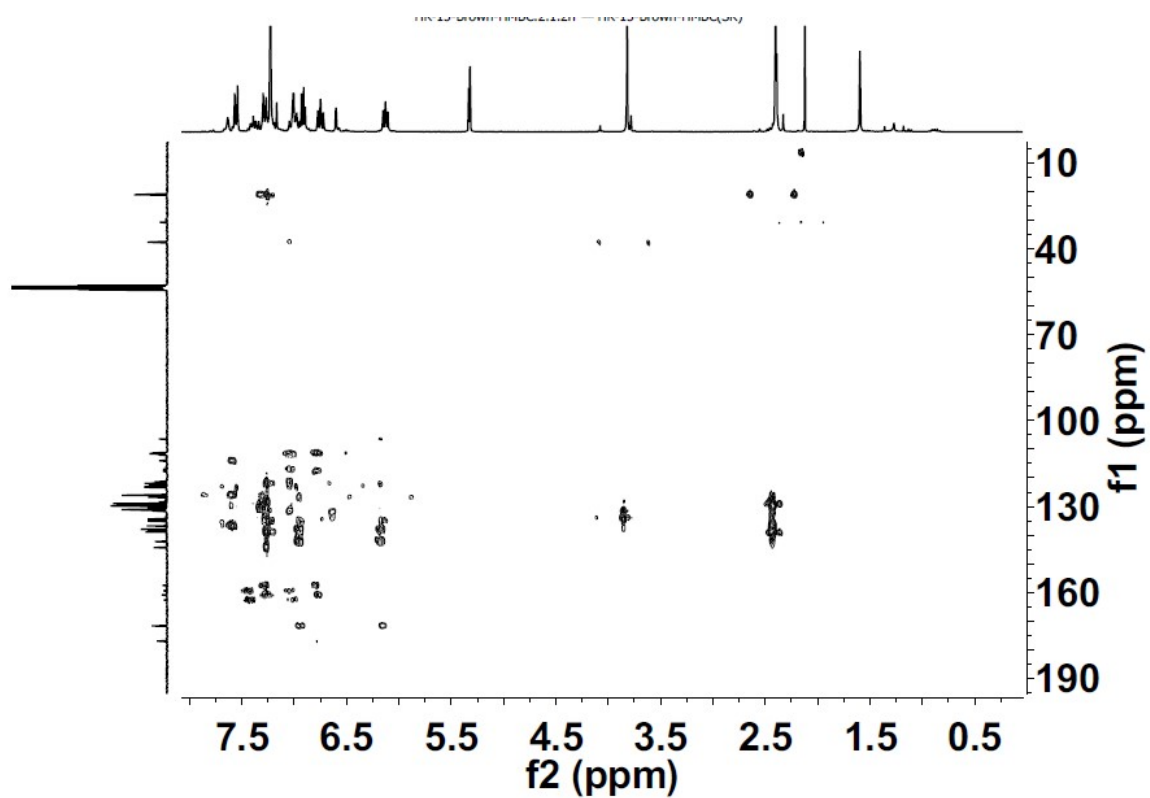


Fig. S28 HMBC NMR spectra of **10** in CD_2Cl_2 at 298 K

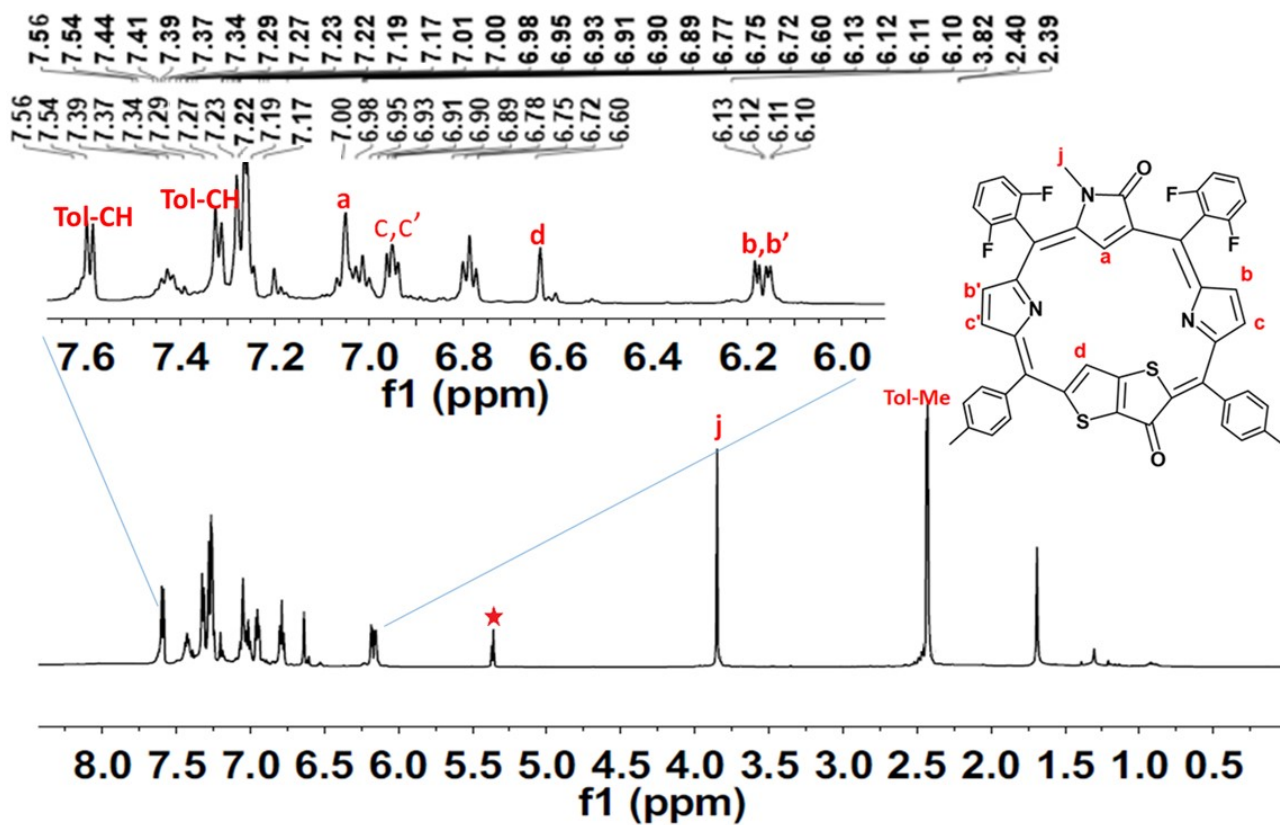


Fig. S29 Complete ^1H NMR spectral assignment of **10** in CD_2Cl_2 at 298 K

4. Electrochemistry

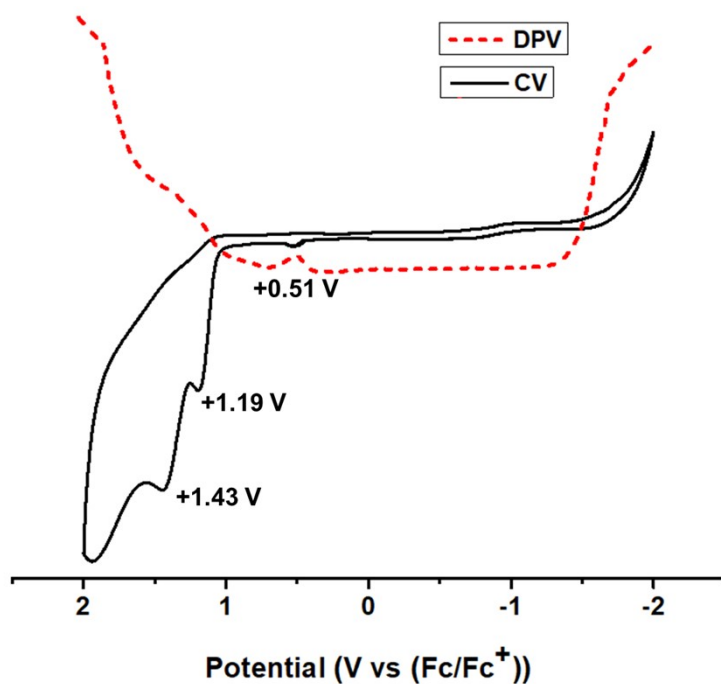


Fig. S30 Cyclic voltammogram of **7** ($\sim 10^{-4}$ M) in dichloromethane containing tetrabutylammonium hexafluorophosphate (0.01M) recorded at 100 mVs^{-1} .

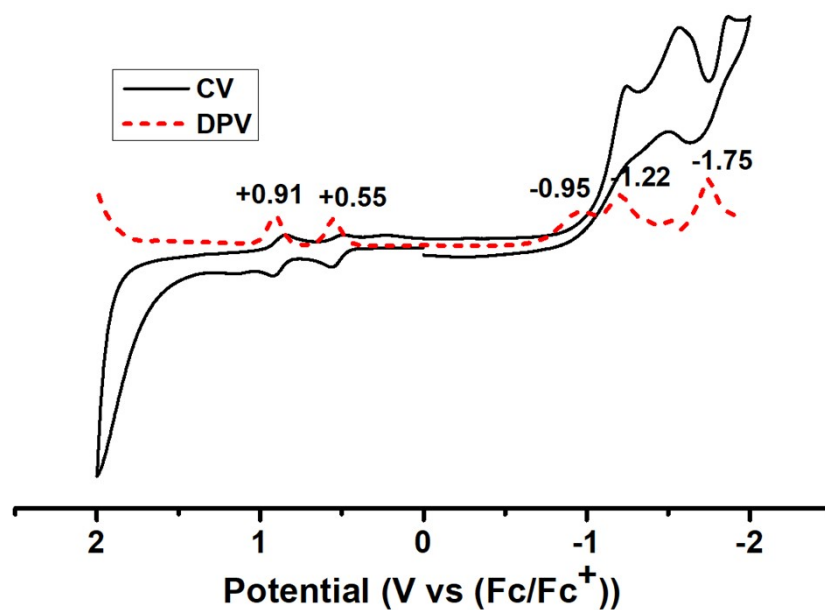


Fig. S31 Cyclic voltammogram of **9** ($\sim 10^{-4}$ M) in dichloromethane containing tetrabutylammonium hexafluorophosphate (0.01M) recorded at 100 mVs^{-1} .

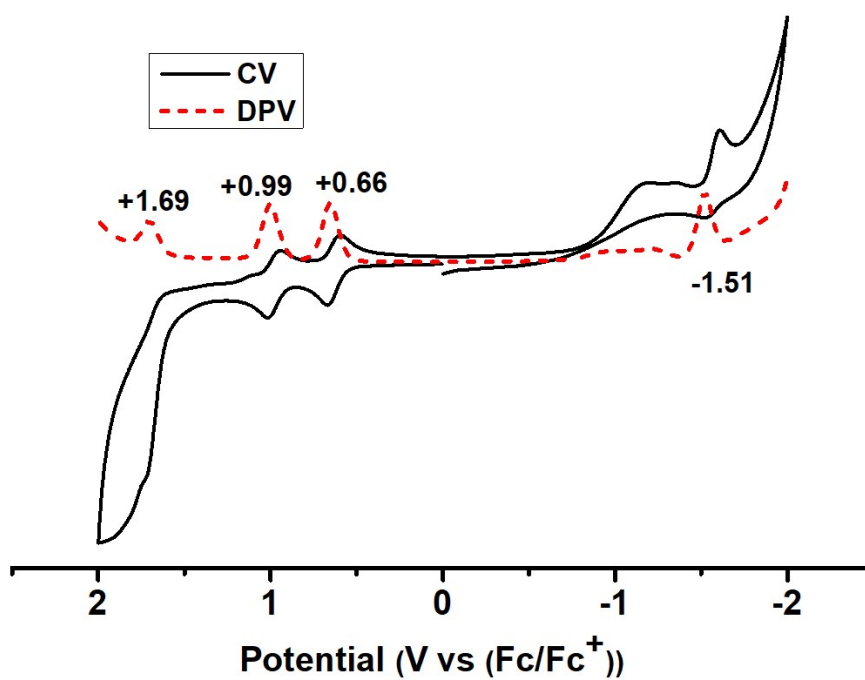


Fig. S32 Cyclic voltammogram of **10** ($\sim 10^{-4}$ M) in dichloromethane containing tetrabutylammonium hexafluorophosphate (0.01M) recorded at 100 mVs^{-1} .

4.0 Crystallographic Data

Table S1. Crystallographic data

Parameters	7
Chemical formula	C ₄₉ H ₃₇ F ₄ N ₃ S ₂
Formula weight	807.2365
Temperature (K)	146
Crystal system	Monoclinic
Space group	P 21/c
a (Å); α (°)	24.971(3); 90.00
b (Å); β (°)	14.4865(19); 100.316(4)
c (Å); γ (°)	12.363(15); 90.00
V (Å ³); Z	4399.9(9); 4
ρ (calc.) g m ⁻³	1.348
μ(Mo Kα) mm ⁻¹	0.299
2θ _{max} (°)	27.570
R(int)	0.0723
Completeness to θ	0.987
Data / param.	10045/6830
GOF	1.040
R1 [F > 4σ(F)]	0.0723
wR2 (all data)	0.1895
max. peak/hole (e.Å ⁻³)	0.414/-0.349
CCDC	2352461

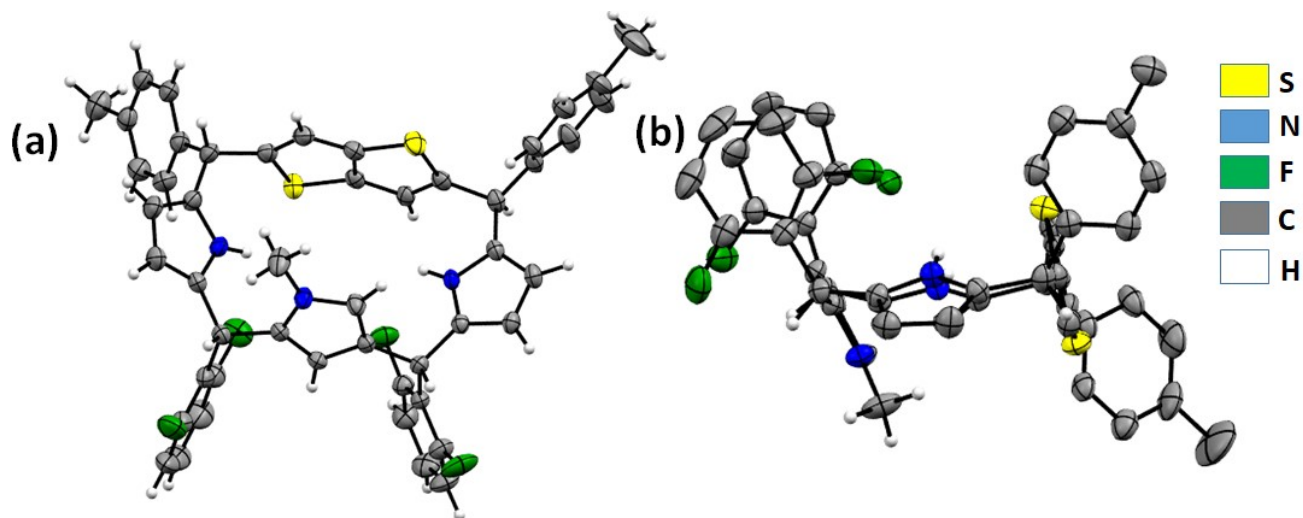


Fig. S33 Crystal structure of 7 (A: top view; B-side view)

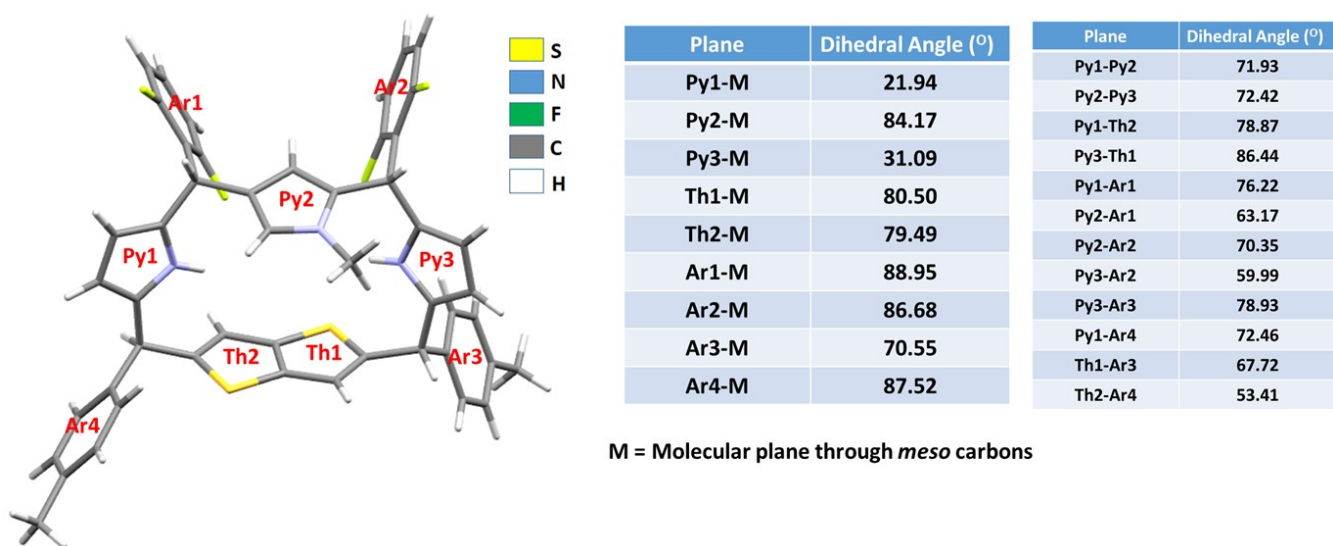


Fig. S33A Crystal structure of **7** (Table shows dihedral angles)

5.0 Theoretical Calculation

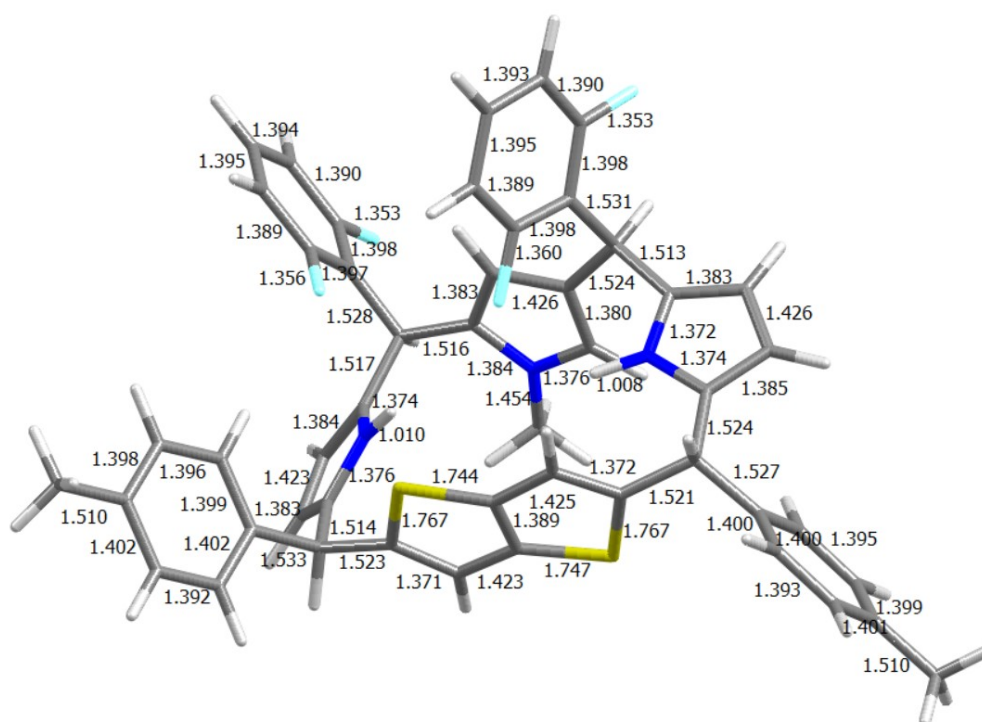


Fig. S34 Optimized geometry of **7** with selected bond length (Å).

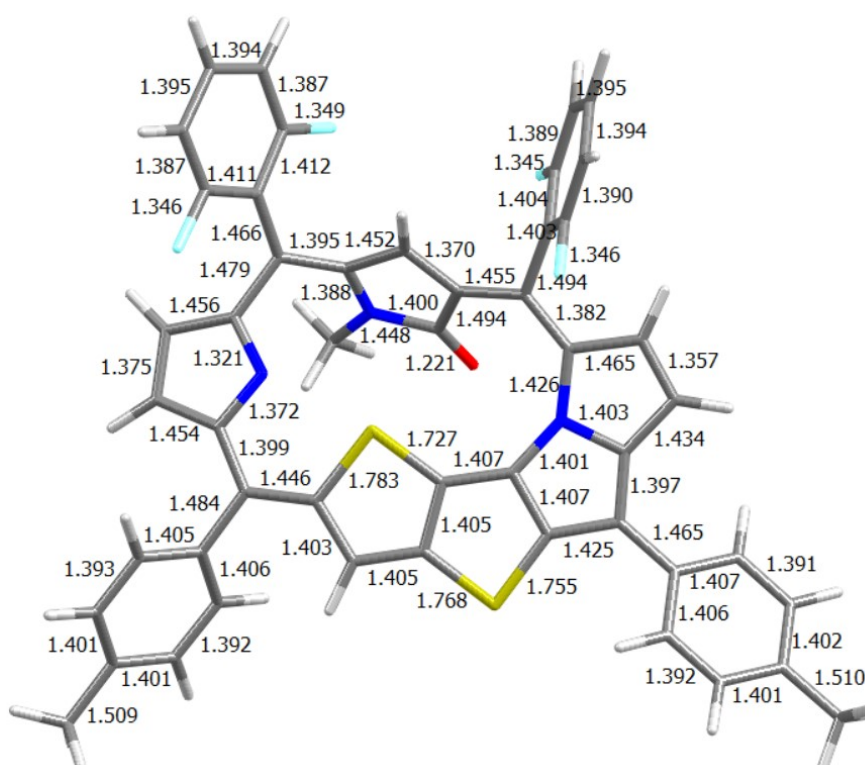


Fig. S35 Optimized geometry of **9** with selected bond length (Å).

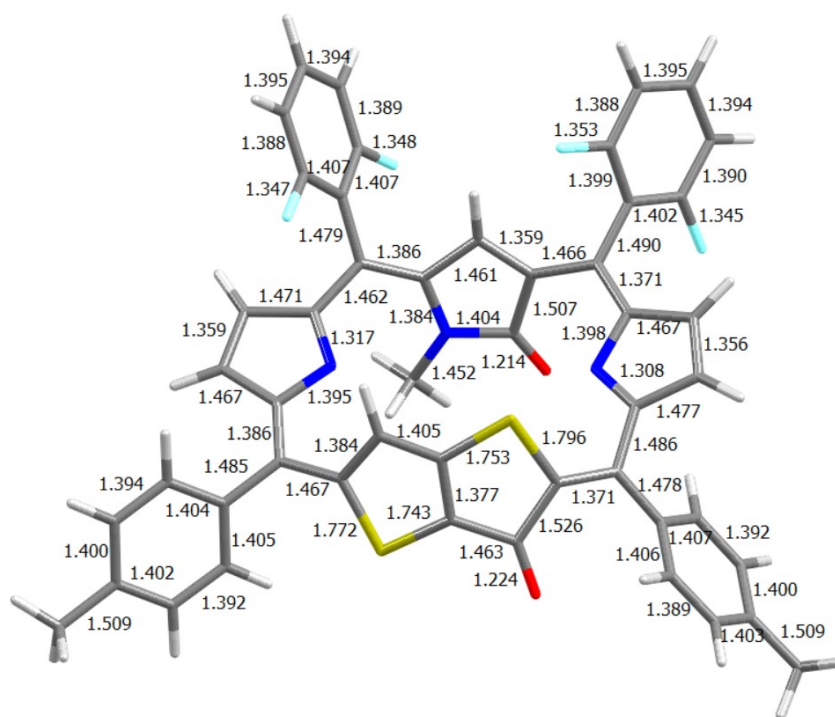


Fig. S36 Optimized geometry of **10** with selected bond length (Å).

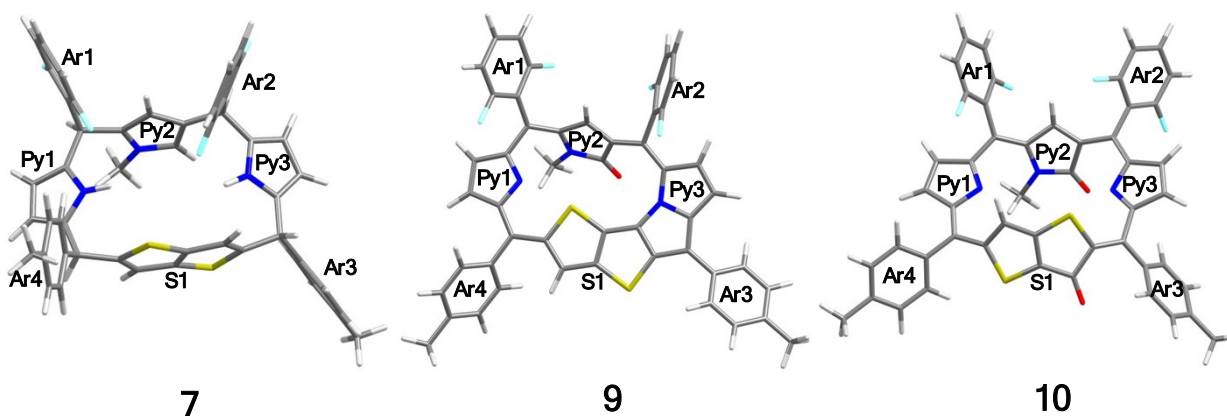


Fig. S37 Label used to measure the important dihedral between the macrocyclic mean plane (M) and the rings of **7**, **9** and **10**.

Table S2. Important dihedral between the macrocyclic mean plane (M) and the rings of **7**, **9** and **10**.

Plane	Dihedral Angle (°)			Plane	Dihedral Angle (°)		
	7	9	10		7	9	10
Ar1-M	83.69	49.77	60.18	Py1-Py2	83.08	56.45	51.20
Ar2-M	88.09	73.53	54.43	Py2-Py3	73.44	45.25	50.99
Ar3-M	79.31	33.39	53.42	Py1-Th2	78.36	22.77	45.45
Ar4-M	70.55	48.10	47.72	Py1-Th1	82.39	19.88	45.00
Py1-M	32.90	17.39	4.96	Py1-Ar1	73.15	66.55	65.01
Py2-M	71.09	52.57	49.81	Py2-Ar1	66.28	73.42	70.62
Py3-M	24.61	7.42	11.85	Py2-Ar2	66.44	77.3	44.08
S1-M	86.73	4.27	43.87	Py3-Ar2	66.08	74.40	64.61
Th1-M	86.19	3.52	45.11	Py3-Ar3	59.84	39.35	64.60
Th2-M	87.31	5.39	43.68	Py1-Ar4	77.06	64.52	57.57
-	-	-	-	Th1-Ar3	57.98	34.99	85.98

-	-	-	-	Th2-Ar4	74.09	42.06	73.72
---	---	---	---	---------	-------	-------	-------

Table S3. Important dihedral between the macrocyclic mean plane (M) and the rings of stereoisomer of **7**.

Plane	Dihedral Angle (°) between the macrocyclic mean plane							
	Ar1-M	Ar2-M	Ar3-M	Ar4-M	Py1-M	Py2-M	Py3-M	S1-M
7	83.69	88.09	79.31	70.55	32.90	71.09	24.61	86.73
Stereoisomer-1	89.51	81.26	75.54	80.97	23.49	71.44	12.68	84.48
Stereoisomer-2	67.90	87.29	80.21	75.27	11.62	62.90	25.23	85.21
Stereoisomer-3	72.11	80.57	74.63	59.58	30.67	62.50	10.85	84.11
Stereoisomer-4	49.56	86.17	67.23	61.80	31.06	65.21	24.32	89.68
Stereoisomer-5	85.83	88.34	79.67	82.48	25.68	69.52	24.88	86.22
Stereoisomer-6	72.40	84.47	67.97	59.67	29.52	62.91	22.39	85.71
Stereoisomer-7	86.37	81.67	75.22	70.12	73.11	73.92	12.51	85.95
Stereoisomer-8	52.17	87.42	62.86	61.53	29.80	61.74	34.04	89.65
Stereoisomer-9	70.14	87.80	63.98	60.72	32.39	59.18	33.85	84.52
Stereoisomer-10	86.60	86.19	64.41	70.41	30.24	74.56	24.67	88.04
Stereoisomer-11	86.29	88.50	61.91	82.16	24.93	69.32	33.43	89.82
Stereoisomer-12	50.02	82.17	74.66	61.67	31.20	65.14	12.92	88.73
Stereoisomer-13	83.96	88.11	60.79	70.94	32.03	70.41	32.19	89.78
Stereoisomer-14	88.95	84.62	67.58	80.49	22.59	72.20	23.75	86.24

Table S4. Calculated energies of the optimized structures and relative energies (ΔE) for plausible isomers of **7**.

	Energy (hartree)	ΔE (kJ/mol)
7	-3249.516115	0.00
Stereoisomer-1	-3249.512879	8.50
Stereoisomer-2	-3249.510230	15.45
Stereoisomer-3	-3249.510479	14.80
Stereoisomer-4	-3249.511195	12.92
Stereoisomer-5	-3249.513499	6.87
Stereoisomer-6	-3249.510837	13.86
Stereoisomer-7	-3249.514654	3.84
Stereoisomer-8	-3249.513113	7.88
Stereoisomer-9	-3249.512328	9.94
Stereoisomer-10	-3249.514880	3.24
Stereoisomer-11	-3249.514403	4.50
Stereoisomer-12	-3249.510754	14.08
Stereoisomer-13	-3249.516818	-1.84
Stereoisomer-14	-3249.513291	7.41

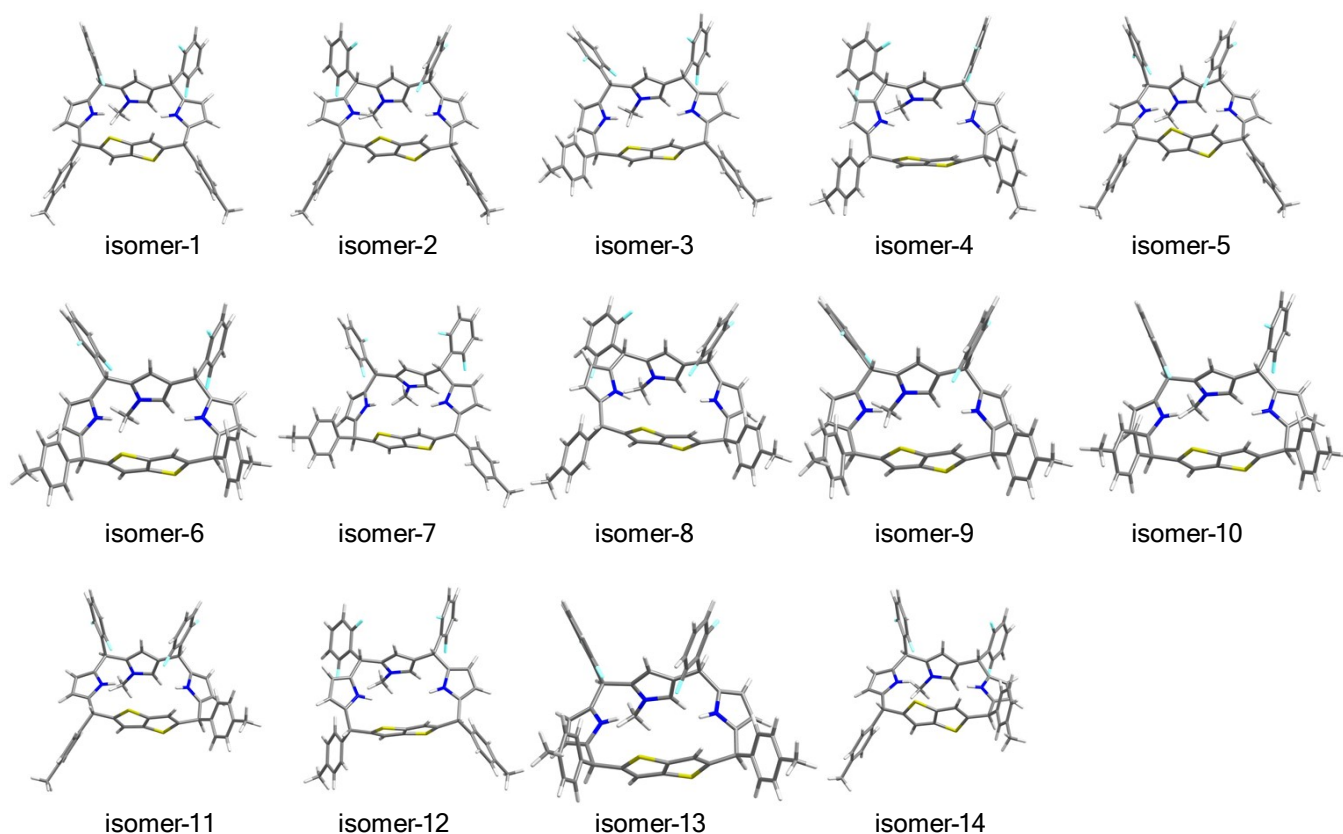


Fig. S38 Optimized geometry of all the possible stereoisomers of **7**.

Table S5. Frontier Molecular Orbital compositions (%) in the ground state for **7**.

	Energy (eV)	Ar1	Ar2	Ar3	Ar4	Py1	Py2	Py3	S1
HOMO-3	-5.678	2.56	0.36	3.13	4.37	25.15	5.94	3.91	54.57
HOMO-2	-5.464	3.27	2.50	2.03	1.72	11.19	52.05	7.56	19.67
HOMO-1	-5.176	5.04	2.11	3.40	5.47	36.14	7.97	25.97	13.90
HOMO	-5.050	2.40	6.32	6.19	1.68	13.03	20.80	a44.39	5.20
LUMO	-0.743	0.21	0.09	4.13	3.69	5.37	0.24	4.62	81.65
LUMO+1	-0.427	82.76	0.18	0.01	1.16	5.36	9.62	0.06	0.85
LUMO+2	-0.325	0.27	84.91	0.83	0.02	0.03	6.37	7.08	0.48
LUMO+3	-0.090	75.39	1.18	2.54	9.11	3.62	2.18	0.17	5.81
LUMO+4	-5.678	2.56	0.36	3.13	4.37	25.15	5.94	3.91	54.57

Table S6. Frontier Molecular Orbital compositions (%) in the ground state for **9**.

	Energy (eV)	Ar1	Ar2	Ar3	Ar4	Py1	Py2	Py3	S1
HOMO-3	-5.815	5.72	1.03	3.59	1.95	25.19	5.35	5.07	52.10

HOMO-2	-5.469	0.83	9.97	15.77	1.57	6.38	12.76	13.32	39.41
HOMO-1	-5.304	23.18	1.30	2.43	6.09	5.21	27.49	12.29	22.00
HOMO	-4.511	11.58	7.88	12.27	1.99	13.60	12.39	14.80	25.47
LUMO	-2.962	10.92	6.92	3.19	12.99	12.61	21.61	14.17	17.60
LUMO+1	-1.951	17.65	3.15	5.94	16.22	19.85	13.05	7.55	16.59
LUMO+2	-1.543	14.85	26.69	7.58	0.89	3.67	24.62	15.31	6.39
LUMO+3	-0.432	4.39	65.23	5.97	2.39	0.50	6.36	13.04	2.13
LUMO+4	-5.815	5.72	1.03	3.59	1.95	25.19	5.35	5.07	52.10

Table S7. Frontier Molecular Orbital compositions (%) in the ground state for **10**.

	Energy (eV)	Ar1	Ar2	Ar3	Ar4	Py1	Py2	Py3	S1
HOMO-3	-6.241	0.52	7.64	18.82	0.26	1.45	10.63	15.30	45.40
HOMO-2	-5.954	6.27	1.25	20.77	2.83	8.21	4.12	4.41	52.13
HOMO-1	-5.336	22.60	0.73	4.43	9.55	14.42	32.25	3.11	12.90
HOMO	-5.148	1.92	1.98	10.53	1.03	1.30	2.40	6.93	73.91
LUMO	-2.848	9.34	13.27	2.56	11.07	10.14	25.11	19.85	8.67
LUMO+1	-2.631	3.44	12.23	9.54	11.59	17.18	7.44	10.58	28.01
LUMO+2	-1.604	24.27	2.09	9.41	10.10	16.40	18.76	3.85	15.13
LUMO+3	-1.537	6.98	13.01	16.28	2.31	3.62	13.04	14.98	29.77
LUMO+4	-6.241	0.52	7.64	18.82	0.26	1.45	10.63	15.30	45.40

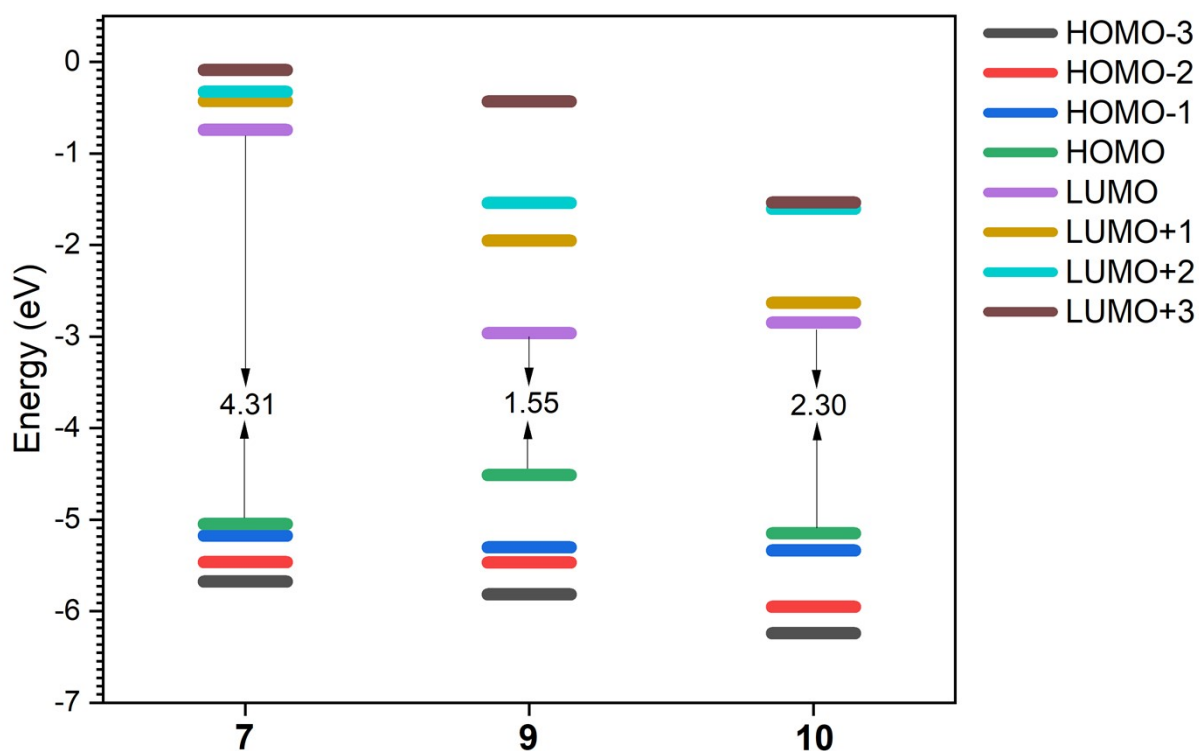


Fig. S39 FMO energy levels of **7**, **9** and **10**

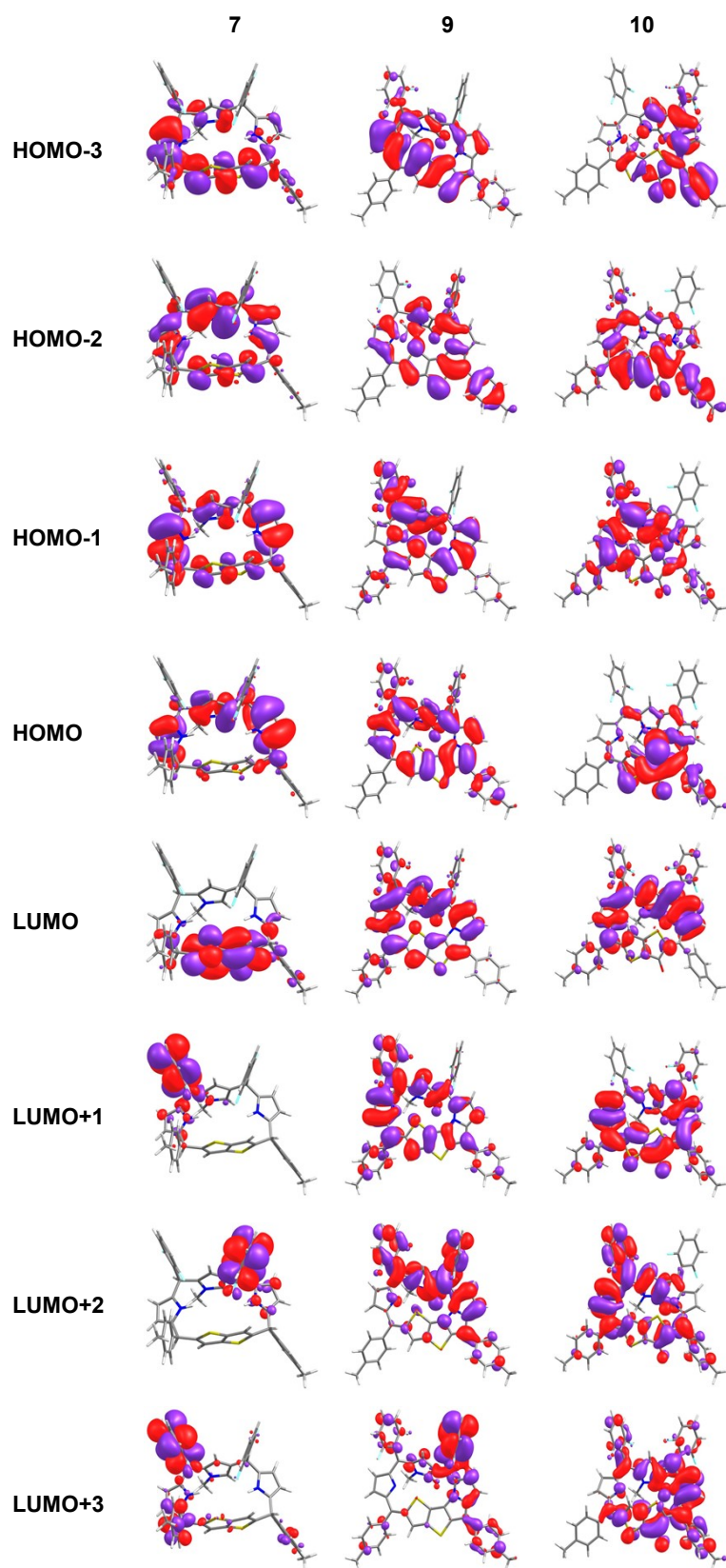


Fig. S40 Highest occupied molecular orbital and lowest unoccupied molecular orbitals of **7**, **9** and **10**

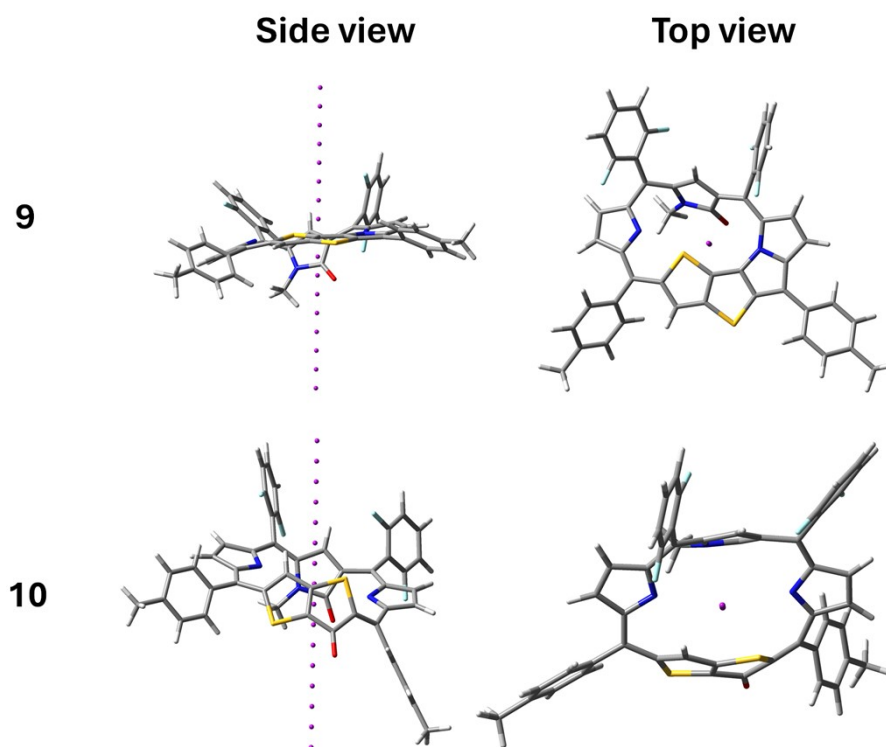


Fig. S41 The centers of macrocycles **9** and **10** for the NICS values were designated at the non-weighted mass of π conjugation pathway of the macrocycles.

Table S8. The calculated nucleus-independent chemical shifts (NICS) values for **9** and **10**.

Distance (Å)	Macrocycle	
	9	10
-8	0.5807	-0.2305
-7	0.8406	-0.3497
-6	1.2701	-0.4865
-5	2.0078	-0.6098
-4	3.1912	-0.7139
-3	3.7092	-0.9822
-2	2.7057	-1.5375
-1	8.4334	-1.7308
0	8.4270	-1.4915
1	9.0511	-1.2194
2	6.9556	-0.8664
3	4.2039	-0.5359
4	2.5202	-0.3736
5	1.5778	-0.2913
6	1.0341	-0.2023
7	0.7054	-0.1111
8	0.4979	-0.0431

Table S9. Harmonic oscillator model of aromaticity (HOMA), multi-center indices (MCI), approximate multi-center bond order for large rings (AV1245 index) and Avmin index values for **9** and **10**.

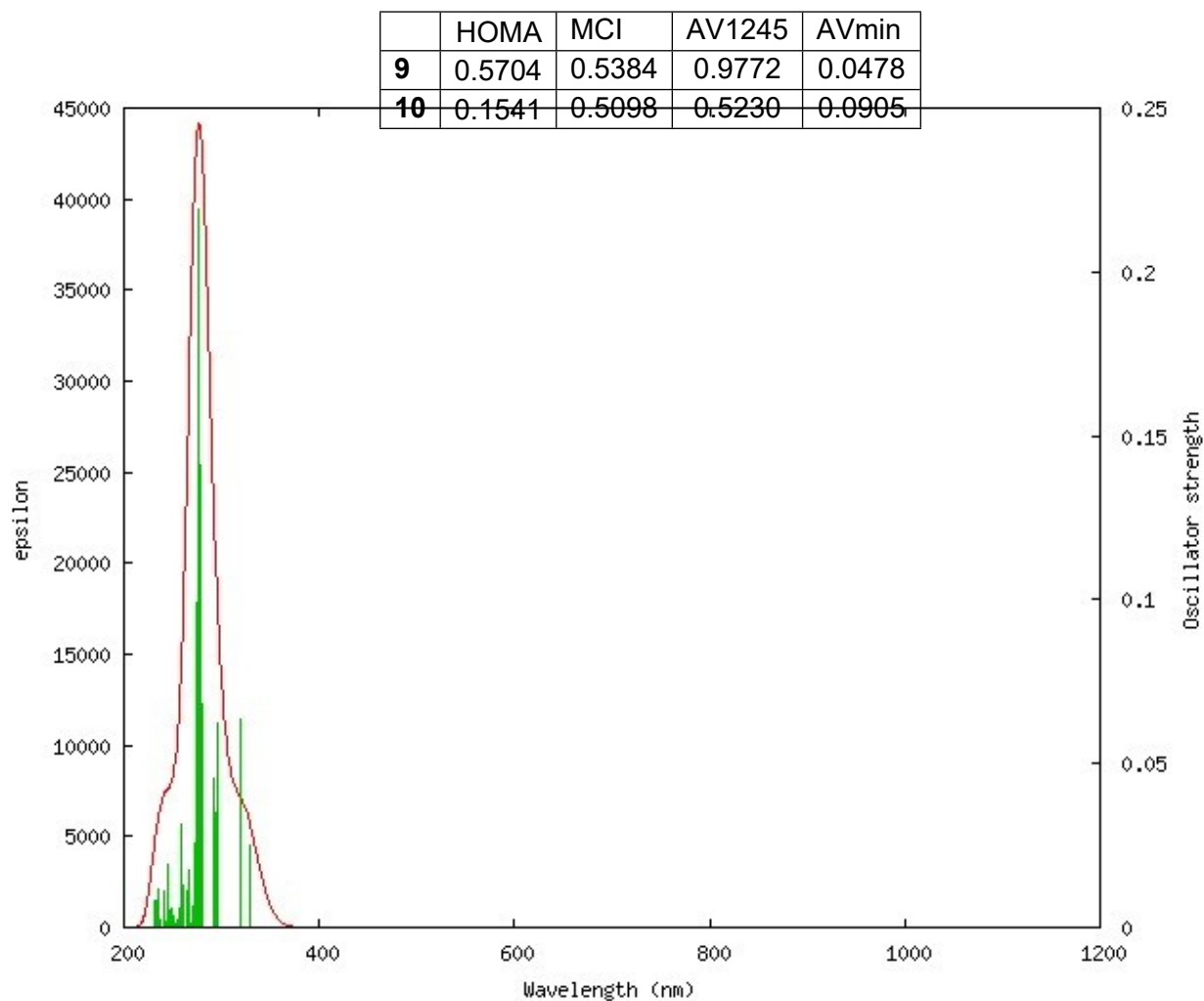


Fig. S42 Computed absorption spectrum of **7** in solvent phase (CH_2Cl_2)

Table S10. Computed absorption maxima (λ_{max} nm), Electronic excitation energies (E, eV), and Oscillator strength (f) of **7** in solvent phase (CH_2Cl_2).

No.	E (cm ⁻¹)	Cal. λ_{\max} (nm)	Oscillator Strength f	Main Contributing Configurations
1	30353.27	329.45	0.0250	HOMO→LUMO (94%)
2	31251.78	319.98	0.0637	HOMO-1→LUMO (93%)
3	33810.19	295.77	0.0621	HOMO-2→LUMO (91%)
4	34032.80	293.83	0.0350	HOMO→LUMO+1 (85%)
5	34290.09	291.63	0.0457	HOMO-1→LUMO+2 (23%), HOMO→LUMO+2 (72%)
6	35791.91	279.39	0.0682	HOMO-3→LUMO (27%), HOMO-1→LUMO+2 (39%), HOMO→LUMO+2 (15%)
7	36045.17	277.43	0.1408	HOMO-3→LUMO (23%), HOMO-2→LUMO+1 (12%), HOMO-1→LUMO+1 (27%), HOMO-1→LUMO+2 (21%)
8	36234.71	275.98	0.2189	HOMO-3→LUMO (32%), HOMO-2→LUMO+1 (11%), HOMO-1→LUMO+1 (37%)
9	36504.91	273.94	0.0992	HOMO→LUMO+3 (72%)
10	36747.68	272.13	0.0259	HOMO-1→LUMO+3 (25%), HOMO→LUMO+4 (58%)
11	36982.39	270.40	0.0067	HOMO-1→LUMO+3 (28%), HOMO→LUMO+5 (12%), HOMO→LUMO+6 (41%)
12	37139.67	269.25	0.0009	HOMO-1→LUMO+7 (21%), HOMO→LUMO+7 (69%)
13	37153.38	269.15	0.0003	HOMO→LUMO+5 (54%), HOMO→LUMO+6 (10%)
14	37391.32	267.44	0.0019	HOMO-1→LUMO+5 (12%), HOMO-1→LUMO+8 (29%), HOMO→LUMO+8 (40%)
15	37490.52	266.73	0.0172	HOMO-2→LUMO+1 (59%), HOMO-1→LUMO+1 (21%)
16	37788.14	264.63	0.0109	HOMO-2→LUMO+2 (84%)
17	38365.64	260.65	0.0060	HOMO-1→LUMO+3 (24%), HOMO→LUMO+4 (10%), HOMO→LUMO+6 (24%)
18	38500.34	259.74	0.0128	HOMO-4→LUMO (82%)
19	38661.65	258.65	0.0020	HOMO-2→LUMO+7 (10%), HOMO-1→LUMO+4 (10%), HOMO-1→LUMO+7 (48%), HOMO→LUMO+7 (24%)
20	38752.79	258.05	0.0314	HOMO-5→LUMO (76%), HOMO-4→LUMO (14%)
21	38975.40	256.57	0.0057	HOMO-2→LUMO+4 (11%), HOMO-1→LUMO+4 (45%), HOMO-1→LUMO+7 (14%)
22	39256.08	254.74	0.0022	HOMO-1→LUMO+5 (17%), HOMO-1→LUMO+8 (21%), HOMO→LUMO+8 (38%)
23	39381.91	253.92	0.0019	HOMO-1→LUMO+6 (35%), HOMO-1→LUMO+8 (20%)
24	39690.82	251.95	0.0013	HOMO-3→LUMO+1 (10%), HOMO-1→LUMO+5 (27%), HOMO-1→LUMO+8 (10%)
25	39797.28	251.27	0.0035	HOMO-3→LUMO+1 (22%), HOMO-2→LUMO+3 (11%), HOMO-1→LUMO+6 (20%)
26	40080.39	249.50	0.0061	HOMO-3→LUMO+1 (51%), HOMO-2→LUMO+3 (26%)
27	40089.26	249.44	0.0026	HOMO-6→LUMO (87%)
28	40308.64	248.09	0.0056	HOMO-3→LUMO+2 (40%), HOMO-2→LUMO+4 (29%)
29	40343.32	247.87	0.0007	HOMO-3→LUMO+2 (50%), HOMO-2→LUMO+4 (24%)
30	40451.40	247.21	0.0054	HOMO-7→LUMO (85%)
31	40621.59	246.17	0.0002	HOMO-2→LUMO+7 (83%)
32	40782.90	245.20	0.0191	HOMO-8→LUMO (84%)
33	40962.76	244.12	0.0012	HOMO-3→LUMO+3 (10%), HOMO-3→LUMO+6 (12%), HOMO-2→LUMO+4 (13%), HOMO-2→LUMO+5 (10%), HOMO-2→LUMO+6 (20%)
34	41153.92	242.99	0.0017	HOMO-3→LUMO+3 (20%), HOMO-2→LUMO+3 (11%), HOMO-2→LUMO+5 (34%)
35	41345.07	241.87	0.0046	HOMO-3→LUMO+3 (11%), HOMO-2→LUMO+5 (10%), HOMO-2→LUMO+6 (43%), HOMO-2→LUMO+8 (14%)

36	41471.70	241.13	0.0066	HOMO-9→LUMO (52%), HOMO-4→LUMO+1 (22%)
37	41487.83	241.03	0.0018	HOMO-9→LUMO (18%), HOMO-4→LUMO+1 (53%), HOMO-4→LUMO+2 (12%)
38	41548.33	240.68	0.0100	HOMO-4→LUMO+1 (18%), HOMO-4→LUMO+2 (76%)
39	41578.97	240.51	0.0111	HOMO-9→LUMO (21%), HOMO-2→LUMO+8 (53%)
40	42062.91	237.74	0.0024	HOMO-3→LUMO+4 (24%), HOMO-3→LUMO+5 (42%)
41	42221.00	236.85	0.0009	HOMO-3→LUMO+3 (12%), HOMO-3→LUMO+6 (31%), HOMO-2→LUMO+6 (14%)
42	42629.92	234.58	0.0118	HOMO-3→LUMO+4 (24%), HOMO-1→LUMO+10 (10%), HOMO→LUMO+10 (38%)
43	42681.54	234.29	0.0036	HOMO-12→LUMO (16%), HOMO→LUMO+9 (27%)
44	42761.39	233.86	0.0079	HOMO-3→LUMO+4 (18%), HOMO-3→LUMO+5 (25%), HOMO-3→LUMO+6 (21%)
45	42950.13	232.83	0.0025	HOMO-3→LUMO+8 (16%), HOMO→LUMO+9 (44%)
46	43055.79	232.26	0.0009	HOMO-3→LUMO+7 (49%)
47	43077.56	232.14	0.0015	HOMO-13→LUMO (15%), HOMO-3→LUMO+7 (25%)
48	43149.35	231.75	0.0024	HOMO-3→LUMO+8 (58%)
49	43347.76	230.69	0.0053	HOMO-14→LUMO+7 (10%), HOMO-10→LUMO+2 (22%), HOMO-5→LUMO+2 (17%), HOMO-3→LUMO+7 (12%)
50	43395.35	230.44	0.0084	HOMO-12→LUMO (14%), HOMO-10→LUMO+2 (14%), HOMO-5→LUMO+3 (19%)

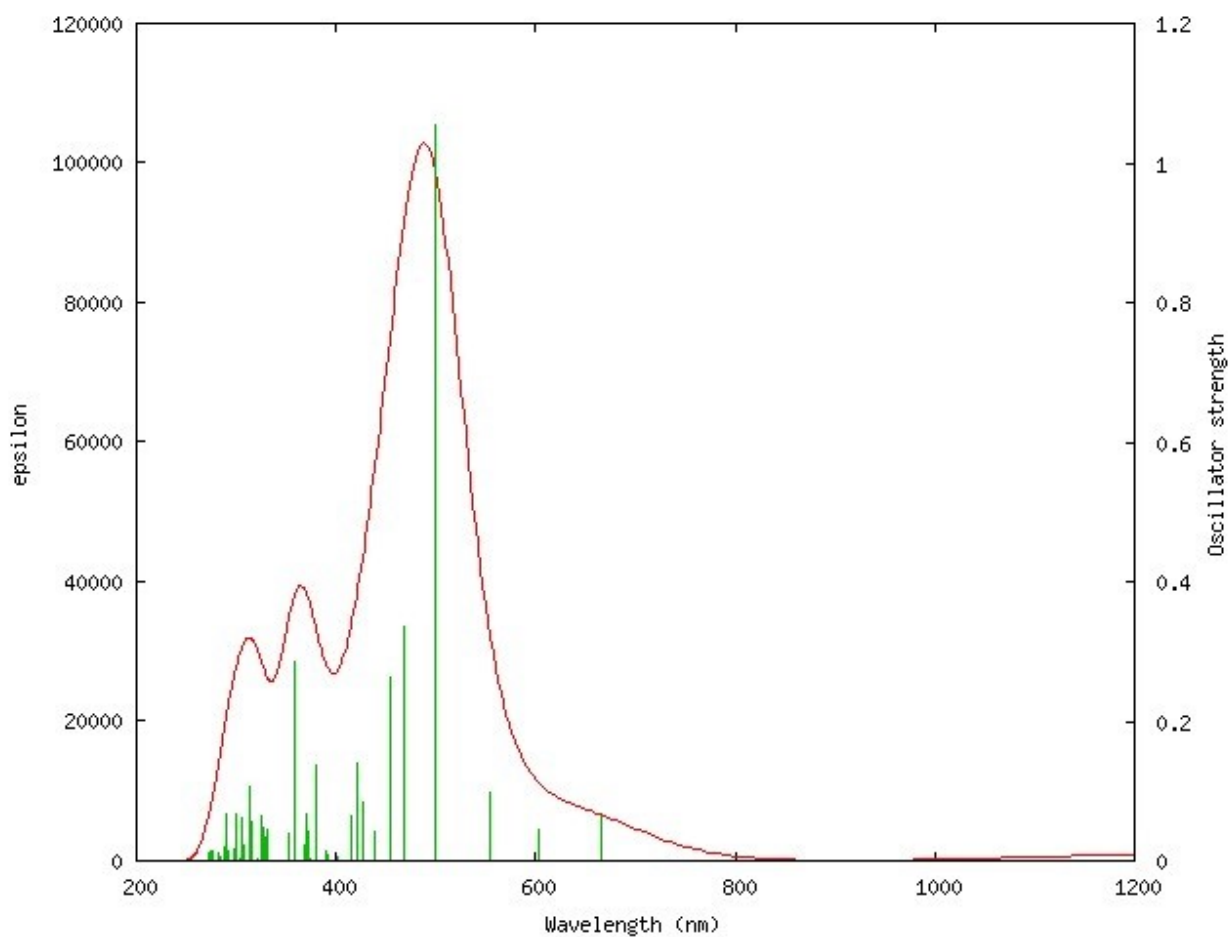


Fig. S43 Computed absorption spectrum of **9** in solvent phase (CH_2Cl_2)

Table S11. Computed absorption maxima (λ_{max} nm), Electronic excitation energies (E, eV), and Oscillator strength (f) of **9** in solvent phase (CH₂Cl₂).

No.	E (cm ⁻¹)	Cal. λ_{max} (nm)	Oscillator Strength f	Main Contributing Configurations
1	7699.42	1298.80	0.0137	HOMO→LUMO (100%)
2	15026.21	665.50	0.0642	HOMO-1→LUMO (81%), HOMO→LUMO+1 (13%)
3	16568.36	603.56	0.0443	HOMO-2→LUMO (70%), HOMO→LUMO+1 (17%)
4	18029.04	554.66	0.0987	HOMO-3→LUMO (67%), HOMO→LUMO+1 (24%)
5	20033.34	499.17	1.0536	HOMO-4→LUMO (12%), HOMO-3→LUMO (24%), HOMO-2→LUMO (15%), HOMO→LUMO+1 (38%)
6	21369.81	467.95	0.3360	HOMO→LUMO+2 (84%)
7	22019.09	454.15	0.2637	HOMO-7→LUMO (12%), HOMO-4→LUMO (39%), HOMO-1→LUMO+1 (12%)
8	22749.02	439.58	0.0426	HOMO-7→LUMO (11%), HOMO-5→LUMO (49%), HOMO-4→LUMO (13%), HOMO-1→LUMO+1 (13%)
9	23391.85	427.50	0.0831	HOMO-4→LUMO (15%), HOMO-1→LUMO+1 (55%)
10	23698.35	421.97	0.1410	HOMO-9→LUMO (11%), HOMO-7→LUMO (24%), HOMO-6→LUMO (13%), HOMO-5→LUMO (33%)
11	24070.17	415.45	0.0654	HOMO-6→LUMO (67%), HOMO-4→LUMO (15%)
12	24892.86	401.72	0.0053	HOMO-2→LUMO+1 (85%)
13	25512.30	391.97	0.0091	HOMO-8→LUMO (62%), HOMO-7→LUMO (15%)
14	25585.70	390.84	0.0043	HOMO-9→LUMO (40%), HOMO-8→LUMO (33%), HOMO-7→LUMO (15%)
15	25658.29	389.74	0.0137	HOMO-13→LUMO (34%), HOMO-11→LUMO (25%), HOMO-9→LUMO (21%)
16	26353.54	379.46	0.1363	HOMO-13→LUMO (17%), HOMO-11→LUMO (30%), HOMO-3→LUMO+1 (21%), HOMO-1→LUMO+2 (18%)
17	26760.05	373.69	0.0027	HOMO-10→LUMO (81%)
18	26813.28	372.95	0.0419	HOMO-12→LUMO (34%), HOMO-11→LUMO (20%), HOMO-3→LUMO+1 (14%), HOMO-1→LUMO+2 (15%)
19	27066.54	369.46	0.0667	HOMO-12→LUMO (14%), HOMO-3→LUMO+1 (17%), HOMO-1→LUMO+2 (51%)
20	27183.49	367.87	0.0230	HOMO-12→LUMO (39%), HOMO-3→LUMO+1 (35%)
21	27920.69	358.16	0.2867	HOMO-2→LUMO+2 (87%)
22	28353.81	352.69	0.0383	HOMO-14→LUMO (87%)
23	30200.03	331.13	0.0443	HOMO-4→LUMO+1 (23%), HOMO-3→LUMO+2 (11%), HOMO→LUMO+3 (31%)
24	30350.85	329.48	0.0325	HOMO-4→LUMO+1 (12%), HOMO→LUMO+3 (25%), HOMO→LUMO+4 (46%)
25	30581.53	326.99	0.0464	HOMO-3→LUMO+2 (10%), HOMO→LUMO+3 (31%), HOMO→LUMO+4 (29%)
26	30814.62	324.52	0.0647	HOMO-4→LUMO+1 (16%), HOMO-3→LUMO+2 (41%), HOMO→LUMO+4 (12%)
27	31040.46	322.16	0.0029	HOMO-15→LUMO (14%), HOMO-7→LUMO+1 (12%), HOMO-5→LUMO+1 (29%), HOMO-4→LUMO+1 (16%), HOMO-3→LUMO+2 (13%)
28	31634.90	316.11	0.0548	HOMO-15→LUMO (50%), HOMO-5→LUMO+1 (12%)
29	31759.91	314.86	0.0277	HOMO-16→LUMO (66%)
30	31922.84	313.26	0.1068	HOMO-16→LUMO (10%), HOMO-7→LUMO+1 (21%), HOMO-6→LUMO+1 (25%), HOMO-5→LUMO+1 (18%)
31	32418.87	308.46	0.0116	HOMO-6→LUMO+1 (27%), HOMO→LUMO+5 (29%)
32	32598.74	306.76	0.0237	HOMO-6→LUMO+1 (11%), HOMO→LUMO+5 (31%),

				HOMO→LUMO+7 (29%)
33	32785.86	305.01	0.0610	HOMO→LUMO+6 (10%), HOMO→LUMO+7 (41%), HOMO→LUMO+8 (24%)
34	32864.90	304.28	0.0027	HOMO→LUMO+5 (12%), HOMO→LUMO+6 (59%), HOMO→LUMO+7 (21%)
35	33099.61	302.12	0.0007	HOMO-9→LUMO+1 (22%), HOMO→LUMO+9 (57%)
36	33382.71	299.56	0.0677	HOMO-5→LUMO+2 (13%), HOMO→LUMO+8 (50%)
37	33647.26	297.20	0.0165	HOMO→LUMO+10 (77%)
38	34180.40	292.57	0.0112	HOMO-9→LUMO+1 (34%), HOMO-7→LUMO+1 (15%), HOMO→LUMO+9 (35%)
39	34274.77	291.76	0.0135	HOMO-17→LUMO (10%), HOMO-5→LUMO+2 (47%)
40	34391.72	290.77	0.0683	HOMO-11→LUMO+1 (22%), HOMO-4→LUMO+2 (38%)
41	34503.02	289.83	0.0022	HOMO-8→LUMO+1 (70%)
42	34540.93	289.51	0.0181	HOMO-17→LUMO (49%)
43	34685.31	288.31	0.0189	HOMO-13→LUMO+1 (10%), HOMO-11→LUMO+1 (33%), HOMO-4→LUMO+2 (31%)
44	35144.24	284.54	0.0041	HOMO-13→LUMO+1 (26%), HOMO-12→LUMO+1 (42%), HOMO-11→LUMO+1 (16%)
45	35282.97	283.42	0.0051	HOMO-10→LUMO+1 (82%)
46	35485.41	281.81	0.0111	HOMO-13→LUMO+1 (25%), HOMO-12→LUMO+1 (50%)
47	36135.50	276.74	0.0131	HOMO-13→LUMO+1 (10%), HOMO-6→LUMO+2 (71%)
48	36372.63	274.93	0.0141	HOMO-9→LUMO+2 (11%), HOMO-7→LUMO+2 (55%)
49	36504.91	273.94	0.0125	HOMO-8→LUMO+2 (83%)
50	36739.61	272.19	0.0119	HOMO-13→LUMO+2 (29%)

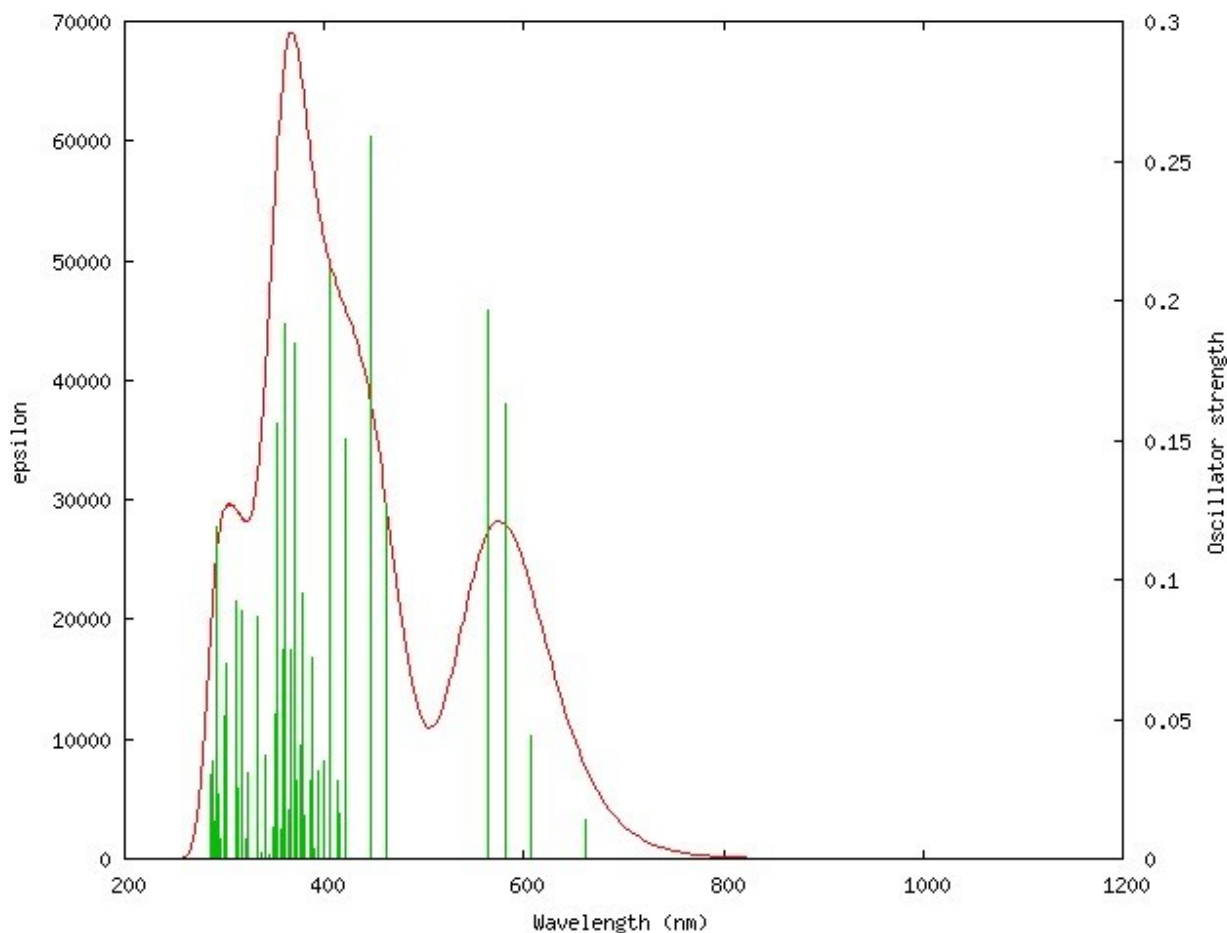


Fig. S44 Computed absorption spectrum of **10** in solvent phase (CH₂Cl₂)

Table S12. Computed absorption maxima (λ_{\max} nm), Electronic excitation energies (E, eV), and Oscillator strength (f) of **10** in solvent phase (CH₂Cl₂).

No.	E (cm ⁻¹)	Cal. λ_{\max} (nm)	Oscillator Strength f	Main Contributing Configurations
1	15111.71	661.74	0.0142	HOMO-1→LUMO (11%), HOMO→LUMO (80%)
2	16498.99	606.10	0.0441	HOMO-1→LUMO (64%), HOMO→LUMO+1 (29%)
3	17206.34	581.18	0.1628	HOMO-1→LUMO+1 (66%), HOMO→LUMO (13%), HOMO→LUMO+1 (10%)
4	17712.06	564.59	0.1963	HOMO-1→LUMO (13%), HOMO-1→LUMO+1 (25%), HOMO→LUMO+1 (54%)
5	21656.94	461.75	0.1272	HOMO-2→LUMO (91%)
6	22396.56	446.50	0.2589	HOMO-2→LUMO+1 (80%)
7	23726.58	421.47	0.1504	HOMO-5→LUMO (10%), HOMO-3→LUMO (14%), HOMO-3→LUMO+1 (21%)
8	24054.85	415.72	0.0160	HOMO-5→LUMO (32%), HOMO-4→LUMO (13%), HOMO-3→LUMO (30%)
9	24207.29	413.10	0.0280	HOMO-5→LUMO (23%), HOMO-3→LUMO (13%), HOMO-3→LUMO+1 (16%), HOMO→LUMO+2 (17%)
10	24621.05	406.16	0.2111	HOMO-4→LUMO (48%), HOMO-4→LUMO+1 (14%), HOMO-3→LUMO (17%)
11	24972.71	400.44	0.0251	HOMO-9→LUMO (10%), HOMO-3→LUMO+1 (30%),

				HOMO→LUMO+2 (30%)
12	25350.99	394.46	0.0316	HOMO-9→LUMO (13%), HOMO-7→LUMO (18%), HOMO-6→LUMO (14%), HOMO-3→LUMO (14%), HOMO→LUMO+2 (15%)
13	25609.89	390.47	0.0038	HOMO-7→LUMO (12%), HOMO-7→LUMO+1 (11%), HOMO-6→LUMO (38%), HOMO-5→LUMO+1 (11%)
14	25746.20	388.41	0.0717	HOMO-7→LUMO (24%), HOMO-5→LUMO+1 (28%)
15	25968.01	385.09	0.0279	HOMO-4→LUMO (11%), HOMO-4→LUMO+1 (20%), HOMO-1→LUMO+2 (30%), HOMO→LUMO+2 (10%)
16	26361.61	379.34	0.0155	HOMO-1→LUMO+2 (11%), HOMO-1→LUMO+3 (26%), HOMO→LUMO+3 (47%)
17	26398.71	378.81	0.0948	HOMO-4→LUMO+1 (38%), HOMO-1→LUMO+2 (24%)
18	26530.18	376.93	0.0409	HOMO-12→LUMO (19%), HOMO-9→LUMO (22%), HOMO-8→LUMO (11%), HOMO-6→LUMO+1 (10%)
19	26853.61	372.39	0.0281	HOMO-9→LUMO (23%), HOMO-8→LUMO (59%)
20	26885.87	371.94	0.0078	HOMO-10→LUMO (79%)
21	26999.60	370.38	0.1847	HOMO-12→LUMO (16%), HOMO-8→LUMO (15%), HOMO-6→LUMO+1 (14%)
22	27279.47	366.58	0.0748	HOMO-6→LUMO (12%), HOMO-1→LUMO+3 (14%), HOMO→LUMO+3 (13%)
23	27515.79	363.43	0.0176	HOMO-7→LUMO (17%), HOMO-7→LUMO+1 (13%), HOMO-6→LUMO+1 (28%)
24	27713.40	360.84	0.1919	HOMO-9→LUMO+1 (35%), HOMO-1→LUMO+3 (18%)
25	27886.01	358.60	0.0745	HOMO-9→LUMO+1 (21%), HOMO-7→LUMO+1 (24%)
26	28069.09	356.26	0.0105	HOMO-11→LUMO (60%), HOMO-11→LUMO+1 (25%)
27	28326.39	353.03	0.1562	HOMO-14→LUMO (12%), HOMO-13→LUMO (21%), HOMO-13→LUMO+1 (11%), HOMO-7→LUMO+1 (11%)
28	28523.19	350.59	0.0515	HOMO-15→LUMO (39%), HOMO-14→LUMO (17%), HOMO-13→LUMO (12%)
29	28735.31	348.00	0.0115	HOMO-13→LUMO (19%), HOMO-13→LUMO+1 (16%)
30	29007.12	344.74	0.0011	HOMO-9→LUMO+1 (11%), HOMO-8→LUMO+1 (81%)
31	29366.85	340.52	0.0372	HOMO-13→LUMO (21%), HOMO-13→LUMO+1 (14%), HOMO-12→LUMO+1 (25%)
32	29703.99	336.66	0.0020	HOMO-10→LUMO+1 (87%)
33	29937.09	334.03	0.0142	HOMO-13→LUMO+1 (24%), HOMO-12→LUMO+1 (46%)
34	30035.49	332.94	0.0049	HOMO-11→LUMO (31%), HOMO-11→LUMO+1 (65%)
35	30095.17	332.28	0.0865	HOMO-15→LUMO (19%), HOMO-14→LUMO (12%), HOMO-14→LUMO+1 (14%), HOMO-13→LUMO (10%)
36	30921.90	323.40	0.0308	HOMO-15→LUMO+1 (17%), HOMO-14→LUMO+1 (39%), HOMO-2→LUMO+2 (21%)
37	31213.07	320.38	0.0073	HOMO-15→LUMO+1 (36%), HOMO-2→LUMO+2 (33%)
38	31487.30	317.59	0.0886	HOMO-17→LUMO (21%), HOMO-16→LUMO (15%), HOMO-14→LUMO+1 (17%), HOMO-2→LUMO+2 (31%)
39	31897.83	313.50	0.0254	HOMO-17→LUMO+1 (11%), HOMO-16→LUMO+1 (30%), HOMO-2→LUMO+3 (25%)
40	32026.08	312.25	0.0921	HOMO-18→LUMO (19%), HOMO-17→LUMO (13%), HOMO-16→LUMO (10%), HOMO-2→LUMO+3 (36%)
41	32162.39	310.92	0.0102	HOMO-17→LUMO (36%), HOMO-16→LUMO (19%), HOMO-2→LUMO+3 (21%)
42	33091.54	302.19	0.0700	HOMO-18→LUMO (54%), HOMO-16→LUMO+1 (19%), HOMO-2→LUMO+3 (10%)
43	33427.88	299.15	0.0511	HOMO-4→LUMO+2 (10%), HOMO-3→LUMO+2 (63%)
44	33777.12	296.06	0.0067	HOMO-17→LUMO+1 (32%), HOMO-16→LUMO+1 (17%),

				HOMO-5→LUMO+3 (13%), HOMO-3→LUMO+3 (12%)
45	34062.64	293.58	0.0232	HOMO-18→LUMO+1 (20%), HOMO-4→LUMO+2 (13%), HOMO-4→LUMO+3 (10%), HOMO-3→LUMO+3 (25%)
46	34161.85	292.72	0.1190	HOMO-18→LUMO+1 (16%), HOMO-17→LUMO+1 (31%), HOMO-4→LUMO+2 (15%)
47	34456.24	290.22	0.0053	HOMO-18→LUMO+1 (28%), HOMO-5→LUMO+2 (45%)
48	34582.87	289.16	0.0136	HOMO-5→LUMO+2 (32%), HOMO-4→LUMO+2 (27%), HOMO→LUMO+4 (13%)
49	34745.80	287.80	0.0349	HOMO-1→LUMO+4 (10%), HOMO→LUMO+4 (51%)
50	34957.12	286.06	0.0302	HOMO-5→LUMO+3 (32%), HOMO-4→LUMO+3 (11%), HOMO- 3→LUMO+3 (10%), HOMO→LUMO+4 (12%)

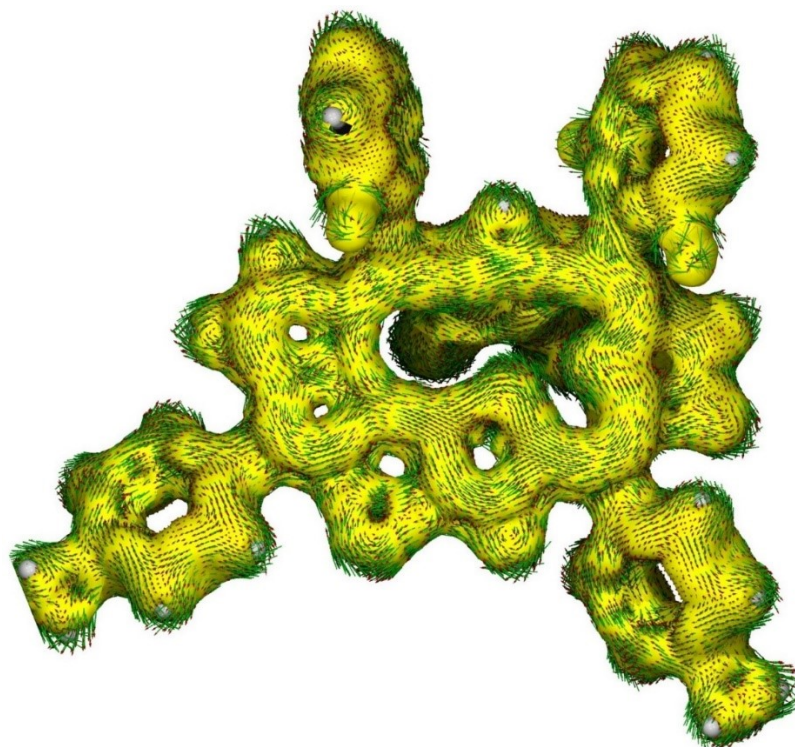


Fig. S45 The Anisotropy of Induced Current Density (AICD) plot of **9**. A continuous anti-clockwise ring current along the macrocycle indicating the anti-aromatic nature of macrocycle

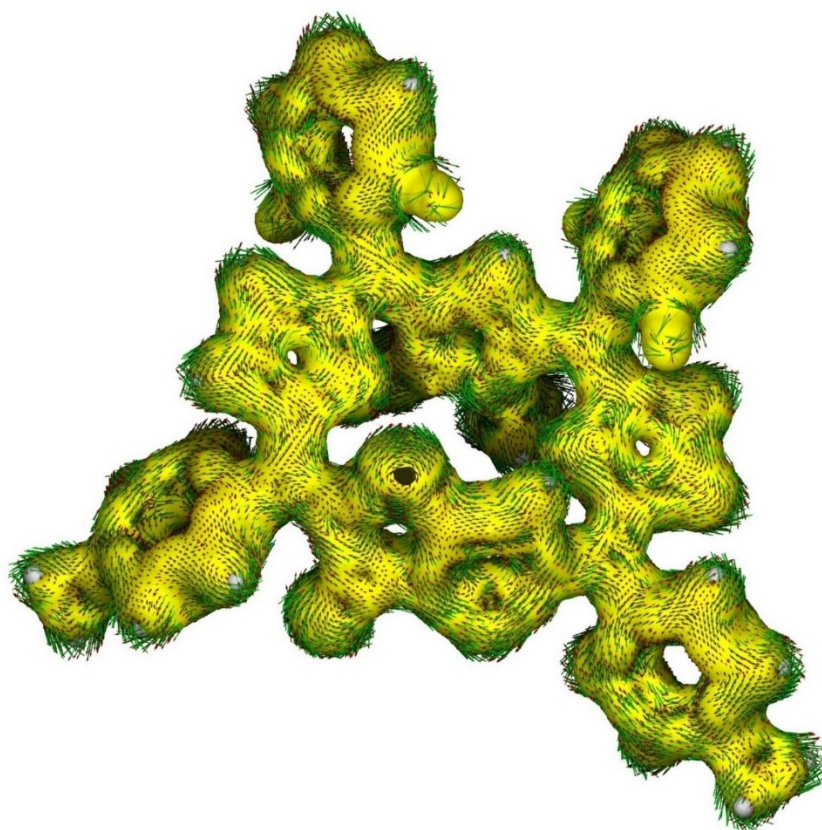


Fig. S46 The Anisotropy of Induced Current Density (AICD) plot of **10**

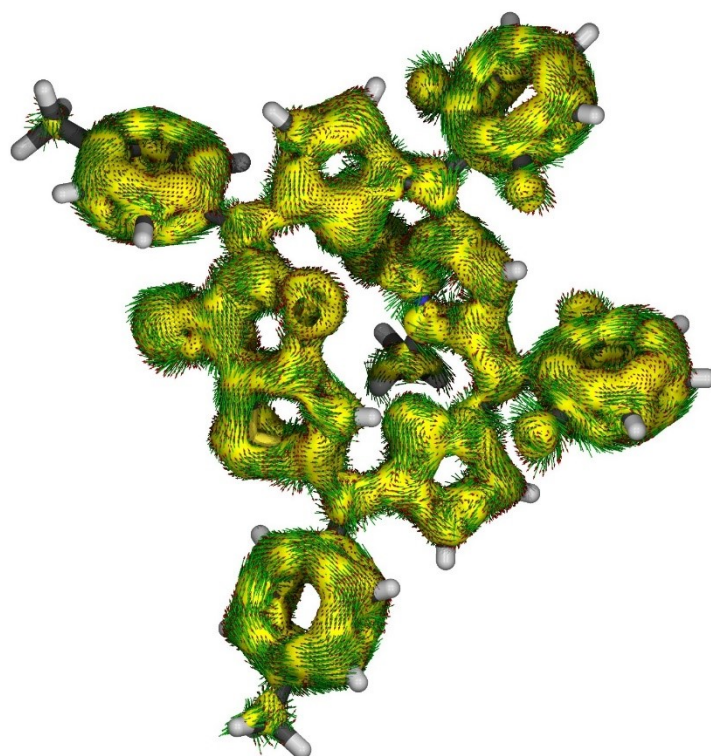


Fig. S47 The Anisotropy of Induced Current Density (AICD)_π plot of **10** indicating the nonaromatic nature of macrocycle

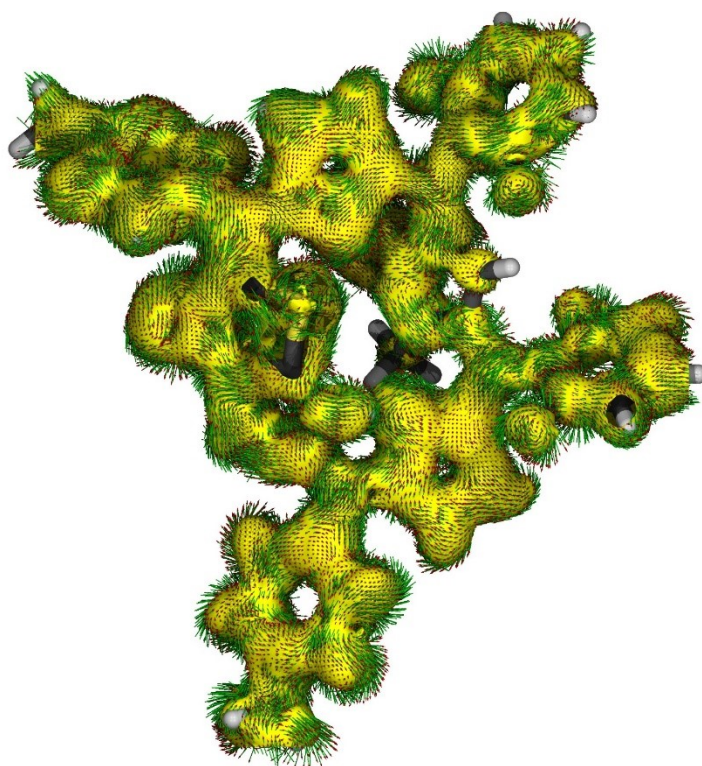


Fig. S48 The Anisotropy of Induced Current Density (AICD)_σ plot of **10** indicating the sigma aromatic nature of macrocycle

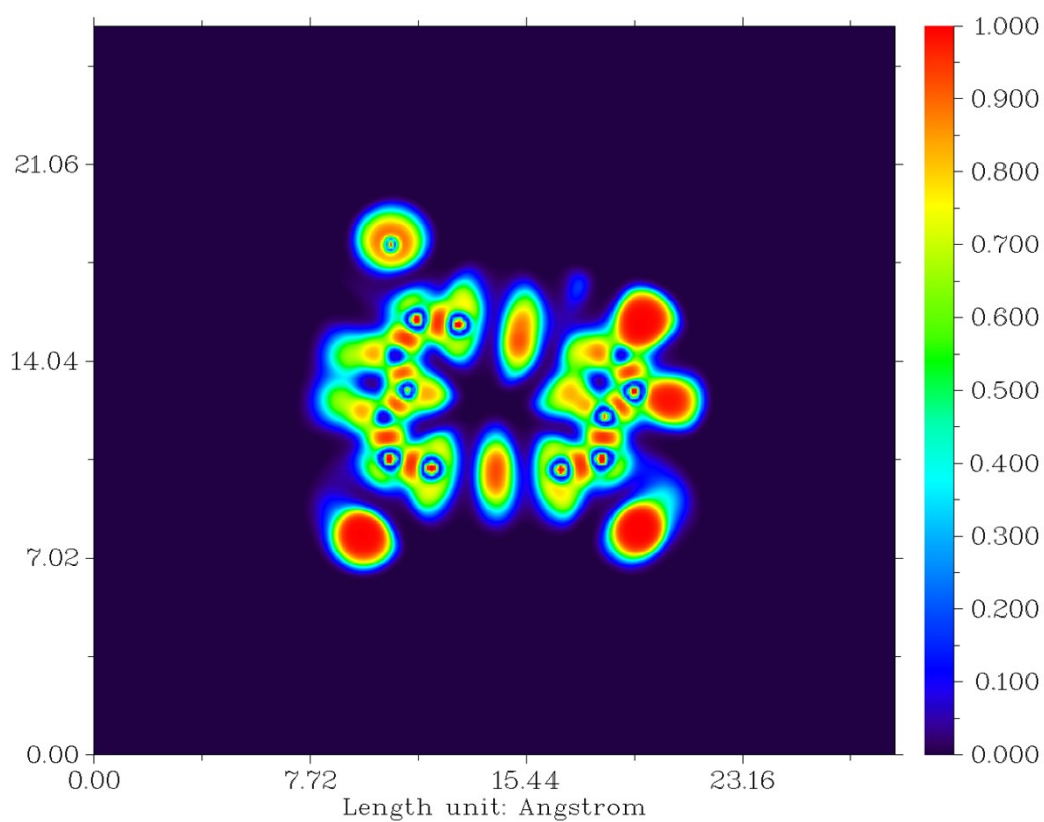


Fig. S49 Color-filled map of the electron localization function of **7**

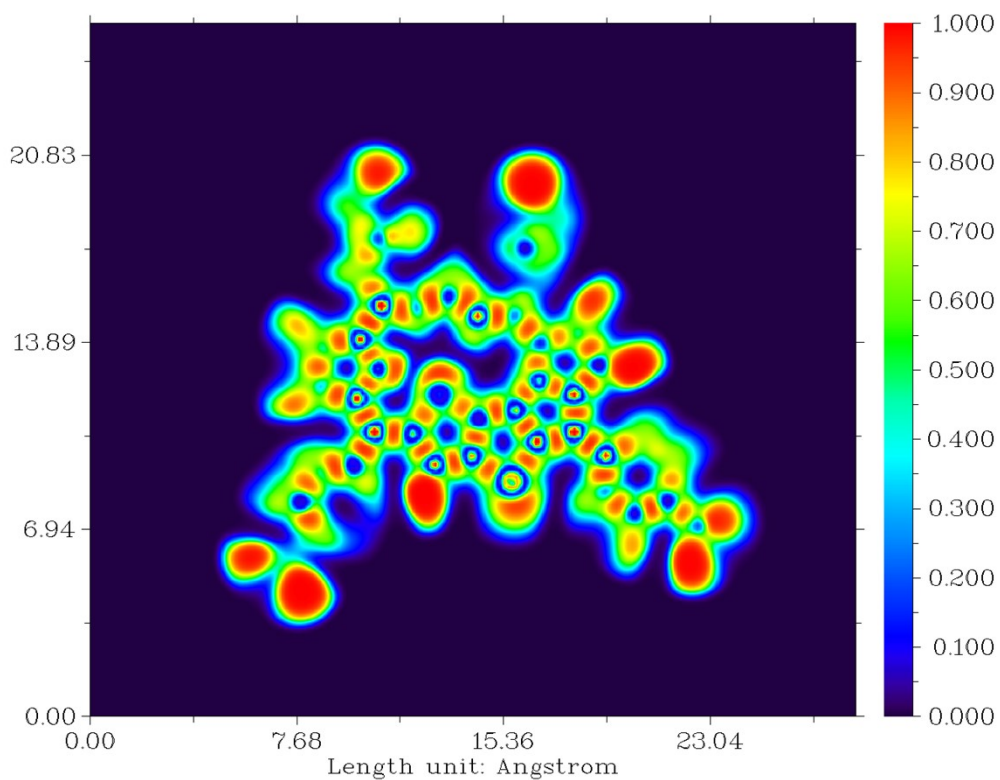


Fig. S50 Color-filled map of the electron localization function of **9**

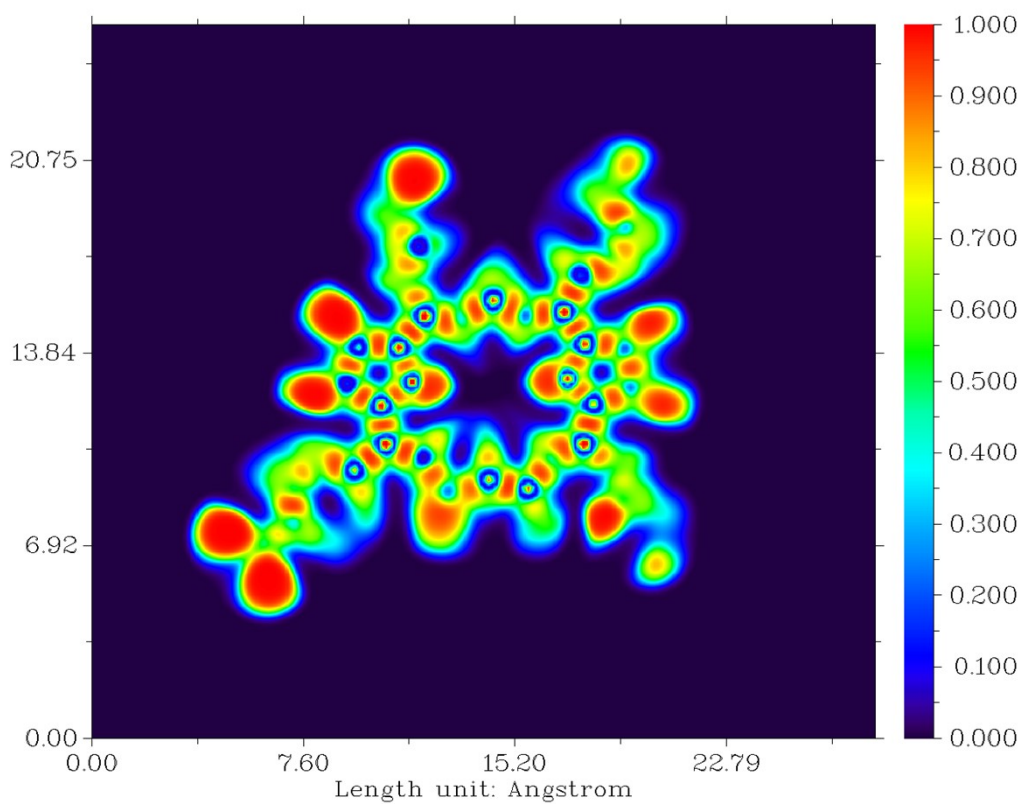


Fig. S51 Color-filled map of the electron localization function of **10**

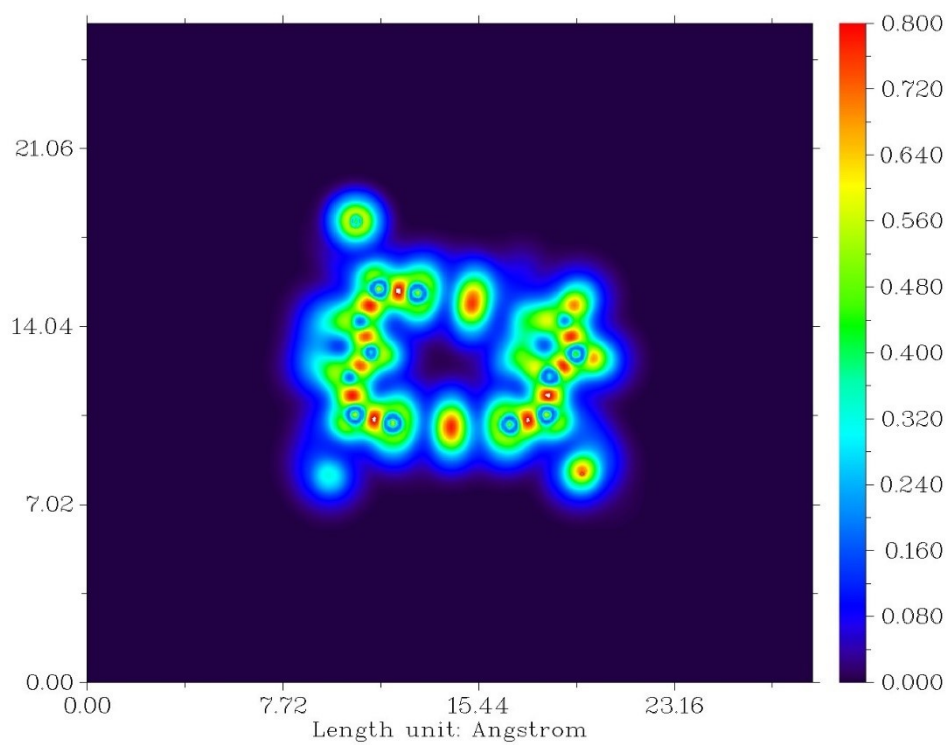


Fig. S52 Computed contour map of the π -localized orbital locator of **7**

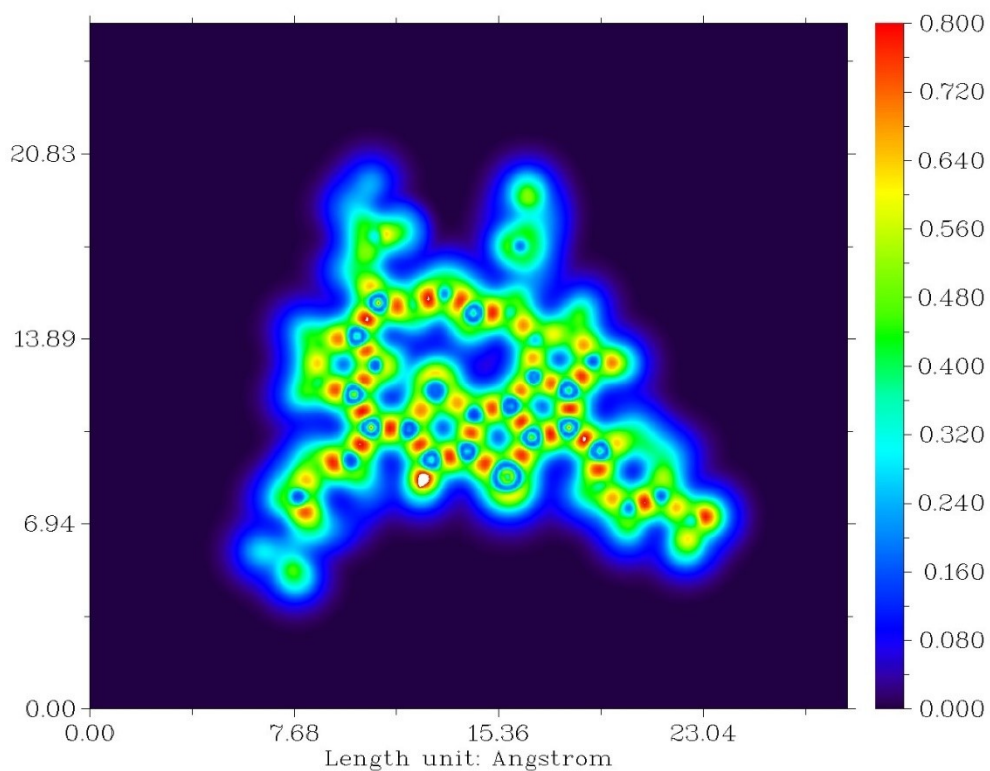


Fig. S53 Computed contour map of the π -localized orbital locator of **9**

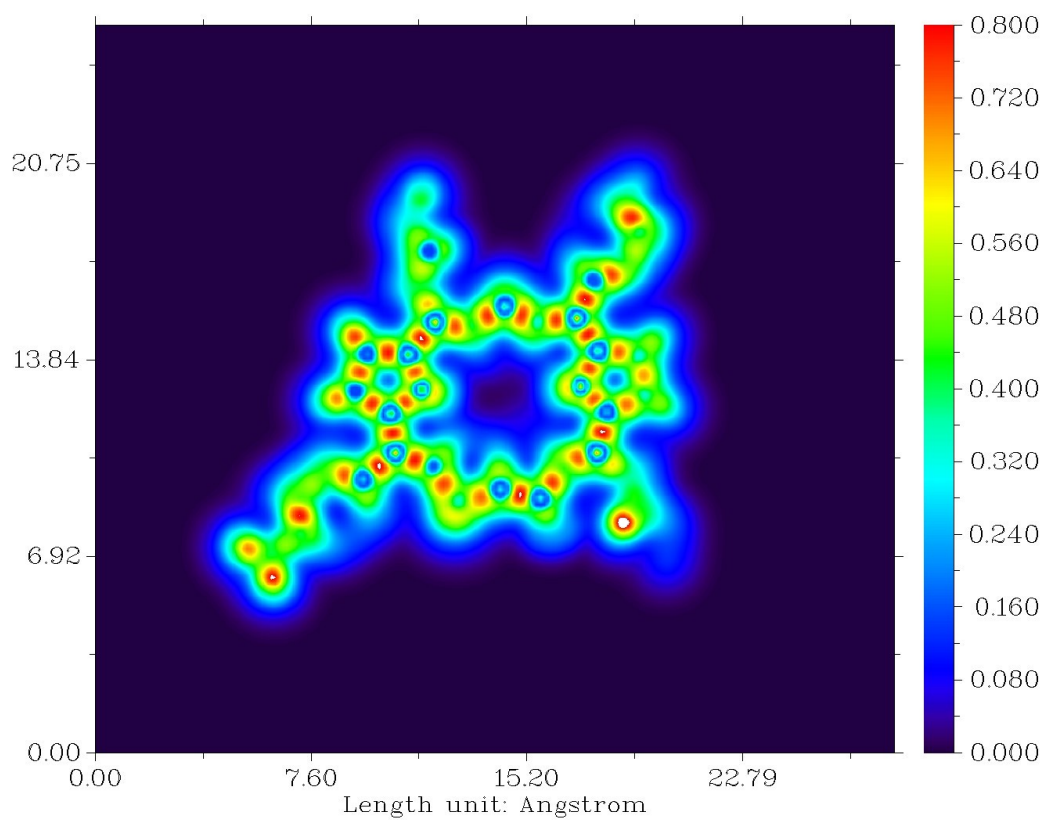


Fig. S54 Computed contour map of the π -localized orbital locator of **10**

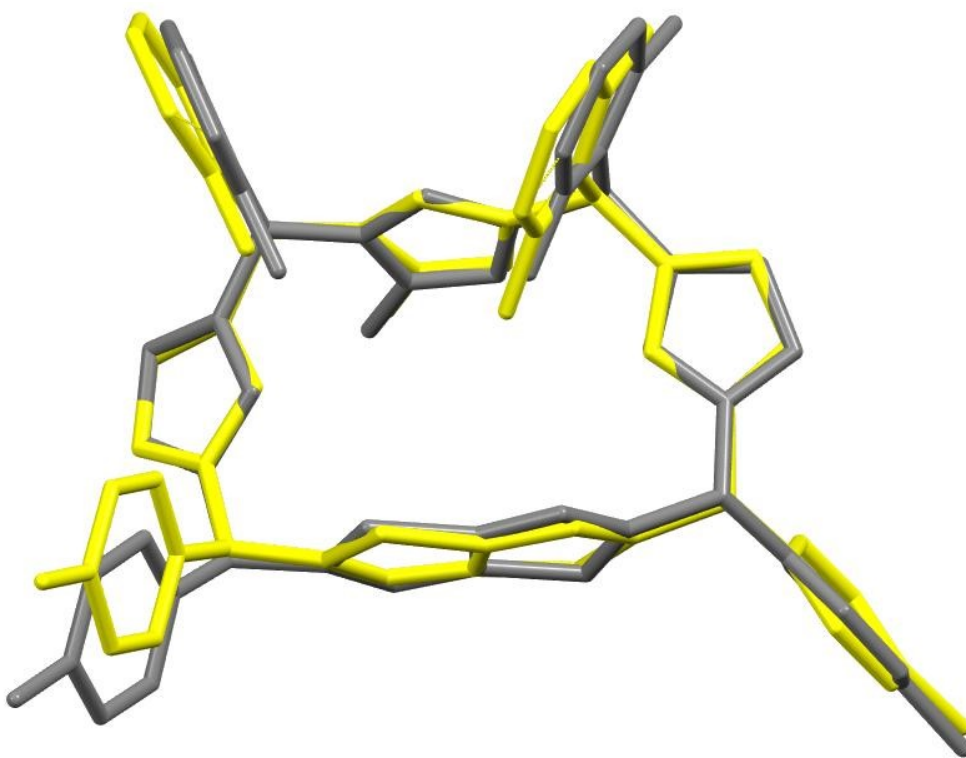


Fig. S55 Overlay plot (DFT, grey and XRD, yellow) of structure **7**. Hydrogen atoms are omitted for clarity.

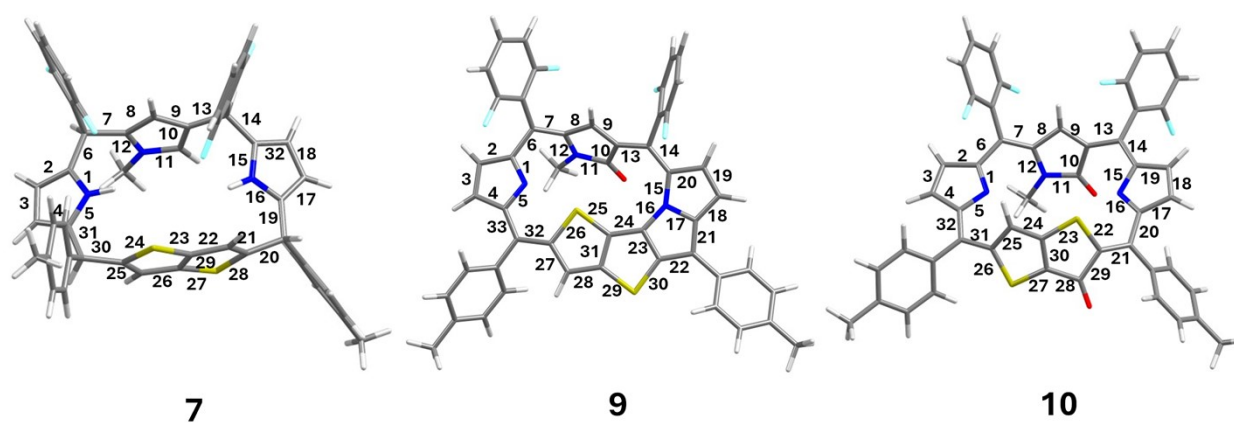


Fig. S56 Label used to show the computed Weiberg Bond Index and π -character of each bond

Table S14. Computed Weiberg Bond Index and π -character of each bond.

Number of Bond	7		9		10	
	Wieberg Bond Index	π -character of the bond	Wieberg Bond Index	π -character of the bond	Wieberg Bond Index	π -character of the bond
1	1.177	0.161	1.478	0.309	1.531	0.435
2	1.521	0.263	1.170	0.182	1.110	0.273
3	1.322	0.302	1.650	0.490	1.722	0.616
4	1.526	0.402	1.163	0.251	1.114	0.138
5	1.177	0.315	1.173	0.406	1.156	0.304
6	0.984	0.405	1.061	0.370	1.107	0.194
7	0.991	0.253	1.450	0.165	1.467	0.301
8	1.522	0.274	1.144	0.165	1.112	0.228
9	1.293	0.353	1.596	0.280	1.659	0.276
10	1.526	0.256	1.006	0.211	0.984	0.155
11	1.169	0.145	1.050	0.261	1.043	0.248
12	1.155	0.164	1.108	0.157	1.120	0.240
13	0.986	0.104	1.108	0.150	1.077	0.210
14	0.991	0.281	1.536	0.505	1.562	0.388
15	1.176	0.327	1.037	0.232	1.130	0.190
16	1.181	0.342	1.070	0.292	1.610	0.388
17	1.523	0.486	1.098	0.430	1.096	0.326
18	1.319	0.186	1.163	0.333	1.738	0.550
19	0.984	0.295	1.677	0.676	1.101	0.167
20	0.998	0.168	1.134	0.168	1.042	0.167
21	1.612	0.312	1.377	0.403	1.624	0.238
22	1.223	0.165	1.240	0.257	1.054	0.188
23	1.126	0.330	1.332	0.359	1.070	0.309
24	1.150	0.394	1.247	0.251	1.278	0.220
25	1.611	0.501	1.102	0.459	1.500	0.333
26	1.233	0.118	1.109	0.509	1.154	0.314
27	1.128	0.275	1.411	0.415	1.130	0.224
28	1.148	0.350	1.342	0.348	1.096	0.172
29	1.410	0.297	1.086	0.498	1.003	0.136
30	0.996	0.295	1.123	0.485	1.417	0.287
31	0.989	0.162	1.313	0.329	1.108	0.126
32	1.526	0.506	1.217	0.232	1.506	0.388
33	-	-	1.397	0.380	-	-

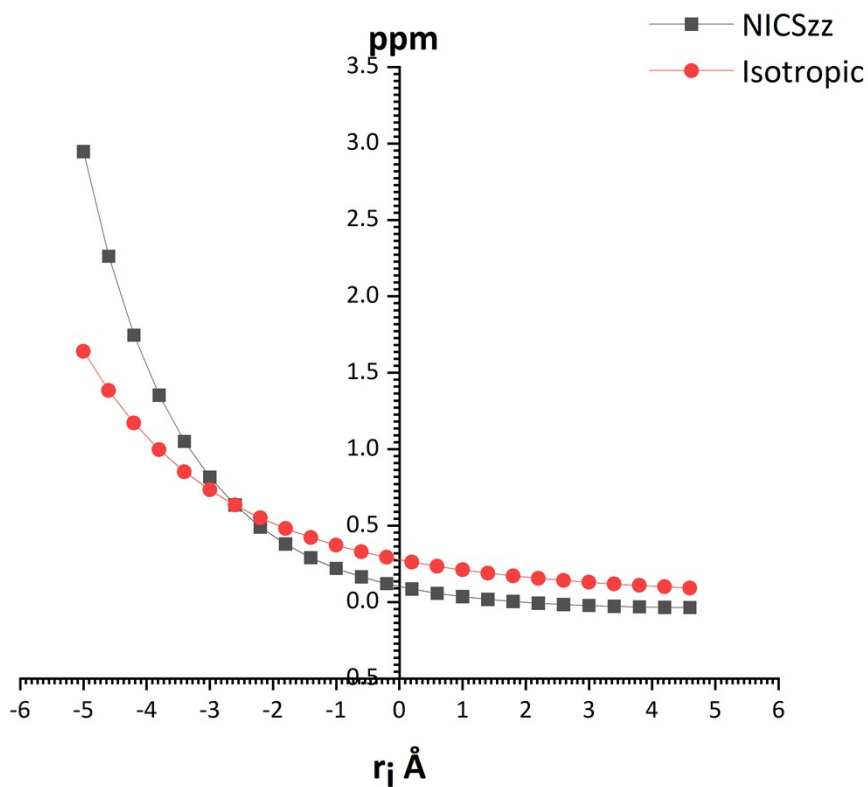


Fig. S57 Isotropic NICS and NICSzz scan plot of **9** where NICSzz is the out of plane contribution

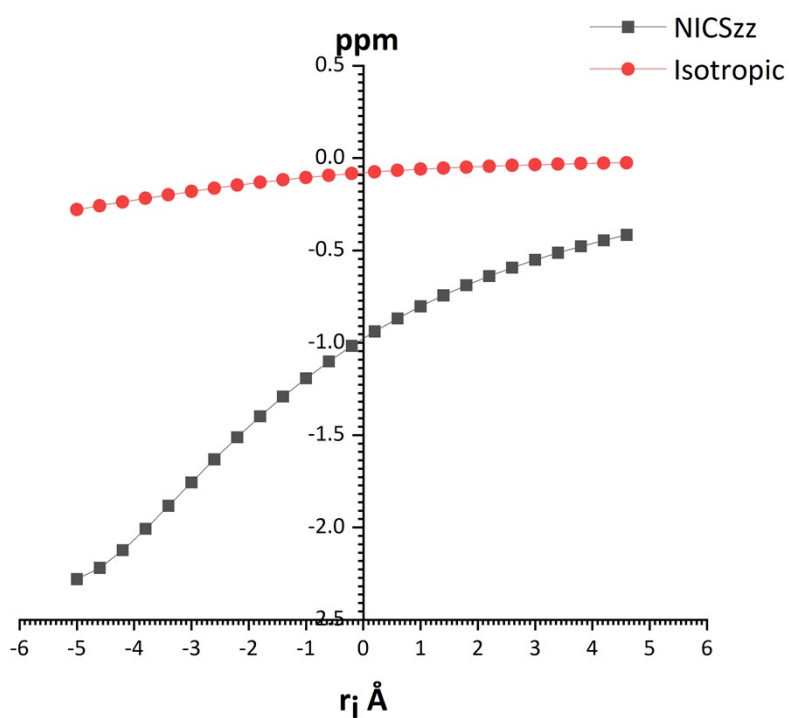


Fig. S58 Isotropic NICS and NICSzz scan plot of **10** where NICSzz is the out of plane contribution

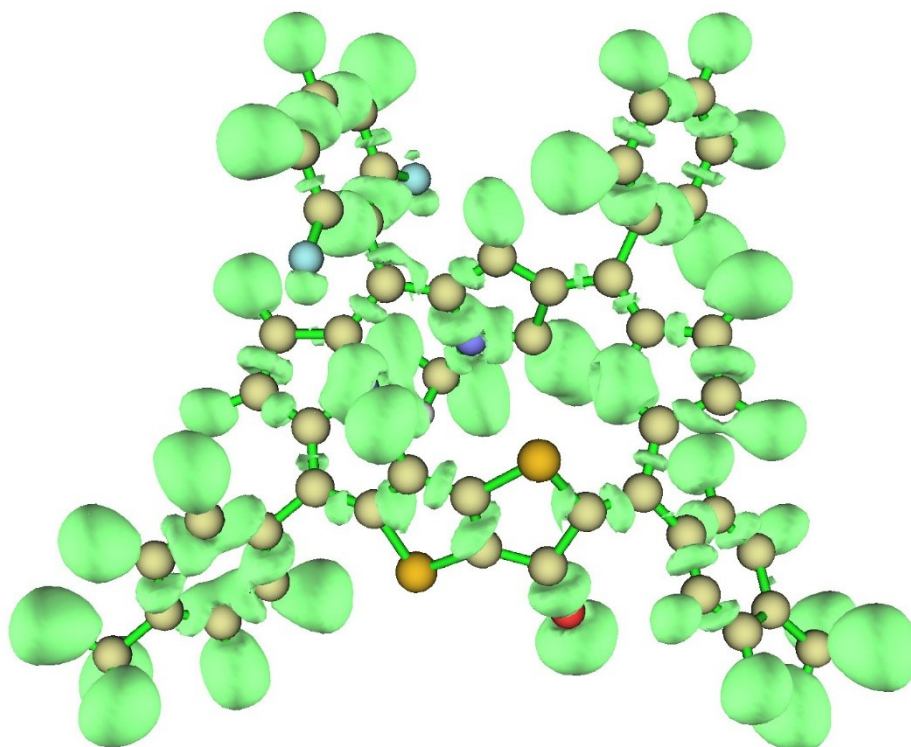


Fig. S59 Computed ELF- σ index of **10**

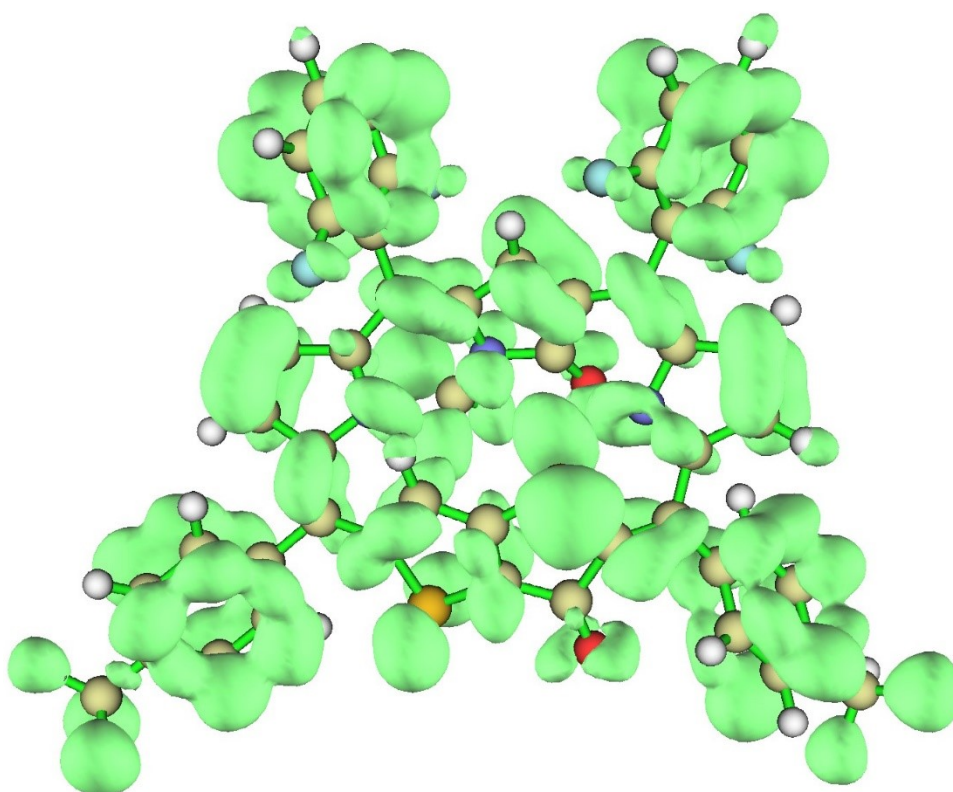


Fig.S60 Computed ELF- π index of **10**

6	0.816764000	-3.380514000	-0.317572000	1	-4.722049000	-0.424906000	1.604960000
6	-1.477964000	-2.413147000	-0.635762000	1	3.616743000	1.210495000	0.537902000
6	-1.067976000	-2.486308000	0.689237000	6	4.433318000	2.044126000	-1.203617000
6	0.229693000	-3.044728000	0.875296000	6	5.332395000	2.800164000	-0.445833000
1	0.727575000	-3.166941000	1.829074000	6	4.542723000	2.215597000	-2.587379000
6	3.406939000	1.134624000	-0.535126000	6	6.272522000	3.666362000	-0.992525000
6	-2.722546000	-1.749358000	-0.832094000	6	5.463782000	3.064414000	-3.188970000
1	-3.188621000	-1.574160000	-1.793605000	6	6.333161000	3.794278000	-2.378641000
6	-3.253327000	-1.295665000	0.345944000	1	6.932730000	4.216778000	-0.332351000
6	1.981298000	1.644526000	-0.706946000	1	5.484510000	3.138555000	-4.270160000
6	1.230357000	2.346709000	0.281102000	1	7.058994000	4.463261000	-2.829306000
1	1.570134000	2.594379000	1.276690000	9	3.712272000	1.517807000	-3.393966000
6	0.004922000	2.691007000	-0.260754000	9	5.289473000	2.687795000	0.902892000
6	1.177797000	1.578954000	-1.828859000	1	2.305425000	-4.418842000	-1.436339000
1	1.361959000	1.136706000	-2.795121000	6	2.820456000	-4.570334000	0.622117000
6	-4.419173000	-0.336970000	0.551329000	6	2.501976000	-5.931381000	0.722505000
6	-3.966208000	1.095470000	0.309497000	6	3.612640000	-3.987853000	1.614316000
6	-4.667735000	2.241751000	-0.023821000	6	2.955604000	-6.718944000	1.784092000
1	-5.727594000	2.291691000	-0.227233000	1	1.881718000	-6.386963000	-0.047089000
6	-3.739162000	3.319350000	-0.067615000	6	4.067378000	-4.759132000	2.686892000
1	-3.955120000	4.349691000	-0.316641000	1	3.884217000	-2.939977000	1.540949000
6	-2.492024000	2.812646000	0.248065000	6	3.742956000	-6.110531000	2.772851000
6	-1.142743000	3.501269000	0.316495000	1	4.681734000	-4.300371000	3.456646000
6	-1.095119000	2.341395000	-2.525721000	1	4.104879000	-6.702672000	3.609883000
1	-1.442308000	3.376048000	-2.587163000	6	2.628109000	-8.192279000	1.855681000
1	-1.944989000	1.707271000	-2.258811000	1	3.489447000	-8.805460000	1.563222000
1	-0.719449000	2.044750000	-3.506412000	1	2.351216000	-8.491300000	2.871951000
6	-5.633437000	-0.750560000	-0.280048000	1	1.799777000	-8.451250000	1.190371000
6	-5.792595000	-0.375856000	-1.619351000	1	-1.253631000	4.406403000	-0.291323000
6	-6.607534000	-1.578413000	0.290992000	6	-0.825104000	4.003966000	1.723841000
6	-6.886715000	-0.823118000	-2.360621000	6	-0.674776000	5.368146000	1.987662000
1	-5.070522000	0.291810000	-2.078133000	6	-0.698630000	3.170411000	2.838750000
6	-7.700483000	-2.020815000	-0.450643000	6	-0.422262000	5.888519000	3.251658000
1	-6.510389000	-1.879242000	1.331363000	6	-0.444614000	3.633035000	4.123317000
6	-7.858758000	-1.655657000	-1.793937000	6	-0.307591000	5.006574000	4.324488000
1	-6.989471000	-0.511712000	-3.397367000	1	-0.319844000	6.960638000	3.372553000
1	-8.445165000	-2.655957000	0.022956000	1	-0.359182000	2.919905000	4.934994000
6	-9.028922000	-2.158993000	-2.605303000	1	-0.109820000	5.389317000	5.320287000
1	-8.826076000	-3.155055000	-3.018389000	9	-0.821173000	1.833167000	2.662024000
1	-9.933870000	-2.241003000	-1.995344000	9	-0.783396000	6.236457000	0.955318000
1	-9.247395000	-1.495835000	-3.447313000				